ESTIMATING ASPHALT BINDER FATIGUE RESISTANCE USING AN ACCELERATED TEST METHOD

By:

Carl M. Johnson

A dissertation submitted in partial fulfillment of
the requirement for the degree of
Doctor of Philosophy

(Civil & Environmental Engineering)

at the
UNIVERSITY OF WISCONSIN – MADISON

2010

Dedicated to my grandfather,

Glenn H. Johnson

ACKNOWLEDGEMENTS

I would like to express my gratitude towards a number of individuals who have helped make this research possible. The first of which is my advisor, Prof. Hussain Bahia, whose guidance and tireless efforts to see this work to its highest potential have been a true inspiration. I would also like to thank my committee members: Profs. Steven Cramer, Tuncer Edil, Michael Plesha, and Dante Fratta, who have all been tremendously helpful in providing their honest feedback and advice over my entire course of study at UW-Madison. Not only has their assistance been related to engineering, but also to educating others, advancing my career and maintaining focus on my life's goals.

I would also like to thank Prof. Jeffrey Russell for his unfailing words of encouragement, which were always greatly appreciated.

To Prof. M. Emin Kutay, Prof. Haifang Wen, and Dr. Wilfung Martono I am especially grateful for the technical expertise they shared in relation to this particular research topic. I would also like to acknowledge the Federal Highway Administration for funding this research, as well as all of the Asphalt Research Consortium members for the collaborative effort to guide asphalt technology to new heights.

Special thanks also go to all of my colleagues at the UW-Madison Asphalt Research Group (past and present), particularly Dr. Raul Velasquez, Dr. Ahmed Faheem and Dr. Rodrigo Delgadillo, who have all been tremendously supportive over the past number of years, and with whom I have shared many of the joys and challenges of scholastic work.

Lastly, and most importantly, I would like to thank my wife, Jessica, along with the rest of my family for their love, support, and patience throughout this process, without which I most certainly would not have succeeded.

ABSTRACT

The main contribution of this study is the introduction of a method to quantify fatigue damage accumulation of asphalt binders using a short-duration test procedure that can be easily implemented into current practice. This was made possible by integrating results from the testing into an analysis procedure based on Viscoelastic Continuum Damage (VECD) concepts. The use of VECD analysis to characterize asphalt mixtures has been in use by researchers for a number of years, and it has been successfully applied in the field of asphalt mixtures to both monotonic and constant applied load amplitude cyclic (time sweep) tests. However, the application of these methods to asphalt binders has encountered a number of challenges. Monotonic testing of binders showed that, in some cases, the undamaged material response to loading is difficult to predict when some types of binder modification are used (e.g. polymers). The duration of time sweep tests is undefined, since it monitors the change in material properties with respect to number of loading cycles, and some high-performing binders can take many hours to show enough degradation to accurately assess their fatigue properties.

These challenges in applying VECD concepts to binders have been resolved by using the Linear Amplitude Sweep (LAS) test. By selecting a specific ramping sequence of strains, and by combining the results with the results of a frequency sweep, it has been shown that estimation of the fatigue performance of asphalt binders can be correlated to mixture performance in the laboratory and to field fatigue performance.

The accelerated loading scheme is found to give highly repeatable results and it takes less than 10 minutes to perform. The estimation of binder fatigue behavior was first validated against binder time sweep testing, followed by comparisons with asphalt mixture fatigue

results, and finally with in-service (field) pavement fatigue performance. A subsequent draft standard procedure is provided, along with recommendations for inclusion of the LAS procedure for specification use.

TABLE OF CONTENTS

LIST OF FIGURES

LIST OF TABLES

1. INTRODUCTION

1.1. Background

There is a significant amount of effort being focused on the development of binder test procedures that can more accurately determine the critical material failure properties associated with pavement distresses such as rutting, fatigue, and thermal cracking. Evaluation of fatigue damage in the binder alone has proven to be challenging, as it typically requires multiple repeated load cycles over a testing period that can last for hours. However, there is little argument that the binder/mastic phase of asphalt concrete is the most critical for resisting fatigue damage, and thus it must be evaluated for fatigue performance.

The search for an improved asphalt binder fatigue test method is an on-going effort related to the improvement of asphalt specifications. The current specification practice of measuring linear viscoelastic dynamic shear modulus and phase angle does well to evaluate the effect of long-term aging on the material properties of asphalt, but it does not include actual evaluation of resistance to damage. Additionally, it does not account for the effect of pavement structure or traffic loading, as it is measured at only one load amplitude and frequency. During the National Cooperative Highway Research Program (NCHRP) Project 9-10, a test method was proposed that applies repeated cyclic loading to a binder specimen using the Dynamic Shear Rheometer (DSR), known as the time sweep (Bahia et al. 2001). The new test was designed to mimic mixture testing and, although developed independently, has its basis in work done in the early 1960's (Pell 1962). The main benefit to this test is a direct application of fatigue-type loading, and if performed at sufficient stiffness levels,

relevant fatigue performance indicators can be measured (Anderson et al. 2001; Martono et al. 2007). However, the suitability of this test for use in specification is questionable due to the possibility of long testing times. Hence, recent work on binder fatigue has focused on the search for test procedures that can be used as "accelerated" fatigue tests (Andriescu et al. 2004; Martono and Bahia 2008; Johnson et al. 2009b).

Multiple test procedures have been under investigation for their abilities to act as a surrogate to the time sweep test. These "accelerated" procedures take significantly less time to perform, but work to unite these methods to time sweep performance via a fundamental link continues to be a challenge. Recent work has suggested that these types of procedures may hold promise in the indication of fatigue performance of asphalt binders (Martono and Bahia 2008; Johnson et al. 2009b), and the results presented in this dissertation show that there may be a benefit to employing accelerated test methods in future specification.

1.2. Problem Statement

Current methods of specifying asphalt binder with regards to its ability to withstand fatigue damage rely on indications from undamaged material properties. Newer fatigue test methods for evaluating the damage-resistance characteristics of binders are impractical for use in specification due to long testing times. There is then a present need to have a testing and analysis methodology that can assess the fatigue damage resistance of asphalt binders in a reasonable amount of time, while still having the ability to incorporate the effects of traffic and pavement structure. A system meeting these goals would be valuable for both government specifying agencies to ensure long-lasting pavements, as well as suppliers of asphalt products that require a high-quality material be delivered to their clients.

1.3. Hypothesis

Fatigue resistance of asphalt binders can be estimated efficiently by accelerating the progression of damage, and using continuum damage principles. The acceleration of damage can be achieved by systematically increasing the load amplitude in a repeated cyclic loading test, known in this dissertation as the linear amplitude sweep (LAS) test. The LAS results, combined with results of undamaged rheological characterization, can be used to predict fatigue resistance of asphalt binders, under various loading and pavement structure conditions. This is possible using Viscoelastic Continuum Damage (VECD) analysis principles already used successfully for asphalt mixtures.

1.4. Objectives

The objective of this research is to develop a testing and analysis methodology that can efficiently determine the fatigue characteristics of asphalt binders. The methodology can then be applied to a specification system that can be used to define binder quality and acceptance for use in pavements based on the expected traffic and pavement structure. This specification system can be used by pavement engineers as a tool to select binders for the design of pavements for fatigue resistance.

2. LITERATURE REVIEW

2.1. Damage in Viscoelastic Materials

2.1.1. Molecular Structure and Effect on Mechanical Response

Asphalt binder is typically regarded as having a colloidal structure, consisting of insoluble asphaltene molecules distributed in an oily matrix, identified as the maltene phase, consisting of aromatics and saturates. Resins present in the material act as a dispersing agent for the asphaltenes molecules (an example of this arrangement is shown in Figure 2.1). The asphaltenes are primarily responsible for giving asphalt its stiffness, as viscosity typically increases as the asphaltenes concentration increases. However, the high amount of secondary bonding in the maltene phase gives asphalt binder its temperature sensitivity. These bonds are easily broken with the addition of heat energy, decreasing stiffness/viscosity as the temperature increases.

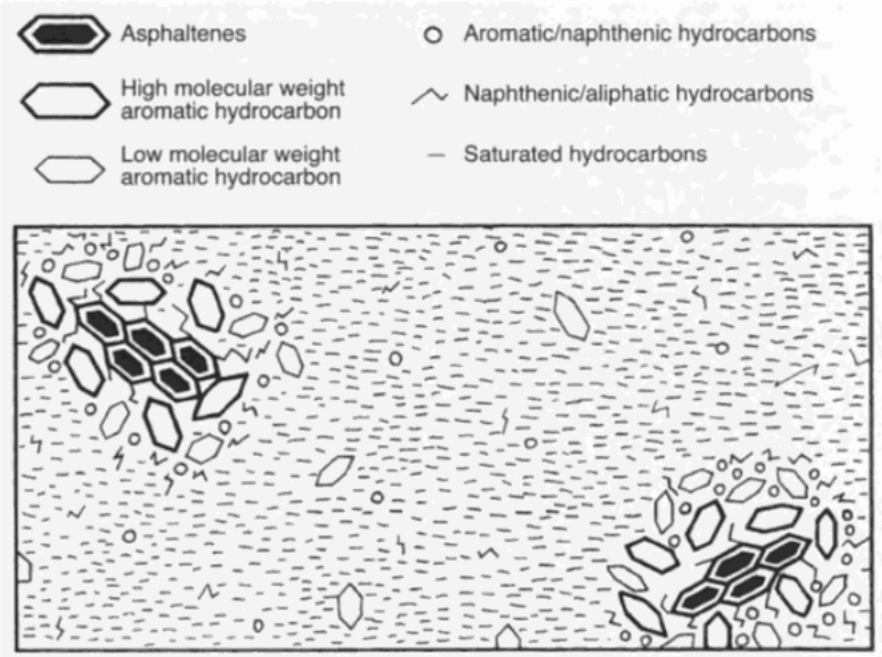

Figure 2.1. Schematic of molecular arrangement in asphalt binder (Read and Whiteoak 2003).

The addition of synthetic polymers to asphalt can add significant performance improvement given appropriate conditions. For example, adding a polymer with high elasticity can help reduce the permanent deformation in mixes resulting from the viscous nature of binder at high temperatures. Studies have shown that polymer modification can also enhance thermal and fatigue cracking resistance (Bahia et al. 2001). For the purposes of this study, fatigue performance was investigated in detail.

Using the colloidal model for binder described above, the material can be thought of as a composite consisting of different types of molecules with varying properties. Compatible polymer types can be dissolved in the maltene phase of the material and act as "reinforcement" due to their ability to form physical cross-links between other polymer molecules, adding strength and elasticity to the binder. However, the binder as a whole is still somewhat heterogeneous in nature, as evidence by comparison tests performed on unmodified

and polymer-modified binders (Read and Whiteoak 2003). The force ductility test consists of a dumbbell-shaped binder specimen that is elongated at a constant displacement rate while recording the stress response. As shown in Figure 2.2, the polymer-modified binder typically shows a secondary peak stress, indicating that the polymer phase provides additional strain tolerance to the material.

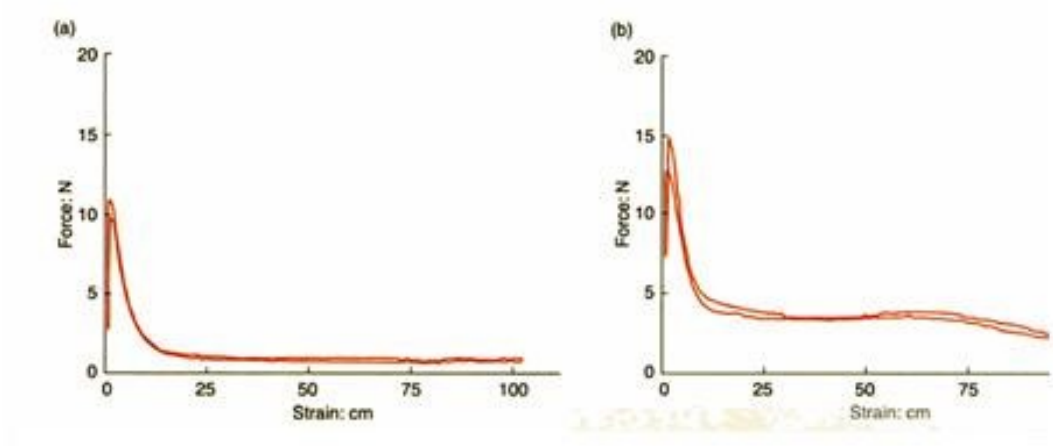

Figure 2.2. Results of force-ductility tests between (a) unmodified and (b) polymer-modified binders (Read and Whiteoak 2003).

This phenomenon has also been seen in recent work on a shear corollary for the force ductility test, known as the Binder Yield Energy Test, or BYET (Johnson et al. 2009a; Johnson et al. 2009b). An 8-mm diameter by 2-mm thick disc of binder is subjected to a constant shear strain rate rotational loading using the Dynamic Shear Rheometer (DSR). The output of the test is a stress-strain plot. As can be seen in Figure 2.3, differences in unmodified and polymer-modified binders are observed. The plot suggests that the asphaltene-maltene relationship is responsible for the initial peak, while secondary peak in the polymer-modified material shows evidence of the strength of the polymer cross-linking.

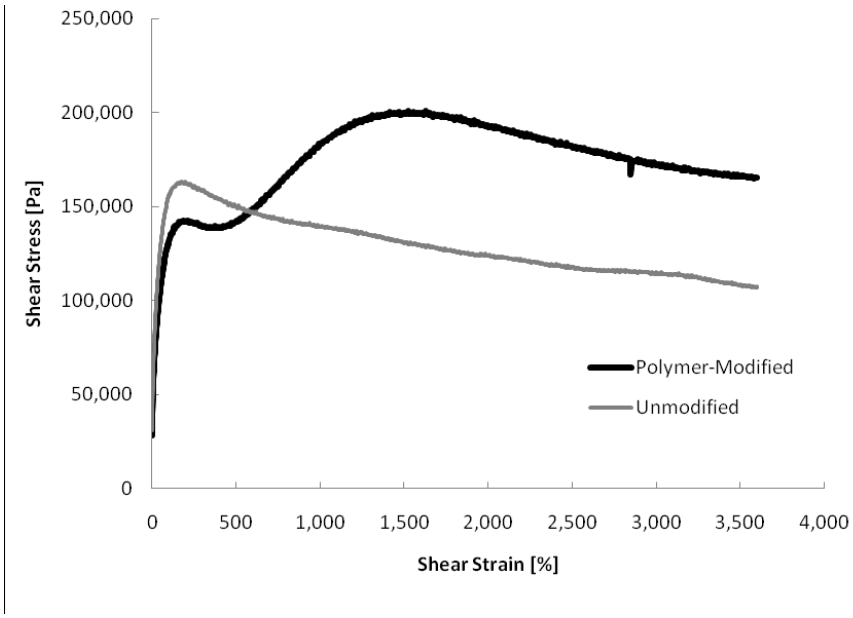

Figure 2.3. BYET results for unmodified and polymer-modified binders.

Another aspect of the chemical composition of asphalt is the fact that organic compounds within the material react with oxygen over time, known as aging, changing both the chemical composition and resulting mechanical properties. Typically, the lighter molecular weight compounds in the maltene phase (namely the aromatics) have been shown to react with more readily, as their percentage by mass of the total material drops with time of exposure to oxygen. This, in turn, leads to a stiffer and more brittle material. This phenomenon is simulated via various methods in current asphalt specifications in order to account for changing material properties with time. Fatigue properties are of notable concern for aging, as brittle materials are more prone to crack growth than those with more ductile properties.

With all of the advances in chemistry and methods to characterize the molecular structure of materials, mechanical characterization of asphalt via its chemical components remains a challenge. The primary reason for this is due to the fact that some binders with

vastly different chemical composition have strikingly similar mechanical properties, and some binders with similar chemical composition exhibit widely varied mechanical behavior. Current research efforts are focused on explaining these observations. However, mechanical characterization remains the best method of evaluating asphalt binder for use in pavements.

2.1.2. Definition of Damage and Design Considerations

As discussed in the previous section, the mechanical properties of a material are largely determined by the nature of the bonding in the material on a molecular level. When this bonding is broken, damage begins to occur. In polymers, this damage can manifest as debonding between the long molecule chains in the material. On a more general scale, damage accumulation is primarily thought of as the decomposition of mechanical properties due to the growth of microcracks or defects in a material (Lemaitre 1992). The damage accumulation process typically begins with the nucleation and subsequent propagation of cracks or defects in a material (Kachanov 1986). These defects coalesce to the point where they eventually lead to a complete failure in the material (i.e. fracture).

The recognition of damage mechanics as a necessary tool in engineering practice has led to the development of design philosophies for consideration of fatigue damage growth, given below in chronological order of their development (Krajcinovic 1996) :

- *Static strength (or infinite life)*: Allowable stresses are limited to a "safe" fraction of the ultimate strength of the material.
- *Safe-life*: Finite fatigue life is measured for the material, and load cycles are kept within that limit.

- *Fail-safe*: Redundant load paths are emphasized to move stresses away from the damaged material to avoid catastrophic failure and perform timely repair.
- *Damage-tolerant*: Fatigue damage is assumed to be inevitable, and focus is placed upon characterizing the residual strength of the material as damage begins to accumulate.

While these design philosophies were initially listed with aircraft design in mind, there are consistencies with pavement design philosophy. The American Association of State Highway Officials (AASHO) Road Test was the first full-scale investigation into the effect of truck traffic on pavement damage. From 1958 to 1960, test tracks located in Ottawa, Illinois were subjected to constant truck traffic, with the resulting pavement distresses being measured and incorporated into a statistical regression equation that is currently used to design pavement thickness (Yoder and Witczak 1975). The methodology is to calculate a thickness that will result in an acceptable level of damage given a predicted amount of traffic loading, akin to the "safe-life" design methodology. Researchers understood that failures were inevitable, but could merely correlate failure to empirical observations. As advanced characterization techniques evolve, such as computer-aided modeling, researchers are currently trying to obtain a better grasp on how pavements perform with increasing damage, in following with the "damage-tolerant" design philosophy. Pavement materials, such as asphalt mixture, are now being evaluated for their ability to withstand loading as damage accumulates. However, the exact method in which to do so is the focus of current research.

2.1.3. Mechanics of Damage in Viscoelastic Materials

Fatigue in polymer materials has been studied, but largely at temperature conditions where the microstructure of the materials under investigation is glassy or crystalline in nature. However, asphalt binder is unique in that it is used under temperature conditions where it behaves as a highly viscous amorphous solid.

One method of quantifying damage is to relate the undamaged material properties to measured material properties during a destructive (damage-inducing) test, an example of which is shown in Figure 2.4. The undamaged properties can be estimated from tests employing small loads, under the assumption that no damage is produced. This is then followed by a destructive test, which gives a response that includes the undamaged constitutive relation coupled with an expression that describes the deteriorating material properties due to damage. This methodology was employed on asphalt mixtures under uniaxial monotonic loading (Kim and Little 1990; Park et al. 1996) using theories on damage growth in viscoelastic media (Schapery 1975; Schapery 1984).

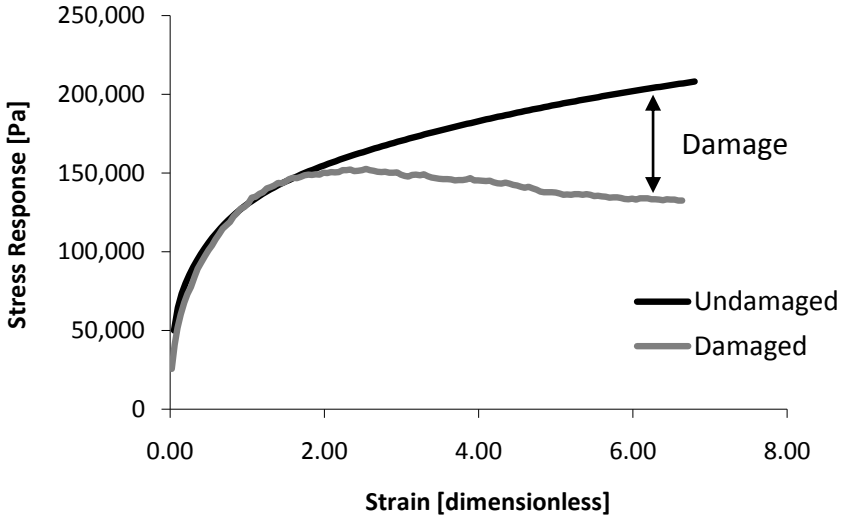

Figure 2.4. Example of discrepancy between the measured damaged response and predicted undamaged response.

The basis for this theory on viscoelastic damage growth is inspired by thermodynamics of irreversible processes. A material has a certain potential to absorb external energy; however, if the material absorbs energy upon an external load via both deformation and energy dissipated due to damage, the process cannot simply be reversed by removing the load since the damage has affected the material's ability to recover to its original state. Therefore, a damage rate (which can also be thought of as the available force for damage growth) can be defined as the change in the material's energy potential (W) with respect to the change in the amount of damage (D) in the material (which is the force required to match that available for damage growth).

$$\frac{\mathrm{d}D}{\mathrm{d}t} = -\frac{\partial W}{\partial D} \tag{1}$$

However, Schapery found that a power law best represented experimental data for viscoelastic materials (Schapery 1975; Schapery 1984). The inspiration for this is based on Paris' Law of crack growth, given as

$$\frac{\mathrm{d}c}{\mathrm{d}N} = A * (\Delta K)^n \tag{2}$$

where: c = crack length,

N = number of loading cycles,

A, n = fracture properties determined by the experimental test,

ΔK = stress intensity factor (SIF) amplitude, depending on the geometry of the test specimen, fracture mode, and crack length.

It was hypothesized by Schapery that damage growth in viscoelastic materials would follow the same type of relationship that Paris' Law defines for crack growth in other materials. Hence, the relationship in Equation (1) becomes

$$\frac{\mathrm{d}D}{\mathrm{d}t} = \left(-\frac{\partial W}{\partial D}\right)^{\alpha} \tag{3}$$

where α is the exponent determining energy release rate.

This relationship serves as a starting point to begin material damage characterization. An appropriate representation of the energy in the material must be determined. For monotonic testing, the area underneath the stress-strain curve is known as the strain energy, and has been used to characterize the damage growth under monotonic loads (Kim and Little 1990; Park et al. 1996; Daniel and Kim 2002). However, under cyclic loading typically associated with fatigue testing, viscoelastic materials have a tendency to dissipate energy due to damping characteristics of the material. This behavior is not damage-related, but changes in this dissipated energy are an indication of damage accumulation. Therefore, the dissipated energy can be used in Equation (3) to account for damage under cyclic loading.

A straightforward method to incorporate the damage parameter *D* is to assign a material response, such as modulus, as function of damage. As damage is typically manifested in experimental data as degradation in material properties, it appears to be an intuitive fit. The exact function associated with damage does not need to be known a priori, as the material response is recorded directly during testing. This way, Equation (3) can be solved to determine the damage accumulation with time, which can then be associated with the relative degradation of material properties at the same corresponding time. If the damage analysis methodology employs Equation (1), and modulus is used as an example of the material property under scrutiny, units for the damage parameter *D* after integration are [stress unit]$^{1/2}$ [time]$^{1/2}$. However, the addition of the exponent in following Paris' Law, as implemented in Equation (3) gives units of [stress unit]$^{\alpha/(1+\alpha)}$[time]$^{1/(1+\alpha)}$.

2.2. Asphalt Pavement Fatigue

Pavement structures are unique in the fact that they are designed to fail, as infinitely durable pavements are cost-prohibitive to produce. Recent efforts have been focused on the design and construction of "perpetual pavements", where an emphasis is placed on high-quality foundation and pavement layers (at a higher initial cost) in hopes of reducing subsequent maintenance and reconstruction costs over the lifetime of the material. However, this option is currently being used in limited cases, and the majority of paved roads in the United States employ more conventional designs that are susceptible to fatigue damage. Fatigue is typically characterized as cracking directly underneath the wheel path due to repeated loading. This cracking allows for both water infiltrating into the pavement's lower layers, possibly weakening them, as well as contributing to a reduced ride comfort. As such, methods to characterize asphalt concrete fatigue in a laboratory have been in use for many years in efforts to obtain a better understanding of this failure mode, and to provide not only fatigue-resistant pavement designs, but also methods for identifying fatigue-resistant paving materials.

One of the most common ways of evaluating the fatigue resistance of asphalt concrete has relied on repeated flexural loading of rectangular beam specimens. Under widespread use since the 1950's (Monismith 1958; Deacon 1965), the flexural fatigue procedure is intended to simulate the response of an asphalt pavement under traffic loading. It identifies a critical condition for pavement fatigue, where spring thaw conditions can lead to saturated conditions in the unbound base layers and decrease support stiffness significantly. This leads to increased pavement deflection with loading, which causes higher strains in the asphalt layer that can ultimately lead to fatigue failure. This failure is typically characterized as "bottom-up

cracking", where tensile strains at the bottom of the pavement structure are responsible for initiating a crack that progressively moves towards the surface of the pavement with successive traffic loads. Based on this concept, pavement design for fatigue resistance involves increasing the asphalt layer thickness in order to limit high tensile strains under the expected traffic loading.

In order to obtain a more complete characterization of an asphalt mixture's fatigue resistance, many researchers have developed models relating the fatigue life of asphalt concrete to the amplitude of the applied load. The most common (Monismith et al. 1970) follow the form of

$$\text{Number of Cycles to Failure} = A \times (\text{Amplitude of Applied Load})^{-B}, \tag{4}$$

where A and B are model coefficients that depend on material characteristics; a graphical example of this relationship is shown in Figure 2.5, also known as a Wohler curve (Schütz 1996). Various parameters have been used for applied load, such as stress and strain by Monismith et al. (1970), as well as dissipated energy (Chomton and Valayer 1972). The relationship has been verified for asphalt binders as well (Bahia et al. 2001). However, in order to obtain the relationship, multiple tests need to be performed. Depending on the fatigue resistance of the material, this can be a time-intensive process.

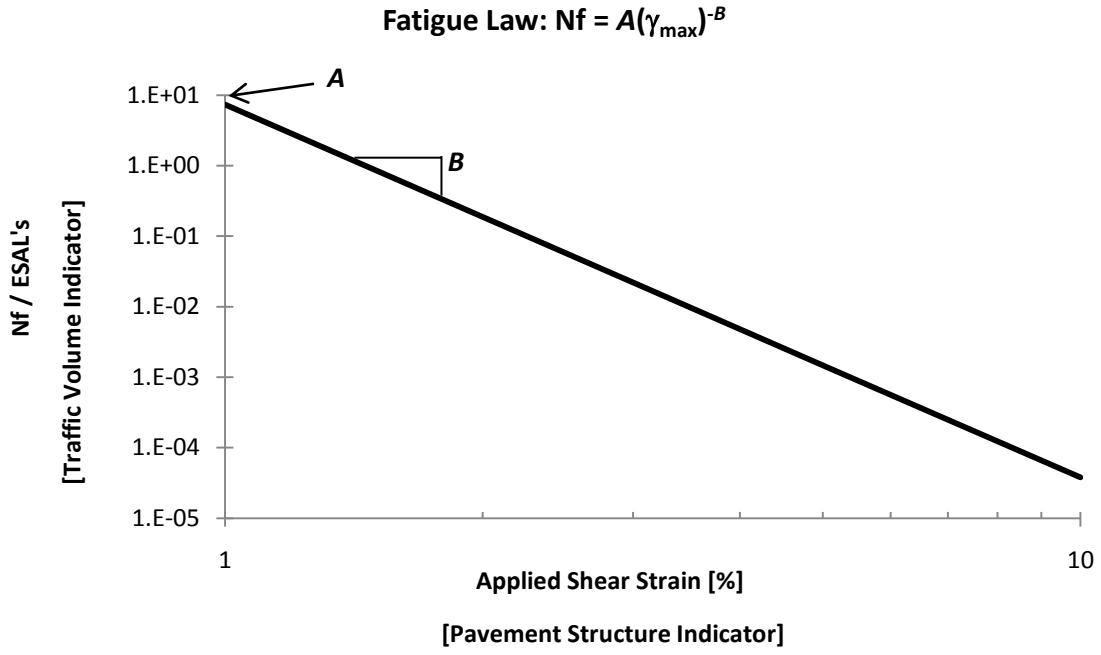

Figure 2.5. Fatigue law for number of cycles to failure versus applied strain amplitude for an asphalt binder.

Many researchers have also employed cylindrical testing geometries to measure fatigue performance of asphalt mixtures under uniaxial loading (Lee and Kim 1998a; Daniel and Kim 2001; Christensen Jr and Bonaquist 2005; Kutay et al. 2008). The benefit of uniaxial load application is that the stress state in the material is relatively uniform across the specimen cross section, which has aided in simplifying the data modeling efforts for the studies referenced above.

Additionally, uniaxial evaluation of cylindrical specimens is being recommended for standardized mechanical evaluation of asphalt concrete for improved pavement design practice (Witczak et al. 2002). While the models employed by this practice vary in form and complexity, the general methodology is to use the dynamic modulus of the material to predict

the strains in the pavement structure at critical locations, with the intent that minimizing the strains at these locations will increase the fatigue life of the pavement (Witczak and El-Basyouny 2004).

In addition to laboratory characterization, there are accelerated full-scale testing methods that are used to simulate traffic loading. These "accelerated pavement testers" (see Figure 2.6) can apply repeated wheel loads in an automated fashion, giving researchers the ability to load the test sections continuously until signs of distress begin to appear. Accelerated testing provides substantial time savings over having to wait for field performance data to become available. Fatigue distress in particular can take many years to manifest in the field, whereas accelerated pavement testing can achieve this in a manner of months (Kutay et al. 2007). With the ability to allow researchers the opportunity to tightly control testing conditions and instrument test sections with sophisticated data acquisition equipment, accelerated testing facilities are a valuable source of information on pavement performance; however, testing conditions do not exactly replicate in-service conditions (e.g. traffic speed and frequency), so caution should be exercised when making direct comparisons between accelerated and in-service pavement performance.

Figure 2.6. Simulated truck tire from accelerated loading facility equipment (From fhwa.dot.gov)

As is shown in the above section, the fatigue resistance of asphalt concrete is a highly sought-after performance characteristic. Methods for measuring fatigue range from small-scale representations of pavement behavior using repeated flexure, to full-scale accelerated testing facilities. Recent efforts have focused on measuring the fundamental mechanical properties of asphalt concrete in an effort to use advanced design practices to combat fatigue damage, and as will be discussed in the next section, further advancements are being made towards modeling the damage growth as an independent property of asphalt concrete.

2.3. Mechanical Behavior of Asphalt Concrete

2.3.1. Contribution of Binder Properties to Global Mixture Properties

Asphalt binder provides both its adhesive and cohesive nature to the mixture of aggregate particles in asphalt concrete. While the aggregate structure provides the majority of the load resistance, the binder serves to cement the aggregates together in order to maintain

the aggregate particle interlock necessary to support traffic loads. It also provides waterproofing characteristics to protect the aggregates in the asphalt mixture, along with underlying foundation aggregate layers that are typically unbound and susceptible to reduction in modulus with the addition of moisture. However, differences in binder mechanical properties have been shown to significantly affect the behavior of asphalt mixtures.

Initially, empirical models were employed to determine the modulus of the mixture based on the relative volumes of asphalt, aggregates, and air voids. The modulus of each component could either be measured or assumed, and a combined value was calculated. This practice developed into a statistical analysis in order to identify critical variables related to the components of asphalt mixture. Regression equations were then formulated in order to use measured material characteristics to estimate mixture modulus. The most recent and widely used example of this is currently implemented in the AASHTO Mechanistic-Empirical Pavement Design Guide (MEPDG) (Witczak and Fonseca 1996). Binder viscosity is the only binder-related parameter in the regression model consisting of twenty terms. However, the equation has a coefficient of determination of 0.95 for 149 mixtures, and is subsequently featured in the MEPDG.

In focusing on the effect of binder on mixture fatigue performance, studies have held mixture aggregate gradations constant while varying the binder type in order to assess whether the selection of different binders (at roughly only 5% of mixture by weight) can significantly affect mixture fatigue performance (Bahia et al. 2001; Kutay et al. 2008). As can be seen in Figure 2.7, there is no question that binder type can have a significant effect on fatigue performance.

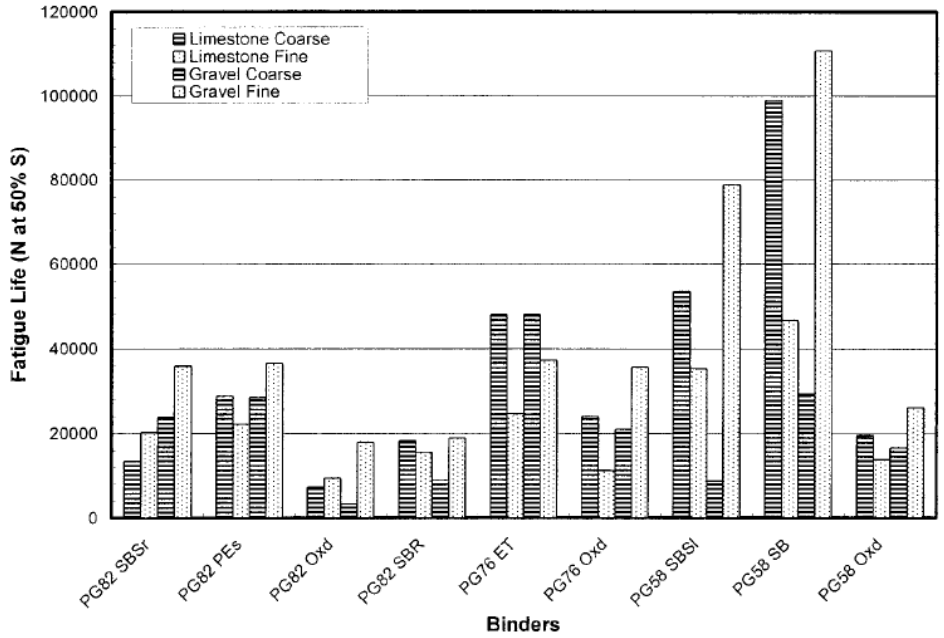

Figure 2.7. Effect of binder type on fatigue performance for various binder and mixture types, where *S* is initial mixture stiffness (Bahia et al. 2001).

The best performing binder type in Figure 2.7 outperforms the worst by over five-fold in some cases, with mixture properties only differing in binder type. When a typical binder content of a mixture is only 5% of the total weight, it becomes apparent that the ability to select superior performing binders for fatigue resistance is an excellent measure for improving overall pavement performance.

2.3.2. Analysis of Strain Distribution in Binder Phase

Efforts to model the complex composite nature of asphalt mixture have been undertaken by researchers hoping to simulate various loading conditions by means of Finite Element Modeling (FEM). A number of studies have used images of cross sections of mixture specimens as the basis for developing two-dimensional models (Wang et al. 1999; Masad et al. 2001; Kose 2002). While three-dimensional models would be more representative, the

computational cost remains a hurdle to researchers. The 2D models have been able to provide valuable insight as to how varied the strain distribution can be within the binder phase of the mixture.

The most prevalent practice is to use the cross sectional image to create a three phase finite element model consisting of aggregates, air voids, and mastic (a combination of asphalt binder and fine particles measuring less than 75μm in their longest dimension). Various loads are then applied, and the range of strains calculated in the mastic phase can be determined, as is shown in Figure 2.8.

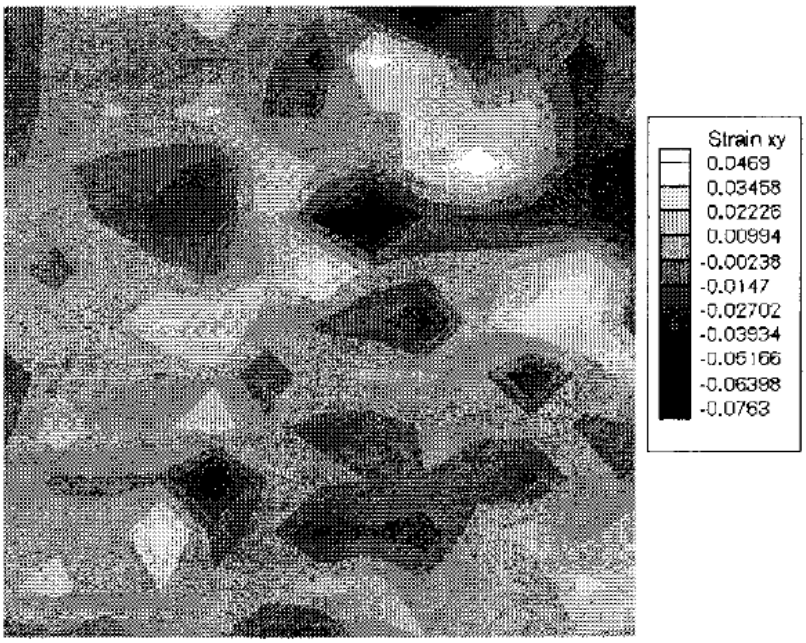

Figure 2.8. Distribution of shear strains in the mastic phase of asphalt mixture under uniaxial loading (Masad et al. 2001).

In order to get to the binder level, a micromechanical model employing composite theories that are based on relative volume of the mastic constituents is used to approximate the ratio of bulk mastic strain to binder strain. Masad et al. (2001) found that FEM results

compared favorably with experimental results derived from digital image analysis of physical specimens under loading, and that the binder phase could experience shear strains as high as 90 times the bulk mixture strain under uniaxial loading. Figure 2.8 displays the relative variation of the mastic shear strain under uniaxial loading, indicating the complex stress and strain states that exist in the binder even under uniaxial loading.

2.3.3. Use of Binder Shear Properties to Determine Damage Characteristics

During the Strategic Highway Research Program (SHRP) efforts to improve asphalt binder specifications, it became apparent that the Dynamic Shear Rheometer (DSR) already in use by the materials science field would be useful tool in characterizing the rheological properties of asphalt binder. Initially, indentation-type tests were examined in order to obtain material characteristics such as creep compliance. However, indentation was abandoned in favor of the DSR as the equipment became more cost-effective, and was more flexible in the types of testing it could perform, such as creep (transient) as well as oscillatory (dynamic) loading. One of the primary objectives of SHRP was to develop a new performance-based specification that could be employed across the United States, and the cost of DSR machines was no longer prohibitive such that contractors and state agencies could purchase and use them to determine advanced material properties previously ignored for asphalt binder. The subsequent specification has been widely adopted, and as a result, a large number of laboratories that test asphalt binders employ the DSR. As such, many research efforts are currently focused on increasing the functionality of the equipment by devising new test methods.

With regards to the previously described complexity of stress and strain states present in an asphalt mixture, binder is assumed to be incompressible with a Poisson's ratio of 0.5, making interconversions between shear and uniaxial material properties relatively straightforward. However, there has been recent work to investigate fatigue properties of binder in tension directly, as cracking in pavements is typically associated with a tensile force opening the crack (Chailleux et al. 2009). Specialized specimen geometry was devised to perform uniaxial tension-compression testing, shown in Figure 2.9.

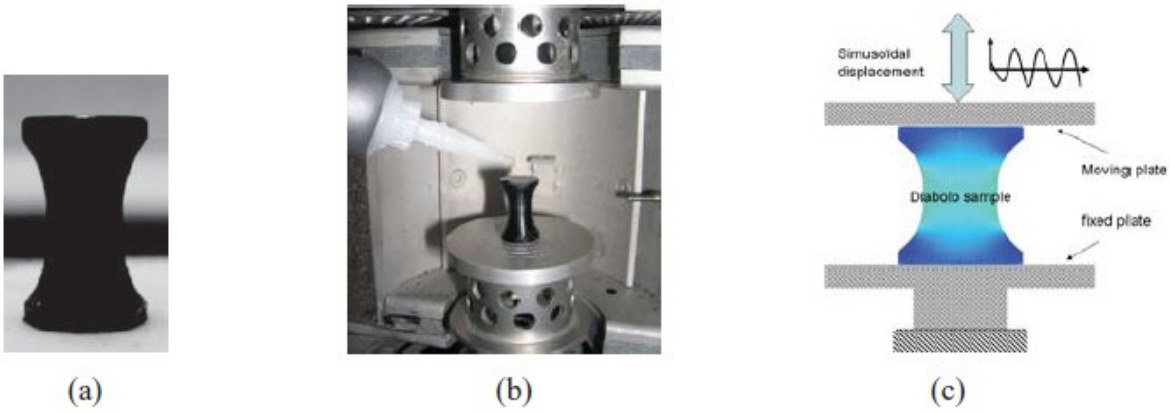

Figure 2.9. Images of the tension-compression specimen (a) upon demolding; (b) being loaded into test equipment using adhesive; (c) schematic depicting loading (Chailleux et al. 2009).

While the equipment to perform this type of testing is not widely available to asphalt researchers, there is currently a "round robin" testing schedule that will allow for a direct comparison of fatigue properties measured in shear to those measured uniaxially. Initial results show that the ranking of fatigue performance from uniaxial binder fatigue tests compare favorably with mixture performance, but only three binders have been tested, two of which with similar fatigue performance characteristics. An expanded testing matrix is planned.

2.4. Use of Viscoelastic Continuum Damage Theory for Asphalt

Based on R.A. Schapery's work on crack growth in viscoelastic media (Schapery 1984), researchers interested in the constitutive modeling of asphalt mixture fatigue have applied the concept of Viscoelastic Continuum Damage (VECD) in an effort to explain this complex phenomenon. VECD primarily uses deviations from linear viscoelastic behavior and stiffness reduction (among other parameters that will be described later) to characterize damage evolution. There has already been much work done in applying this to asphalt mixtures, and the research has shown that material parameters derived from this model can accurately predict damage evolution in asphalt mixtures irrespective of the testing temperature or mode of loading (Kim and Little 1990; Park et al. 1996; Lee et al. 2000; Daniel and Kim 2002; Kim et al. 2002b; Lee et al. 2003; Daniel et al. 2004; Christensen Jr and Bonaquist 2005). The obvious benefit of this is that one can use test results from a single set of conditions to predict the behavior of that material under any variety of alternate conditions, making the experimental characterization of the damage resistance properties of a material far more efficient to perform. The background for the development of the VECD analysis process for asphalt concrete is presented next.

To begin, efforts were initially placed on the constitutive modeling of asphalt concrete. Work done by Kim and Little (1990) used the uniaxial response of an asphalt concrete prismatic specimen under a monotonic constant strain rate to compare with the predicted undamaged response using viscoelastic constitutive equations. The relaxation modulus [$E(t)$] was measured directly using stress relaxation, and the constitutive equation relating stress (σ) and strain (ε) as a function of time for viscoelastic materials, given by Equation (5), was used to predict the monotonic response.

$$\sigma(t) = \int_0^t E(t-\tau)\frac{\partial \varepsilon}{\partial \tau}\mathrm{d}\tau \tag{5}$$

Upon loading of the asphalt concrete specimens in direct tension under a constant strain rate, the measured stress was compared to the predicted stress obtained from undamaged material properties using Equation (5). As the specimen becomes damaged, the measured stress typically begins to decrease in relation to the predicted response, as previously shown in Figure 2.4. This discrepancy is used as a method to quantify damage growth in a material by adding a term to the constitutive equation in order to match experimental data.

Subsequent research incorporated Schapery's theory of work potential to model damage growth as an independent material property (Park et al. 1996). The fundamental basis for the theory relies on attributing changes in the work done in a system to a damage parameter. Under uniaxial monotonic loading, the work performed (W) is described by the strain energy density:

$$W = \frac{1}{2}(E)(\varepsilon)^2 \tag{6}$$

where E = modulus;

ε = uniaxial strain.

The modulus, *E*, can be described as a function of the amount of damage present in the material, and it is this relationship between modulus (or more generally, material integrity) and damage intensity that is used to characterize the material's damage resistance properties. Equation (6) can then be included into Equation (3) in order to quantify damage accumulation.

Determination of the α parameter in Equation (3) has been of substantial interest on its own. Use of Schapery's variation of Paris' Law, given by Equation (2), has been the basis for this work. Schapery (1975) was able to show that the parameters *A* and *n* were related to viscoelastic material properties, specifically that

$$n = 2\left(1 + \frac{1}{m}\right) \tag{7}$$

where m = the exponent of the creep compliance versus time power law, i.e. $J(t) = J_0 + J_1 \times (t)^m$. Further development of Equation (7) led to the generalized J-integral to account for large deformations (Schapery 1984):

$$\frac{\mathrm{d}a}{\mathrm{d}t} = f_1(J_v)^k \tag{8}$$

where J_v = energy release rate;

f_1, k = material-dependent parameters

It was found that k was equal to $1 + 1/m$ in the case that both the maximum stress in the failure zone and fracture energy are constant.

This relationship was used to determine the initial value of α from Equation (3) by Park et al. (1996), which was then iteratively altered to match experimental data. Additional research on application of Equation (3) to cyclic loading found that $\alpha = 1 + 1/m$ best described the results from controlled strain testing (Lee and Kim 1998a).

Moving forward, the work potential theory was used to begin quantification of the damage parameter D. To do so, Equation (3) is typically numerically integrated in order to calculate the damage accumulation from experimental data (Lee and Kim 1998b). First, the chain rule can be utilized, relating modulus E to damage D:

$$\frac{\mathrm{d}E}{\mathrm{d}D} = \frac{\mathrm{d}E}{\mathrm{d}t}\frac{\mathrm{d}t}{\mathrm{d}D} \tag{9}$$

Then, combining Equation (3), Equation (6), and Equation (9) yields the following relation (Kutay et al. 2008):

$$\frac{\mathrm{d}D}{\mathrm{d}t} = \left(-\frac{\varepsilon^2}{2}\frac{\mathrm{d}E}{\mathrm{d}t}\right)^{\frac{\alpha}{1+\alpha}} \tag{10}$$

The damage parameter with respect to time can then be calculated by rearranging Equation (10) and numerically integrating in the form of a Riemann sum:

$$D(t_N) \cong \sum_{i=1}^{N} \left[\frac{1}{2}\varepsilon^2(E_{i-1} - E_i)\right]^{\frac{\alpha}{1+\alpha}} (t_i - t_{i-1})^{\frac{1}{1+\alpha}} \tag{11}$$

where the damage is calculated at data point *N* by summing the incremental damage for each data point *i*.

Daniel and Kim (2002) used this formulation to relate the damage measured from cyclic fatigue tests to damage from monotonic strength tests. For this study, the strain, ε, was replaced with predicted undamaged strain, and Young's modulus, *E*, was replaced with the normalized material integrity. For monotonic tests, material integrity was defined as measured stress divided by predicted stress at each data point; for cyclic tests, it was defined as the measured dynamic modulus at the given cycle divided by the initial undamaged dynamic modulus. Results showed that the relationship between material integrity and damage intensity was consistent regardless of the mode of loading, as shown in Figure 2.10. This study is an important milestone in the development of VECD application to asphalt testing, as it showed its ability to characterize the fatigue behavior of the material for multiple testing conditions using the data from a single, short-duration procedure.

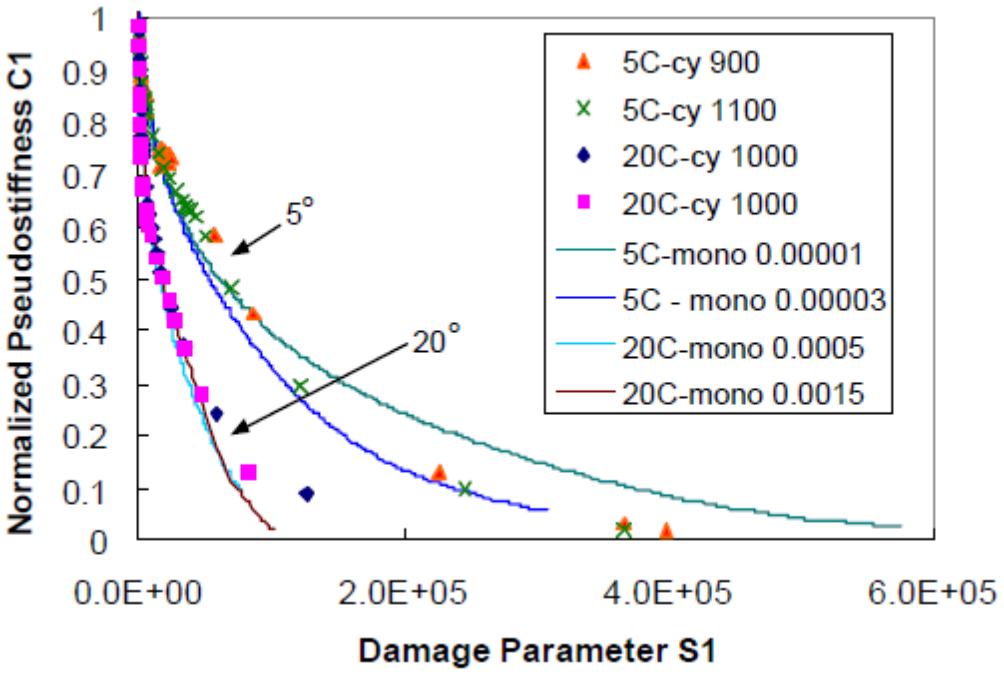

Figure 2.10. Characteristic damage curves from Daniel & Kim (2002) showing agreement between monotonic and cyclic test results. (Note: For this study, material integrity is denoted by the parameter "C1", and damage by the parameter "S1".)

While VECD analysis showed initial promise in relating monotonic to cyclic loading, cyclic data had to be resolved as a series of short monotonic loads, and information regarding the energy dissipated during each load cycle was not included in the analysis. This was addressed in a later study that replaced Equation (6) in the damage calculation with the dissipated energy under strain-controlled cyclic shear loading using the following equation (Kim et al. 2006):

$$W = \pi \cdot I_D \cdot \gamma_0^2 \cdot |G^*| \cdot \sin\delta \tag{12}$$

where I_D = initial undamaged dynamic shear modulus [MPa] divided by a modulus of 1 MPa;

γ_0 = applied shear strain amplitude;

$|G^*|$ = dynamic shear modulus [MPa];

δ = phase angle [degrees].

The reason for shear loading was due to the testing conditions for this study, where small cylinders consisting of asphalt binder and fine aggregates (i.e. sand) were cyclically loaded in torsion. Equation (11) was then modified as follows:

$$D(t) \cong \sum_{i=1}^{N} [\pi I_D \gamma_0^2 (|G^*| \sin \delta_{i-1} - |G^*| \sin \delta_i)]^{\frac{\alpha}{1+\alpha}} (t_i - t_{i-1})^{\frac{1}{1+\alpha}} \quad (13)$$

Fatigue tests were performed at different applied strain amplitudes on a number of differing binder types, with the data analyzed using Equation (13). The value of $|G^*| \sin\delta_i$ for each test was plotted against the corresponding value of $D(t_i)$, and the following mathematical model was fit to the results:

$$|G^*| \sin \delta = \mathrm{C}_0 - \mathrm{C}_1 (D)^{\mathrm{C}_2} \quad (14)$$

where C_0, C_1, and C_2 are model coefficients. Substituting Equation (14) into Equation (12) and taking the derivative with respect to D yields

$$\frac{\mathrm{d}W}{\mathrm{d}D} = -\pi I_D C_1 C_2 (D)^{C_2 - 1} (\gamma_{max})^2$$

(14)

Equations (3) and (14) were then combined to create a closed-form solution to determine the number of cycles to failure given a value of the damage parameter *D* at failure:

$$N_f = \frac{f\left(D_f\right)^k}{k(\pi I_D C_1 C_2)^{\alpha}} (\gamma_{max})^{-2\alpha}$$

(15)

where $k = 1 + (1 - C_2)\alpha$;

f = loading frequency, Hz;

D_f = damage accumulation at failure.

Simplification of Equation (15) is performed by grouping the following parameters:

$$A = \frac{f\left(D_f\right)^k}{k(\pi I_D C_1 C_2)^{\alpha}}$$

(16)

$$B = 2\alpha$$

(17)

Performing this simplification yields the relationship shown in Equation (4), specifically where

$$N_f = A(\gamma_{max})^{-B} \tag{18}$$

However, the number of fatigue tests needed to develop this model is drastically reduced by employing VECD concepts in the analysis. Theoretically, one can perform a fatigue test at relatively high strain amplitude, which will fail after a relatively low number of cycles. Then, with the data from this test, the fatigue model shown in Equation (18) can be developed and used to predict the fatigue life at any other strain condition.

There has been a significant effort to further investigate traditional material characterization methods with the goal of isolating the damage characteristics of an already complex viscoelastic material. The results of this work have shown great promise in defining the fatigue performance of asphalt concrete; however, the asphalt binder itself is the weakest component of this pavement material, and is ultimately responsible for the cracking that is seen since the aggregates themselves are not deteriorating. In the following section, efforts to characterize fatigue performance on the asphalt binder level will be discussed.

2.5. Current Research & Practice for Asphalt Binder Fatigue

2.5.1. Current Performance-Based Specification for Asphalt Binder Fatigue

During the Strategic Highway Research Program (SHRP) efforts in the late 1980's and early 1990's, asphalt binder specifications transitioned from index properties to mechanical properties based on responses relevant to pavement performance; for example, the dynamic shear modulus of asphalt binder became of interest due to the tendency of aggregates to apply shear loads to the binder between them under dynamic loading from traffic. The result of this

research was a new performance-based specification system for asphalt binder, now known as AASHTO M 320 (AASHTO 2007), or Superpave (SUperior PERforming Asphalt PAVEments). Dynamic shear properties are measured using the Dynamic Shear Rheometer (DSR), as shown in Figure 2.11.

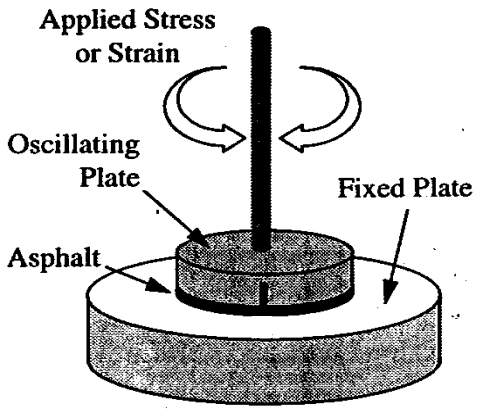

Figure 2.11. Schematic of the Dynamic Shear Rheometer.

The current fatigue specification parameter is based on minimizing the energy dissipated per loading cycle under the assumption that large values indicate the energy is dissipated by creating new surfaces in the material, i.e. cracking. The parameter $|G^*| \sin\delta$ was ultimately decided upon for specification use, as the other terms used to calculate dissipated energy are constant regardless of the material being tested, and $|G^*| \sin\delta$ is the measured response. Based on field performance data, a maximum value of 5 MPa was selected as the specification limit.

However, subsequent research has shown that $|G^*| \sin\delta$ lacks the ability to indicate resistance to fatigue damage (Bahia et al. 2001; Bahia et al. 2002; Tsai et al. 2005) . The primary concern is that $|G^*| \sin\delta$ is merely an initial measure of undamaged linear viscoelastic

properties, and it may be unsuitable to extrapolate this property to predict damage after the multiple loading cycles typically associated with fatigue damage.

2.5.2. National Cooperative Highway Research Program Project 9-10

Beginning in 1996, the National Cooperative Highway Research Program (NCHRP) sponsored research efforts to investigate the emerging practice of modifying asphalt binders and its effect on the current Superpave specifications. The research team was charged with the tasks of both identifying the shortcomings of the first iteration of Superpave, as well as suggesting improvements to better characterize modified asphalts.

The findings from NCHRP Project 9-10 (*Superpave Protocols for Modified Asphalt Binders*) identified the general lack of correlation between mixture fatigue performance and $|G^*| \sin\delta$, therefore the development of improved binder fatigue testing procedures has been pursued. During NCHRP 9-10, the time-sweep (TS) test was introduced as a binder-specific fatigue test performed in the DSR, where the specimen is subjected to repeated cyclic shear loading in either controlled-stress or controlled-strain mode (Bahia et al. 2002; Bonnetti et al. 2002). The TS allowed for the binder to go beyond linear viscoelastic behavior measured by Superpave and into the damage accumulation range. Results from this testing gave a much higher correlation with mixture fatigue performance ($R^2 = 0.84$), indicating that the TS was a promising procedure for evaluating binder fatigue characteristics. Upon the publication of *NCHRP Report 459* (Bahia et al. 2001), further research was performed to evaluate the suitability of time-sweep testing for accurate characterization of binder fatigue. It was reported in subsequent studies (Anderson et al. 2001; Shenoy 2002) that at modulus values lower than 5 MPa, the outer edges of the binder specimen subjected to TS testing could

become unstable and begin to flow. This "edge effect" can manifest itself as a drop in modulus due to changes in the sample geometry, which is indistinguishable from fatigue damage to the DSR data acquisition equipment.

In response to this issue, additional research investigated these geometry effects by comparing the TS for binders against the torsion cylinder geometry (Martono et al. 2007). The torsion cylinder geometry was established in earlier studies (Kim et al. 2002a; Kim et al. 2006) and consists of a sand-asphalt mixture that is used to represent the thin-film behavior of asphalt binder within the mix. For the study performed by Martono et al. (2007), the torsion cylinder represented geometry unaffected by edge effect, as it was significantly stiffer and more resistant to unstable flow than binder alone. By subjecting parallel plate and torsion cylinder geometries to the same loading scheme, the effect of geometry on fatigue life was evaluated. The absolute dissipated energy was significantly different between the two geometries (as they consisted of fundamentally different materials), but when the dissipated energy was normalized to the unit volume of the sample and plotted against fatigue life, both geometries showed comparable fatigue trends. Extensive statistical modeling showed that geometry had little effect on fatigue behavior with respect to binder type and the applied loading, indicating that edge effects are not a significant factor in binder fatigue results.

2.5.3. Development of the Stress Sweep

Following the work done to evaluate the time sweep as a valid binder fatigue testing procedure, researchers recognized that the time sweep is a very lengthy test, and thus began investigating a procedure to accelerate the damage accumulation in the binder specimens (Martono and Bahia 2008). The procedure, known as the stress sweep, uses repeated cyclic

loading at a constant frequency, but the controlled-stress level is increased incrementally over the duration of the test. By increasing the amount of applied energy from the DSR, the material accumulates damage much faster that the time sweep, leading to shorter times to binder failure. The binders used for the stress sweep study were used previously in an Federal Highway Administration (FHWA) Accelerated Loading Facility (ALF) fatigue study (Kutay et al. 2007). The ALF test consisted of applying multiple passes of a simulated truck wheel load on full-scale pavements constructed using different types of binder. The fatigue crack length at 100,000 passes was measured for each section, and the binders were ranked accordingly. The goal of Martono's stress sweep study was to first compare the results with those from time sweep testing, and evaluate the ability of each test to give the same ranking of the performance from the ALF test. As is common with most fatigue research, failure was defined as a 50% reduction in $|G^*|$ for both procedures, with the shear stress at failure (τ_f) being the parameter used to rank the materials' performance for stress sweep, and number of cycles to failure (N_f) used for the time sweep. The value of $|G^*|$ at failure for both test types correlated well, indicating a relationship between the two tests. The time sweep tests gave identical rankings to the ALF using N_f. This was achieved by using strain-controlled testing at relatively high strain levels of 5% and 7% (for reference, the current Superpave fatigue specification typically uses 1% strain).

The stress sweep was not completely accurate in its rankings of ALF performance using τ_f. However, it still showed some similarity in performance. While damage characteristics from the stress sweep correlated well with the time sweep, the ability of the stress sweep to indicate pavement fatigue performance needs further investigation.

2.5.4. Binder Yield Energy Test

As previously described in Section 2.1.1, the Binder Yield Energy Test (BYET) is a monotonic constant shear strain rate test that employs the DSR and the same specimen geometry as the current SuperPave standard (Johnson et al. 2009b). The test was developed in response to the efforts in the asphalt community to explore the relationship between the monotonic and cyclic damage accumulation in mixtures to indicate fatigue characteristics (Daniel and Kim 2002; Roque et al. 2004) .

The initial analysis of the BYET data showed that by taking the area under the stress-strain curve (referred to as the "Yield Energy", shown in Figure 2.12) and comparing it to the observed fatigue cracking from the FHWA ALF experiment showed an intuitive and promising correlation, as shown in Figure 2.13.

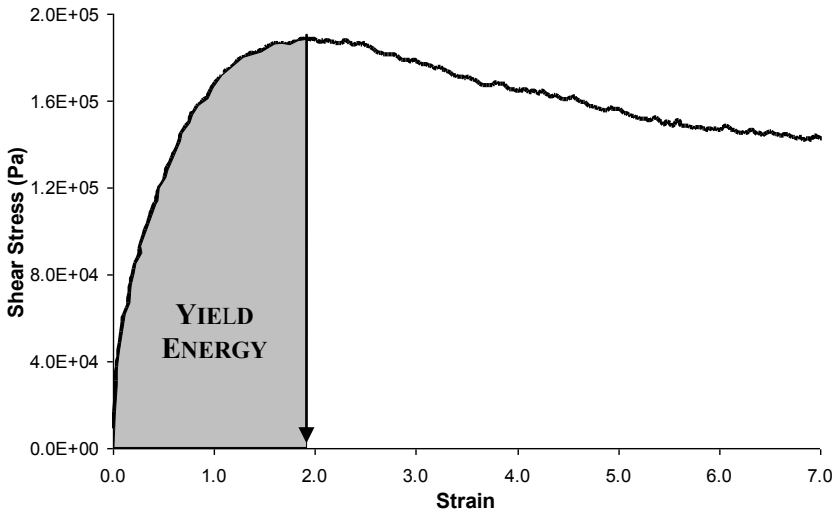

Figure 2.12. Visual representation of the Yield Energy parameter from the BYET (Johnson et al. 2009b). Note that strain is in absolute units, not percentage.

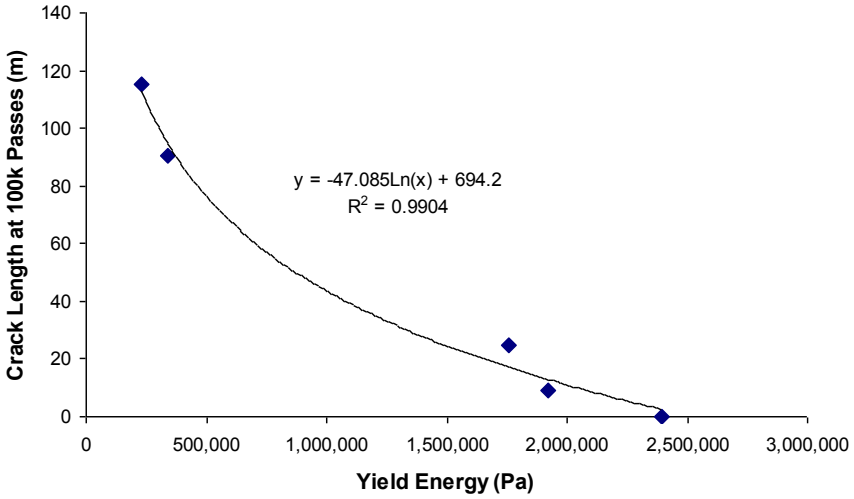

Figure 2.13. Correlation between Yield Energy and ALF pavement cracking (Johnson et al. 2009b).

However, the search for a fundamental explanation of the relationship between Yield Energy and pavement fatigue cracking via VECD analysis proved challenging. As is shown in Figure 2.4, the undamaged response of the binder is predicted from linear viscoelastic properties using the constitutive relation given by Equation (5). This is then compared to the measured response from the BYET, during which damage is assumed to have occurred. Unfortunately, not all materials showed a reduction in material integrity in comparison to the predicted undamaged response as the shear strain during the test increased. Most notable in the polymer-modified binders investigated, the linear viscoelastic properties were unable to predict the strain-hardening behavior at high shear strain levels, as shown in Figure 2.14. The likely reason for this was due to the fact that linear viscoelastic properties are determined from tests at small strain levels (less than 1% strain) in order to avoid damaging the material; at very high strains (greater than 300%), the polymer component in the binder becomes more pronounced in its contribution to the overall mechanical properties.

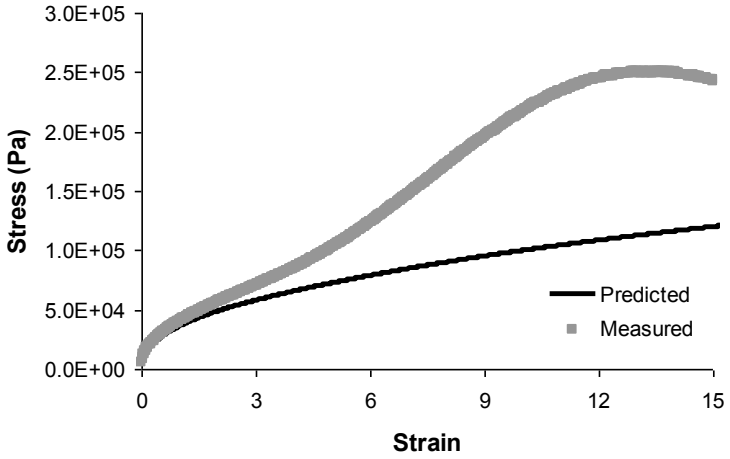

Figure 2.14. Comparison of the undamaged predicted response and measured response for a polymer-modified binder using the BYET.

Quantifying the effect of the polymer additive to the high strain response of the overall binder mechanical properties continues to be a hurdle to accurately determining the characteristics of damage growth using the BYET. Understanding the damage properties of the binder is essential for accurately predicting its failure, and has thus prevented the BYET from adoption as an accelerated fatigue performance test.

Currently, there is no method to predict the number of cycles needed to cause failure in asphalt binder from accelerated test methods. However, the foundation laid by each of the studies mentioned in this chapter will lead to an improved binder fatigue test method that is not only suitable for determining the fatigue performance, but can also do so in an efficient manner that can be employed in specification use without adding to the already extensive testing requirements put in place by current SuperPave standards.

3. RESEARCH METHODOLOGY AND EXPERIMENTAL PLAN

3.1. Research Methodology

The research methodology will consist of four main tasks, listed below, and summarized in Table 3.3.

3.1.1. Task 1: Literature Review

The literature review consisting of a background covering damage in viscoelastic materials, mechanical behavior of asphalt concrete, and asphalt pavement fatigue distress in general has been performed and is presented in Chapter 2. In order to address the modeling concepts employed in this study, a full review of viscoelastic continuum damage modeling approaches was also performed, with a current state-of-the-art segment to bring the research focus to present-day efforts.

3.1.2. Task 2: Experimental Design and Testing

The second task begins with the design of the experimental matrix. Test development consists of the investigation of a number of controlled variables with a subset of asphalt binders of widely varying material properties. Upon completion of this initial testing, the data was analyzed and modeled to determine the effect of these variables on determining the fatigue performance of the binders. From this modeling, the optimum testing and analysis protocols were determined. The following aspects have been investigated in detail:

- Efficiency of testing protocols to determine model inputs
- Significance of the selected testing temperature

- Robustness of model with respect to stress- versus strain-controlled testing mode

Validation efforts employ a comprehensive set of binders in order to create a database of binder fatigue results to further develop the models by relating accelerated binder fatigue performance to actual mixture and pavement fatigue performance.

A detailed description of the materials and test methods for test development and validation efforts are described later in this chapter.

3.1.3. Task 3: Model Refinement and Validation

By utilizing the prediction models, the third task focuses on the validation and refinement of the modeling procedure. Existing mixture and pavement fatigue performance data will be used as the basis for validation and refinement. Refinement involves the investigation of the relationship between predicted fatigue life from binder testing to the measured mixture and pavement fatigue performance for correlations that can be used to refine model coefficients and inputs, as well as develop specification limits to define acceptable performance.

3.1.4. Task 4: Development of Standard Protocol and Recommendations

The final task is the recommendation of a proposed test protocol that can indicate asphalt binder fatigue performance from accelerated testing in such a manner that is implementable as a specification-type procedure. The procedure is outlined in a style similar to current AASHTO standards as a draft. Recommendations for further development are then presented.

3.2. Experimental Methods and Variables

In order to predict the damage growth in asphalt binder, undamaged viscoelastic properties are needed to establish the proper frame of reference to assess damage accumulation, and destructive testing is needed to determine the damage model coefficients. Methods for measuring these properties are listed below. All binder testing methods employ the Dynamic Shear Rheometer, which is set up to evaluate the SuperPave standard specimen geometry of 8 mm in diameter and 2 mm in thickness.

3.2.1. Frequency Sweep Test

The frequency sweep test is a useful method for determining the undamaged viscoelastic properties of asphalt binder in the DSR. The procedure consists of applying constant low-level load amplitude to avoid damaging the specimen over a range of loading frequencies (typically from 0.1 to 30 Hz due to equipment limitations). This is performed at multiple temperatures as the mechanical properties of asphalt are especially sensitive to temperature changes. With the resulting data, one can use the principle of time-temperature superposition to construct a rheological master curve (Ferry 1980). The data for each testing temperature is shifted to align with data from one reference temperature, which allows one to determine mechanical properties across a wider range of reduced (shifted) frequencies than originally tested, as shown in Figure 3.1.

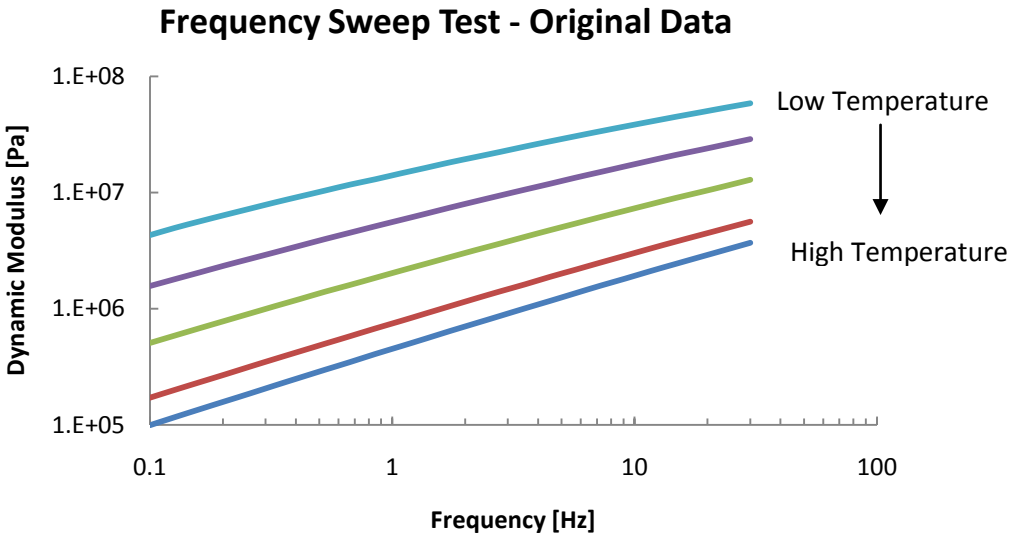

(a)

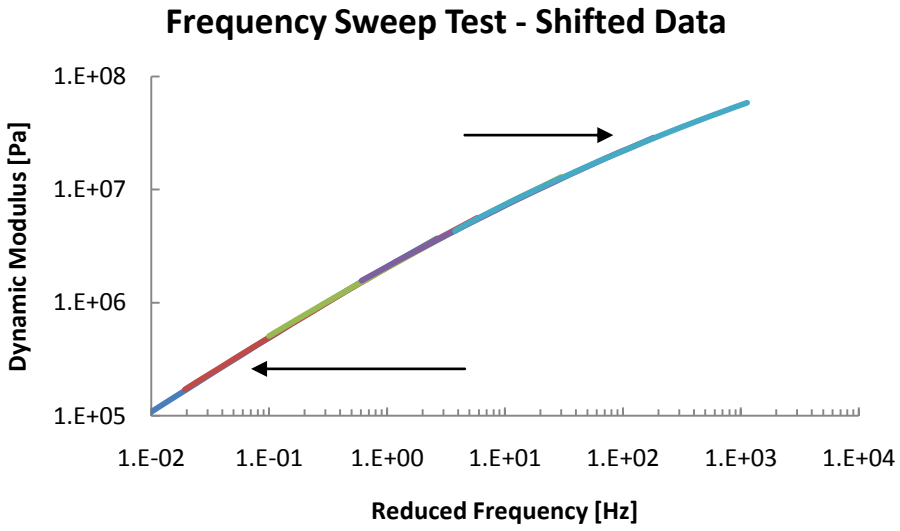

(b)

Figure 3.1. (a) Original data from frequency sweep at different temperatures, and (b) data with horizontal shift factors applied.

The shifting of frequency sweep data is achieved by performed least-squares regression to fit the data to a rheological model relating mechanical properties (typically dynamic shear modulus for asphalt binder) to frequency of loading. Model coefficients and horizontal shift factors are determined simultaneously using software such as the Solver functionality in Microsoft Excel™. During NCHRP 9-10, the following model was used to relate dynamic shear modulus to reduced frequency (Bahia et al. 2001):

$$|G^*|(f') = |G^*|_e + \frac{|G^*|_g - |G^*|_e}{[1 + (f_c/f')^k]^{m_e/k}} \tag{19}$$

where f' = reduced frequency, Hz.

$|G^*|_e = |G^*|$ as $f' \rightarrow 0$, equilibrium dynamic modulus, equal to zero for binder;

$|G^*|_g = |G^*|$ as $f' \rightarrow \infty$, glassy dynamic modulus, assumed to be equal to 1 GPa for binder;

f_c = location parameter with dimensions of frequency;

k, m_e = shape parameters, dimensionless.

The horizontal shift factors are also fit to the Williams-Landel-Ferry equation (Williams et al. 1955) in order to determine the shift factor for any given temperature:

$$\log \frac{a_T(T)}{a_T(T_0)} = -\frac{c_1(T - T_0)}{c_2 + (T - T_0)} \tag{20}$$

where a_T = temperature shift-factor;

T_0 = reference temperature;

c_1, c_2 = constants.

The relationship between phase angle (δ) and reduced frequency can then be modeled by (Bahia et al. 2001):

$$\delta(f') = 90I - (90I - \delta_m)\left\{1 + \left[\frac{\log(f_d/f')}{R_d}\right]^2\right\}^{-m_d/2} \quad (21)$$

where δ_m = phase angle at f_d, the value at inflection;

f_d = location parameter with dimensions of frequency;

R_d, m_d = shape parameters, dimensionless;

$I = 0$ if $f' > f_d$, 1 if $f' \leq f_d$.

Given the three previous models, one can reasonably determine the dynamic modulus and phase angle for any combination of frequencies and temperatures, which can be useful in comparing test data at varying frequencies and temperatures. For this study, frequency sweep tests were conducted at 7, 13, 19, 25, and 28°C to cover the range of typical intermediate temperatures associated with fatigue testing. A range of frequencies from 0.1 – 30 Hz (specific frequencies are selected by the DSR controller software) were used at an applied shear strain of 0.1% in order to avoid damaging the specimen. The master curves that were

developed could then be used to determine appropriate testing temperatures that target specific initial conditions. In order to determine the appropriate testing temperature, the concept of iso-stiffness testing is employed (Shenoy 2002; Santagata et al. 2009). However, the concept is slightly modified in order to incorporate both modulus and phase angle. Rather than selecting a temperature for each material that results in the same modulus, the temperature at which the parameter $|G^*|\cdot\sin\delta$ achieves a value of 5 MPa (the current SuperPave specification limit) is used. This is done to ensure that each binder possesses similar initial mechanical properties at the start of each fatigue test, making it easier to isolate their relative fatigue performance.

Additionally, the relaxation modulus for each binder can be approximated from frequency sweep test data. The shear relaxation modulus, $G(t)$, is used to calculate the damage exponent α used in Equation (3). Using the inter-conversions presented by Schapery and Park (Schapery and Park 1999), one can obtain reasonable estimates of relaxation modulus as follows.

First, data is converted from Hertz to angular frequency (ω), and the dynamic modulus [$|G^*(\omega)|$] and phase angle [$\delta(\omega)$] for each frequency is converted to storage modulus, $G'(\omega)$:

$$G'(\omega) = |G^*(\omega)| \times \cos\delta \tag{22}$$

The slope, n, of the log $G'(\omega)$ versus log ω plot is calculated, beginning with the second data point, at each frequency as follows:

$$n = \frac{\log G'(\omega_i) - \log G'(\omega_{i-1})}{\log \omega_i - \log \omega_{i-1}} \tag{23}$$

The value for *n* at each point can then be used to calculate the following parameter, λ':

$$\lambda' = \Gamma(1 - n) \times \cos(\pi n/2) \tag{24}$$

where Γ is the gamma function, $\Gamma(x) = (x - 1)!$.

Storage modulus for each frequency [$G'(\omega)$] can then be converted to relaxation modulus through the following approximation:

$$G(t) = \left(\frac{1}{\lambda'}\right) G'(\omega) \tag{25}$$

3.2.2. Stress Relaxation Test

For the purposes of this study, the most direct method of determining the relaxation modulus of asphalt binder is to perform a stress relaxation test in the DSR. The test consists of applying a constant shear strain, as shown in Figure 3.2, and measuring the resulting drop in torque required to maintain that strain as the stresses in the material relax. As a general rule, data collection should begin after an interval of at least ten times the amount of time required to apply the loading ramp, otherwise known as "rise time" (t_r). The relaxation modulus, $G(t)$,

is measured as the stress at a given time divided by the constant applied strain level. Typical results are shown in Figure 3.3.

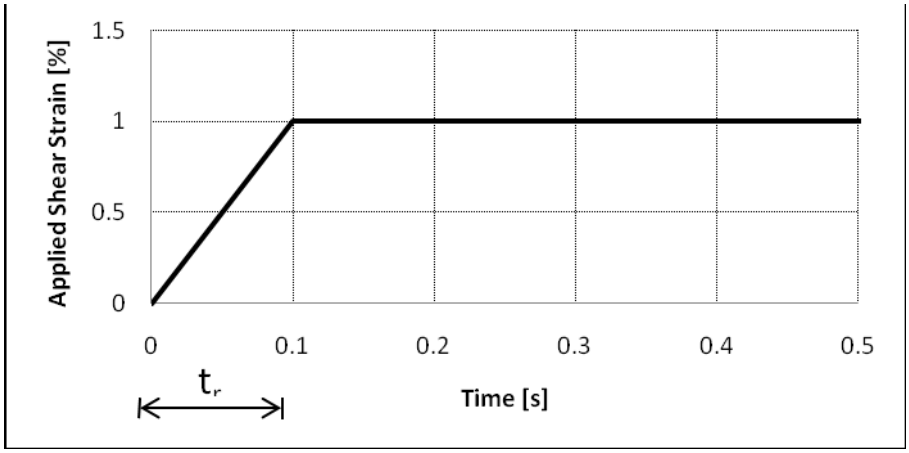

Figure 3.2. Depiction of the loading ramp for the stress relaxation test, with a rise time t_r of 0.1 seconds.

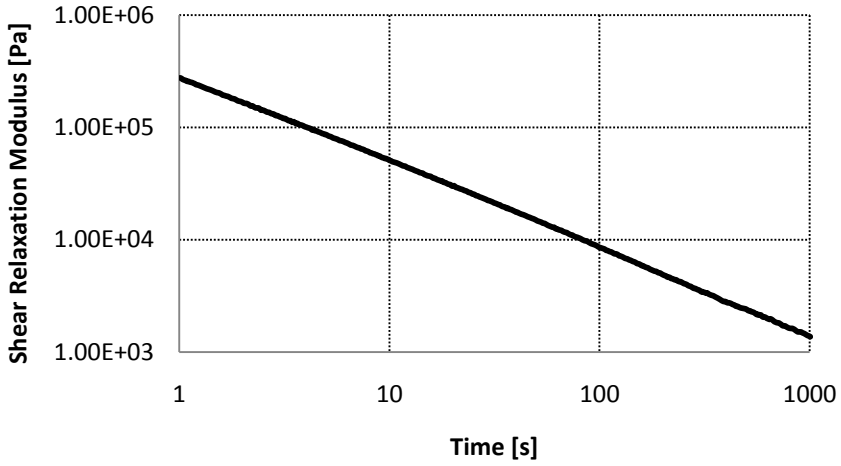

Figure 3.3. Example data from the stress relaxation test.

3.2.3. Time Sweep Test

As was previously discussed in Chapter 2, the time sweep test is simply a repeated cyclic loading test at constant amplitude to measure the fatigue life of asphalt binders. As shown in Figure 3.4, constant cyclic shear strain amplitude testing results in a decrease in the

stress response as fatigue damage progresses. For this study, loading frequency is 10 Hz. Strain-controlled testing is performed in order to ensure that there is zero mean displacement throughout the duration of the test. Two load amplitudes were employed in order to construct the relationship between load amplitude and fatigue life shown in Equation (18).

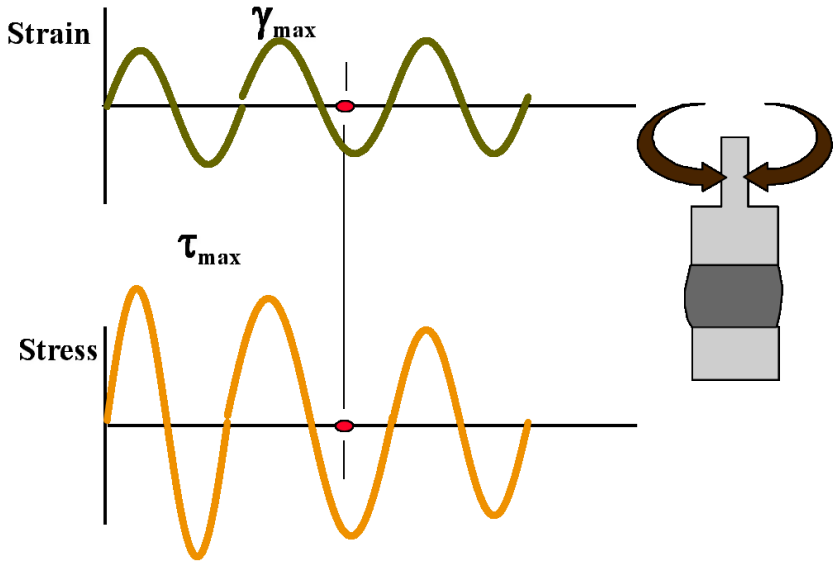

Figure 3.4. Schematic of time sweep load and response.

The damage accumulation can be modeled using Equation (13) shown above, and the resulting fatigue model coefficients *A* and *B* are calculated to characterize the fatigue properties of each binder.

3.2.4. Linear Amplitude Sweep Test

The linear amplitude sweep (LAS) test is the primary method under investigation as an accelerated fatigue procedure. The test is performed using the DSR in strain-controlled mode at the same temperature and loading frequency as the time sweep, but the load amplitude is systematically increased to accelerate damage in the specimen. An initial 100 cycles is

applied at 0.1% strain to determine undamaged linear viscoelastic properties. Each subsequent load step consists of 100 cycles at a rate of increase of 1% applied strain per step for 20 steps, beginning at 1% and ending at 20% applied strain. A graphical example of this loading scheme is shown in Figure 3.5.

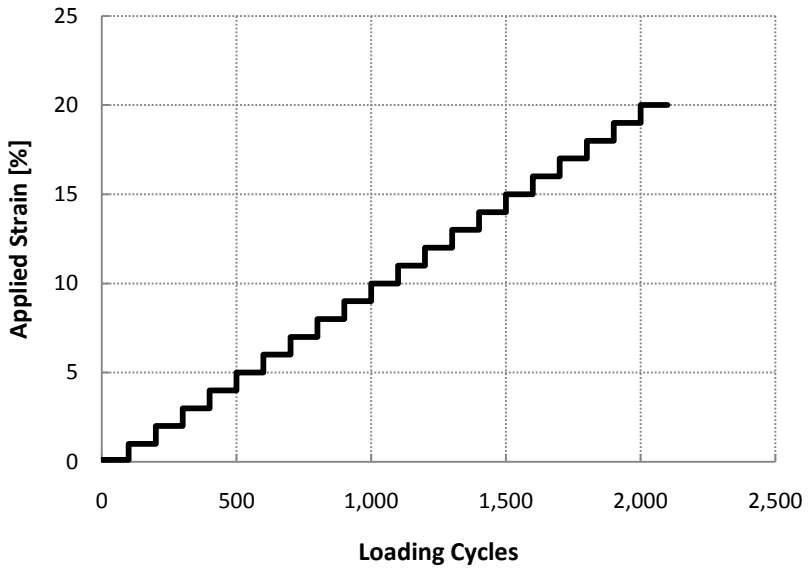

Figure 3.5. Loading scheme for the LAS test employed in this study.

For first portion of this study, a similar stress-controlled loading scheme is employed to investigate the effect of loading mode on damage accumulation modeling. An initial 100 cycles is applied at1 kPa to determine undamaged linear viscoelastic properties. Each subsequent load step consists of 100 cycles at a rate of increase of 50 kPa applied stress per step for 20 steps, beginning at 50 kPa and ending at 1,000 kPa applied stress. Validation testing employs strain-controlled testing only. This is done in order to ensure that there is zero mean displacement throughout the duration of the test.

The damage accumulation for the LAS can then be determined in the same fashion as the time sweep using Equation (13), with the fatigue damage model coefficients *A* and *B* calculated for comparison to results from more traditional fatigue testing of both binders and mixtures.

3.3. Materials

3.3.1. Asphalt Binders

The asphalt binders under investigation for this study span a broad range of mechanical properties. All materials were subjected to simulated short-term aging using the Rolling Thin Film Oven (RTFO) as specified by AASHTO T 240-09, "Effect of Heat and Air on Rolling Film of Asphalt". The short-term aging is intended to represent the oxidative state of the asphalt binder in laboratory mixtures, as mixture fatigue data is available for a number of binders and can be used to validate the ability of accelerated binder testing to indicate mixture fatigue performance.

Four binders, one unmodified and three polymer-modified, which are commonly used in pavement construction, were used for test development (see Table 3.1). Two types of modification, styrene-butadiene-styrene (SBS) rubber and ethylene terpolymer, were employed as they represent the most commonly used in practice at the present. For validation efforts, a comprehensive set of materials, spanning all types of characteristics, were used (see Table 3.2). Asphalt mixture/performance data is available for all validation binders, which is essential for validating the accelerated binder fatigue test results.

3.3.2. Asphalt Mixture/Pavement Data

In designing this experiment, special attention was paid to procure a number of binders that have associated mixture and/or pavement fatigue performance data available for validation purposes. For laboratory-tested asphalt mixtures previously evaluated by other researchers, uniaxial tension-compression data is available. This test is analogous to the fully-reversed loading applied by the DSR under strain-controlled conditions. Additionally, accelerated pavement fatigue test results are also available for a small number of binders, giving critical information on the full-scale performance of these materials under carefully controlled conditions similar to actual field performance. Finally, binders used to construct field sections that have been carefully monitored by the FHWA's Long Term Pavement Performance program are available to investigate the ability of accelerated binder fatigue to indicate in-service fatigue performance.

3.4. Experimental Design

Four binders, one unmodified and three polymer-modified, were used for test development. The testing temperature was selected as described above in Section 3.2.1 such that each material possesses similar values for initial dissipated energy. Testing was also performed at 5°C, which corresponds to spring thaw conditions in states that experience freezing temperatures. This condition is critical to fatigue performance, as the structure below the pavement is typically saturated due to snow melt, and thus its ability to support the pavement layer is greatly diminished. This weakening of the base materials can often lead to accelerated fatigue damage due to larger displacements under wheel loading, which increases

the strain in the bottom of the pavement layer. The testing matrix is given in Table 3.1 (an "X" indicates one replicate).

Table 3.1. Developmental testing matrix.

Binder	Testing Temp	Frequency Sweep	Stress Relaxation	Strain – Controlled Sweep	Stress-Controlled Sweep	5% Time Sweep	7% Time Sweep
64-28 Unmodified	SuperPave IT	XX	XX	XX	XX	XX	XX
	5°C		XX	XX			
64-28 SBS Polymer	SuperPave IT	XX	XX	XX	XX	XX	XX
	5°C		XX	XX			
58-34 Terpolymer	SuperPave IT	XX	XX	XX	XX	XX	XX
	5°C		XX	XX			
64-34 Terpolymer	SuperPave IT	XX	XX	XX	XX	XX	XX
	5°C		XX	XX			

Frequency sweep tests span a range of temperatures as described above, so additional testing at 5°C is not necessary. Stress relaxation data is essential for the calculation of damage from the accelerated binder fatigue data, therefore testing at both temperatures is needed. The strain-controlled LAS is the primary focus of this study; thus, testing was performed at two temperatures to determine the effect of temperature on fatigue performance rankings. However, the stress-controlled LAS and time sweep tests were only performed at one temperature as they are intended only to evaluate the ability of the strain-controlled LAS to indicate their performance.

Validation efforts employ a more comprehensive set of binders in order to create a database of binder fatigue results to further develop the models relating accelerated binder fatigue performance to actual mixture and pavement fatigue performance. Testing temperature were selected to match the corresponding mixture and pavement fatigue testing conditions, as this portion of the study is primarily focused on validating the damage model as opposed to

investigating temperature effects. For Long-Term Pavement Performance (LTPP) data, the binder testing temperature was selected as the SuperPave intermediate temperature for the binder used in the corresponding test section. The testing matrix is given in Table 3.2. A summary of the experimental variables is presented in Table 3.3.

Table 3.2. Validation testing matrix.

	Mix / Pavement Fatigue Data Type		Proposed Binder Testing		
Asphalt Binder	**Laboratory Mix Fatigue Data**	**Pavement Fatigue Data**	**Testing Temp [°C]**	**Alpha Measurement**	**Amplitude Sweep**
70-22 Unmodified	Uniaxial Push-Pull - 19°C	Accelerated Loading	19	X	XX
Air-blown Oxidized	Uniaxial Push-Pull - 19°C	Accelerated Loading	19	X	XX
Crumb Rubber – Terminal Blend	Uniaxial Push-Pull - 19°C	Accelerated Loading	19	X	XX
Ethylene Terpolymer	Uniaxial Push-Pull - 19°C	Accelerated Loading	19	X	XX
SBS - Linearly Grafted	Uniaxial Push-Pull - 19°C	Accelerated Loading	19	X	XX
64-28 Unmodified	Uniaxial Push-Pull - 20°C	N/A	20	X	XX
64-28 Polyphosphoric Acid	Uniaxial Push-Pull - 20°C	N/A	20	X	XX
64-34 SEM Matls.	Uniaxial Push-Pull - 20°C	N/A	20	X	XX
76-22 Citgo	Uniaxial Push-Pull - 20°C	N/A	20	X	XX
64-28 2% Latex Rubber	Uniaxial Push-Pull - 20°C	N/A	20	X	XX
LTPP 04-B901 [PG76-10]	N/A	Field Performance	SuperPave IT	X	XX
LTPP 09-0902 [PG64-28]	N/A	Field Performance	SuperPave IT	X	XX
LTPP 09-0961 [PG58-34]	N/A	Field Performance	SuperPave IT	X	XX
LTPP 34-0901 [PG64-22]	N/A	Field Performance	SuperPave IT	X	XX
LTPP 34-0961 [PG76-28]	N/A	Field Performance	SuperPave IT	X	XX
LTPP 35-0902 [PG64-22]	N/A	Field Performance	SuperPave IT	X	XX
LTPP 37-0962 [PG76-22]	N/A	Field Performance	SuperPave IT	X	XX
LTPP 89-A902 [PG52-40]	N/A	Field Performance	SuperPave IT	X	XX

Table 3.3. Experimental variables and procedures

Control Variables	**Levels**		**Response Variables**	
Asphalt binder	Test Development – 4 Validation – 18		Measured:	$\|G^*\|$ and phase angle master curves
Modification type	Test Development – 2 Validation ≥ 6			Relaxation modulus [$G(t)$]
Testing temperature	Test Development – 2 Validation – 1		Calculated:	Fatigue life [Nf]
Loading mode	Test Development – 2 Validation – 1			Damage model coefficients
Applied time sweep load level	Test Development – 2 Validation – N/A			

3.5. Considerations for Accelerated Binder Testing

3.5.1. Assumptions

The main assumption for the LAS is that damage growth is a material characteristic that is independent of the mode of loading. Following the concepts presented by the Miner-Palmgren rule (Miner 1945), the damage accumulated at different load amplitudes during a test can be summed to determine the total damage accumulation in the specimen. The current version of the MEPDG uses this concept to calculate the total amount of damage in the pavement due to varying types of truck loads, using Equation (26):

$$D = \sum_{i=1}^{T} \frac{n_i}{N_i} \tag{26}$$

where D = damage,

T = total number of periods,

n_i = actual traffic for period i, and

N_i = allowable failure repetitions under conditions prevailing in period i.

The LAS test assumes that the change in energy due to damage is independent of the amplitude of the applied load. Each step applies a systematically increasing applied load to ensure that damage occurs, but the smaller applied loads ensure that the damage growth

between data points is small enough to give good resolution for the trend of decreasing material integrity with increasing damage.

Additionally, non-linear behavior is not separated from damage during the calculations. Ways to determine the threshold between non-linearity are currently being examined as part of the Federal Highway Administration's Asphalt Research Consortium effort (2007), but for the purposes of this research, modulus reduction and changes in phase angle due to non-linearity are deemed undesirable and are included in the damage accumulation. It is common practice in engineering to design for components to perform within the linear limits of their mechanical behavior in order to avoid the uncertainty associated with non-linear behavior, and its association with being an indication of impending damage if load amplitude continues to increase.

The measured response for the DSR testing geometry is measured at the outer edge of the circumference of the test specimen. The parallel plate geometry creates an uneven shear stress distribution in the specimen when loaded; however, changing from parallel plates to a cone-and-plate geometry can remedy this by creating a uniform stress distribution, as shown in Figure 3.6.

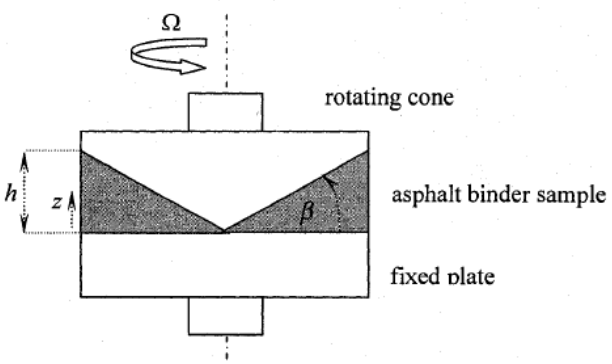

Figure 3.6. Cone-and-plate DSR geometry.

However, it has been shown that the difference between dynamic properties measured in the parallel plate and cone-and-plate geometries is not significant (Kim et al. 2001). Additionally, commercially available cones are typically only available in diameters down to 20mm. This creates a substantial increase in torque demand on the equipment to achieve the same level of shear strain as the 8mm parallel plate geometry, hence the parallel plates are often employed for practicality purposes.

3.5.2. Limitations

During cyclic sinusoidal loading, the applied strain rate is continuously changing. However, if the sine wave is idealized as a triangle wave, as shown in Figure 3.7, one can assume the linear slope is constant other than switching from positive to negative during fully reversed loading. During the LAS test, the testing frequency is held constant while the load amplitudes are systematically increasing. Using the same idealized triangle wave, the strain rate now increases with each increase in amplitude. As the binder is highly time-dependent in its mechanical properties, this increasing strain rate undoubtedly has an effect on the measured response. The frequency at each amplitude step can be altered in order to account for this, and would serve to ensure a consistent and more precise measured response.

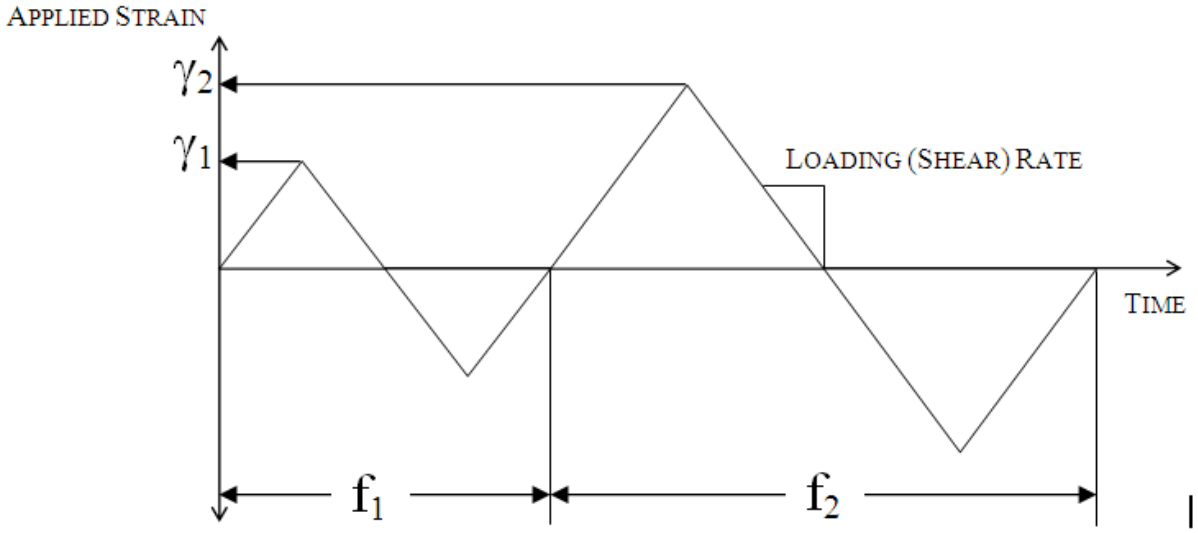

Figure 3.7. Idealized triangle wave during the LAS with varying frequencies.

However, this begs the question of relevance in practical application. Indeed, as damage theoretically accumulates in a pavement (causing greater deflections), traffic does not slow down to accommodate this. Furthermore, Wohler curves developed to describe the effect of loading amplitude on fatigue life of binders are predominately generated using the same frequency of loading for multiple amplitudes (Bonnetti et al. 2002; Delgadillo and Bahia 2005). This leads the fact that one who investigates fatigue damage must be aware of the types of loading expected, and whether strain rate or loading frequency are more important. In pavement materials testing, traffic is primarily represented by loading frequency, while the strain rate is highly varied within the binder phase of an asphalt mixture as indicated previously. Therefore, the testing frequency during the LAS test will remain constant with the understanding that the binder strains in a mixture are far too varied to target a specific strain rate.

4. TEST METHOD DEVELOPMENT

In this section, findings from the test development portion of the study are presented to determine the effect of a number of controlled variables on determining the fatigue performance of the binders.

4.1. Materials and Test Methods

Four binders (one unmodified and three polymer-modified) were selected for the preliminary investigation. It should be noted that the binder grades listed in Table 4.1 include the effect of modification (where applicable), as each binder was sampled after being produced by various commercial suppliers. As such, the exact amount of each modifier is not known. All testing was performed after RTFO-aging in order to simulate the aging in laboratory-prepared mixtures, which is intended for use in future work to compare fatigue performance of binders and mixtures.

The intermediate testing temperatures were determined from rheological master curves for both $|G^*|$ and phase angle (shown in Figure 4.1), which were measured from frequency sweep testing using 0.1% applied strain amplitude over a range of 0.1 – 30 Hz and temperatures from 7° - 28°C. The resulting intermediate testing temperatures are given in Table 4.1. Testing was also performed at 5°C to simulate spring thaw conditions.

Frequency sweep test results were also used to calculate the α parameter for VECD analysis using the conversion method outlined in Section 3.2.1. Additionally, stress relaxation tests were performed in the DSR at intermediate temperatures listed in Table 4.1 and 5°C. Shear strain was held at a constant 1% strain for 1,000 seconds while the resulting stress relaxation was measured by the DSR.

Time sweep and LAS tests were performed as described previously. The strain amplitudes for the time sweep tests were 5% and 7%, and each test was run until at least a 30% reduction in complex shear modulus was attained.

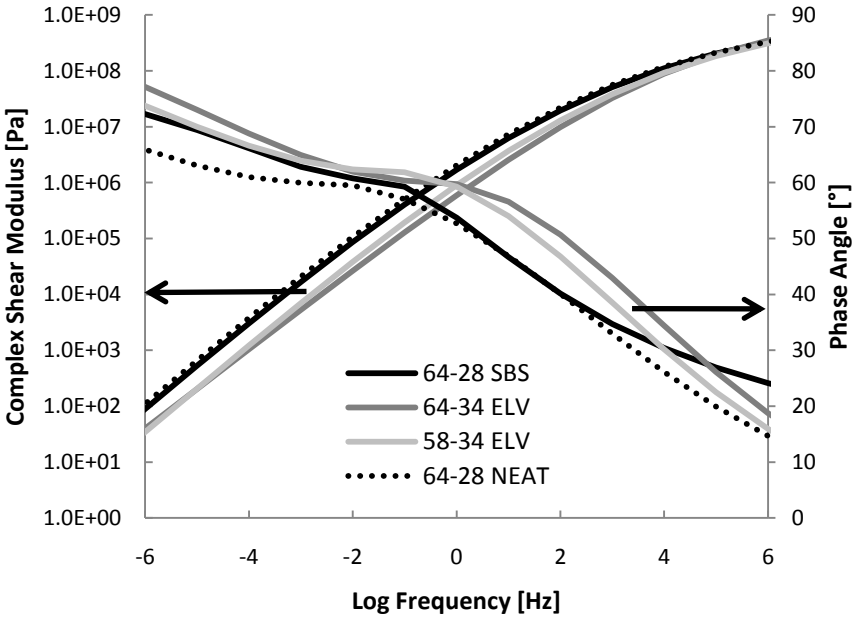

Figure 4.1. Rheological master curves for the binders used in this study.

Table 4.1. Description of binders

Binder PG Grade	Modification Type	Intermediate Testing Temperature [C°]
64 - 28	None	13.1
64 - 28	SBS	12.1
58 - 34	Elvaloy®	8.6
64 - 34	Elvaloy®	6.2

4.2. Time Sweep Results

The choice of time sweep failure criterion for the initial portion of the study was N_{P20}, which is based on the dissipated energy ratio documented in previous work in the area of

binder fatigue (Bahia et al. 2001; Bonnetti et al. 2002; Delgadillo and Bahia 2005). This primarily serves as a starting point to begin ranking the relative performance of the materials. It became apparent upon review of the time sweep results that the SBS-modified binder has substantially higher fatigue damage resistance as compared to the other binders when measured in this fashion at the 5% applied strain amplitude. For the 7% applied strain amplitude, the polymer-modified binders all appear to perform similarly, but the unmodified binder is clearly the least fatigue resistant using this failure criterion.

Table 4.2. Binder 5% time sweep test results.

Binder	N_{P20} - 5% strain (Replicate 1)	N_{P20} - 5% strain (Replicate 2)	N_{P20} - 5% strain (Average)
64 – 28 SBS	123,000	144,000	133,500
64 – 34 ELV	32,100	33,000	32,550
58 – 34 ELV	14,700	18,600	16,650
64 – 28 NEAT	24,600	25,500	25,050

Table 4.3. Binder 7% time sweep test results.

Binder	N_{P20} - 7% strain (Replicate 1)	N_{P20} - 7% strain (Replicate 2)	N_{P20} - 7% strain (Average)
64 – 28 SBS	13,500	13,800	13,650
64 – 34 ELV	17,100	11,700	14,400
58 – 34 ELV	11,400	11,400	11,400
64 – 28 NEAT	6,300	6,900	6,600

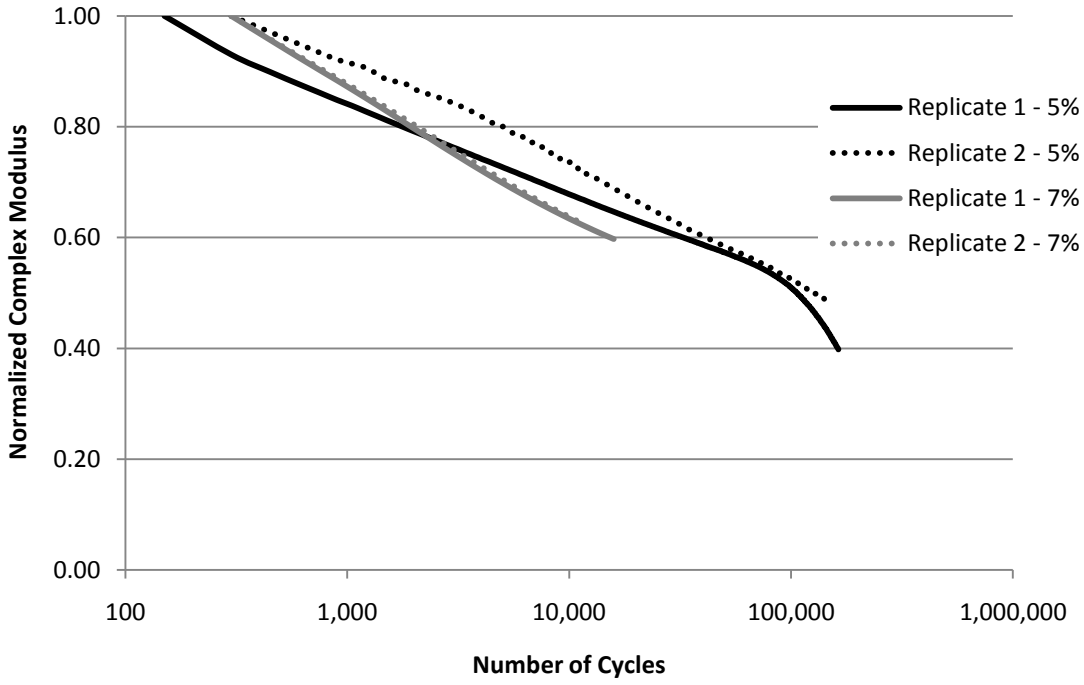

Figure 4.2. Time sweep results for the 64-28 SBS binder at 5% and 7% strain amplitude.

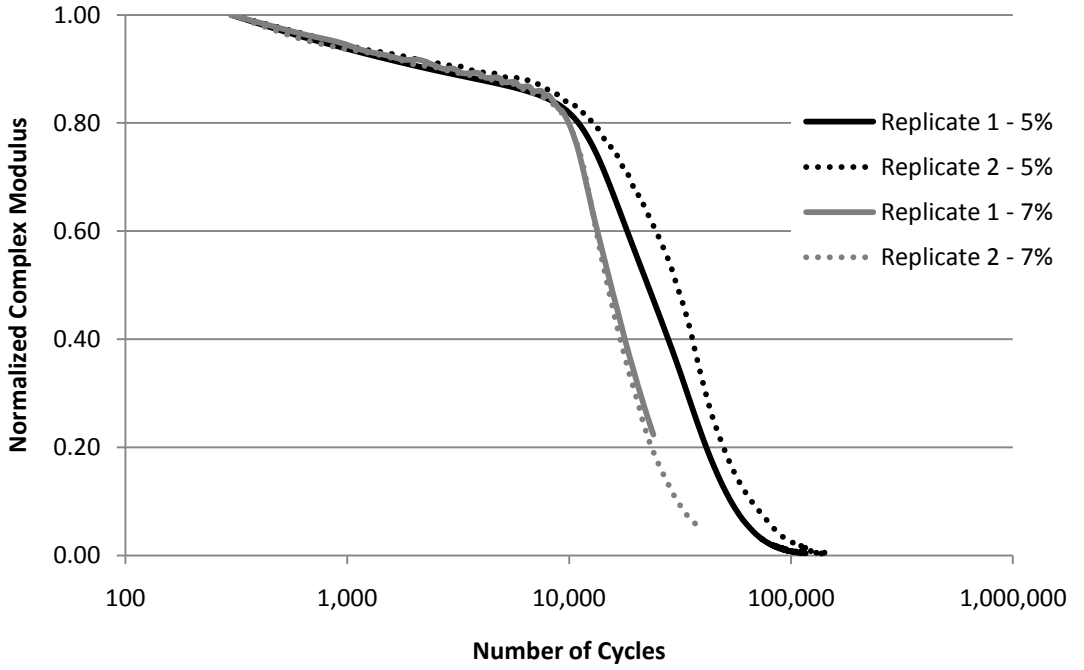

Figure 4.3. Time sweep results for the 58-34 ELV binder at 5% and 7% strain amplitude.

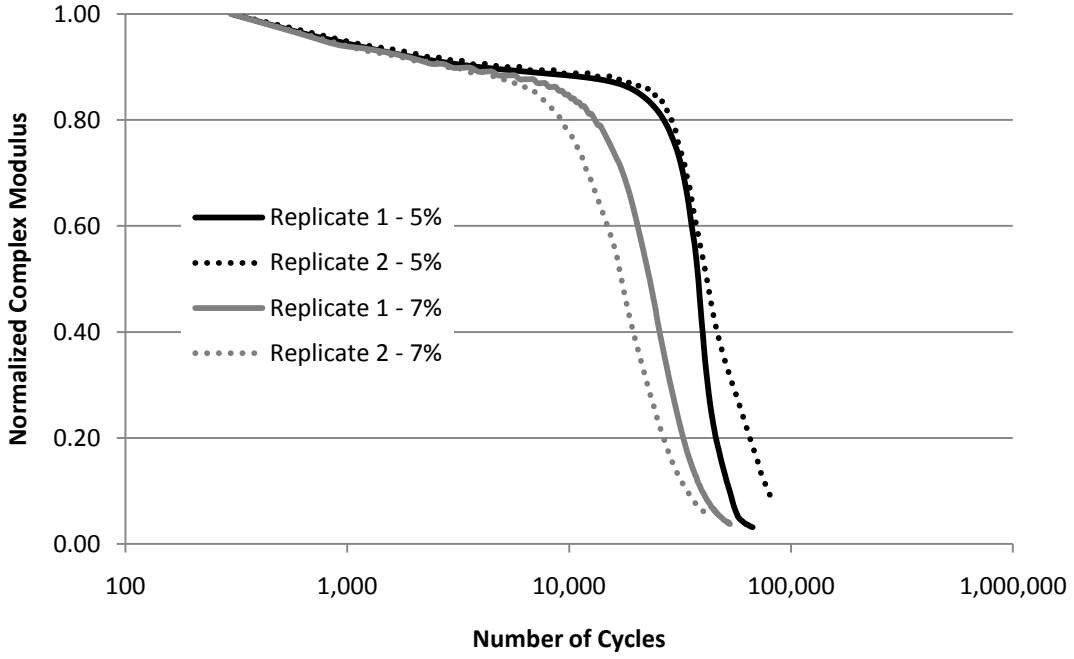

Figure 4.4. Time sweep results for the 64-34 ELV binder at 5% and 7% strain amplitude.

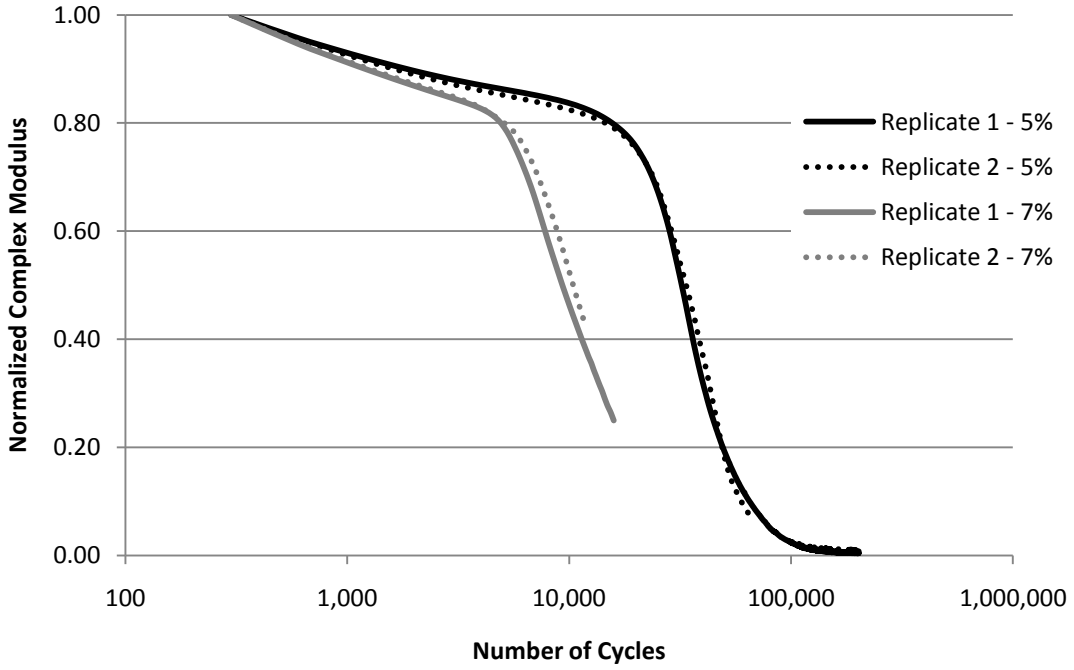

Figure 4.5. Time sweep results for the 64-28 NEAT binder at 5% and 7% strain amplitude.

4.3. Linear Amplitude Sweep Results

The results from the LAS testing give varying material responses at high strains, i.e. greater than 10%. The stress response is plotted against the applied strain in Figure 4.6 through Figure 4.9 from the DSR output.

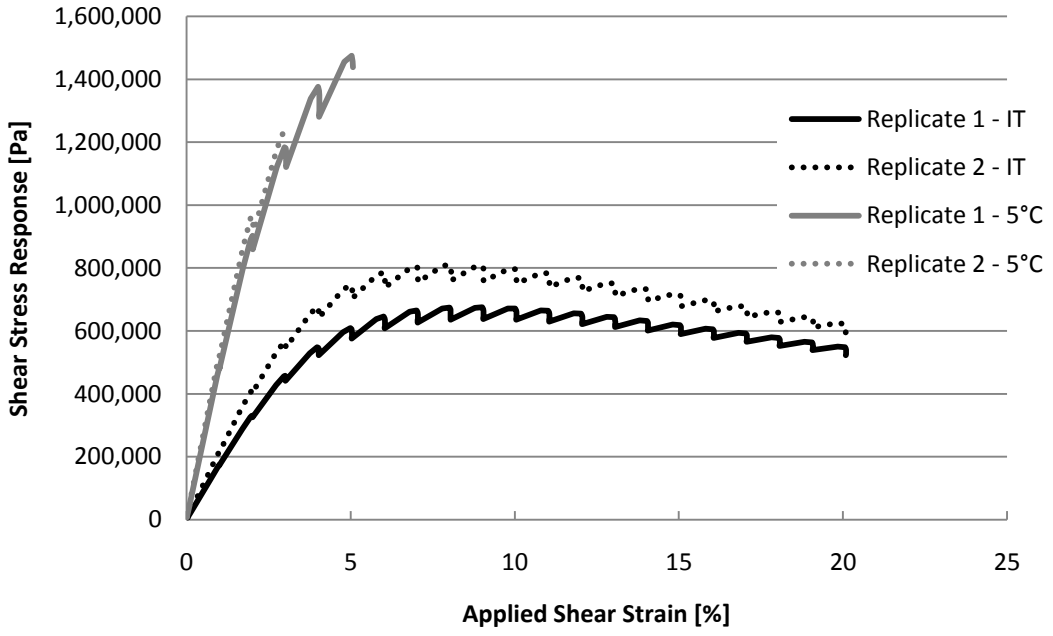

Figure 4.6. LAS results for the 64-28 SBS at intermediate temperature (IT) and 5°C.

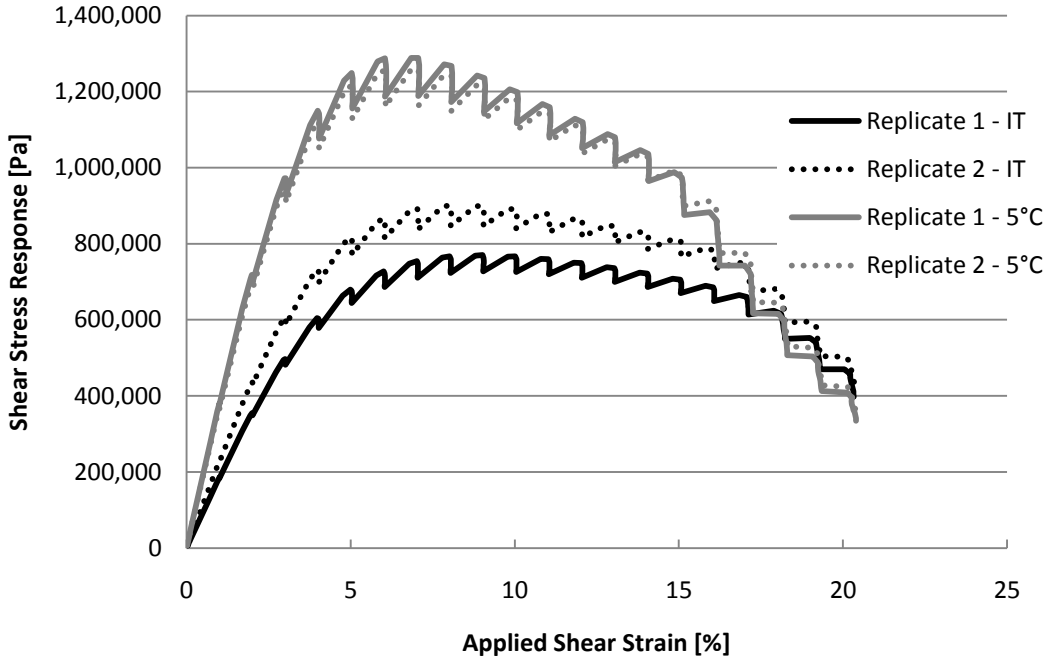

Figure 4.7. LAS results for the 58-34 ELV at intermediate temperature (IT) and 5°C.

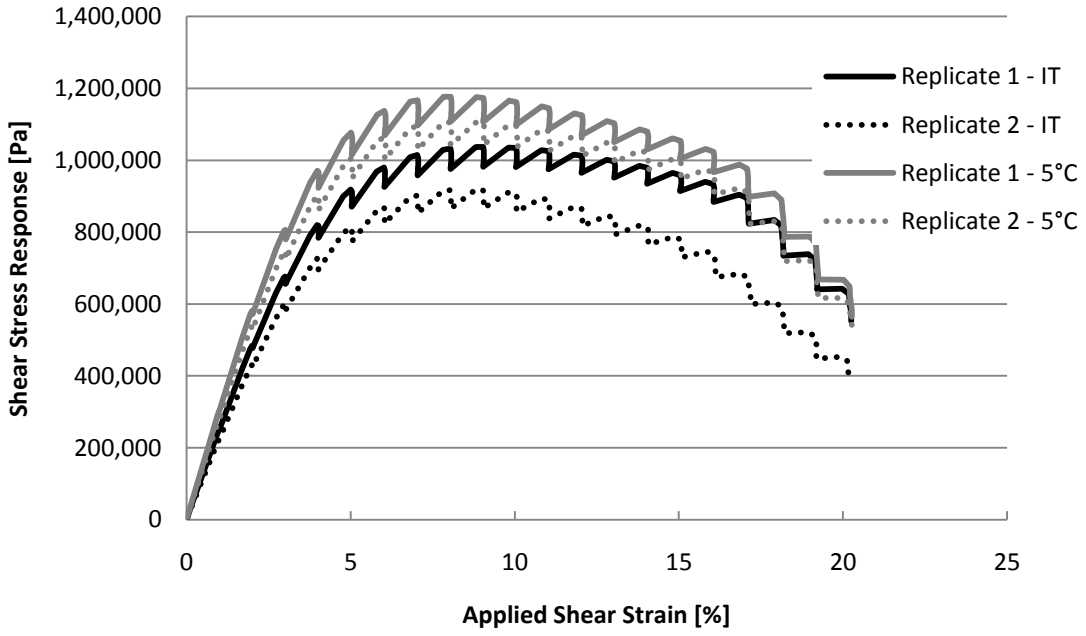

Figure 4.8. LAS results for the 64-34 ELV at intermediate temperature (IT) and 5°C.

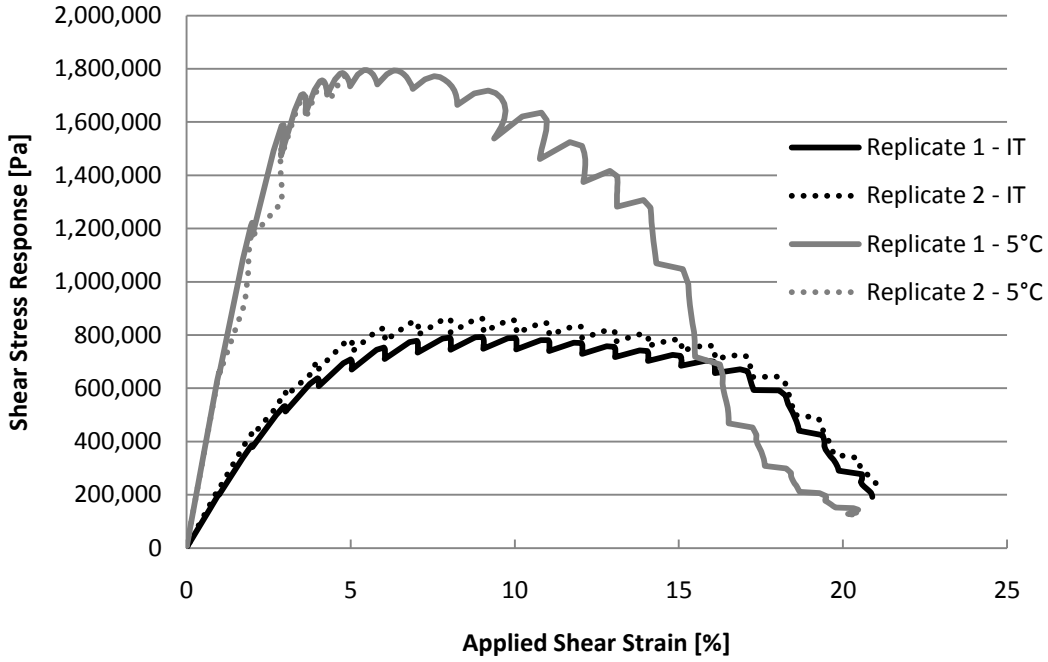

Figure 4.9. LAS results for the 64-28 NEAT at intermediate temperature (IT) and 5°C.

The assumption that damage is occurring during this test is based on the decrease in stress response for constant applied strain amplitude. If no damage were occurring, the stress response would also remain constant, as is seen at lower strain levels in the figures above. However, as depicted in detail in Figure 4.10, stress response shows a systematic degradation for a constant strain level at high amplitudes.

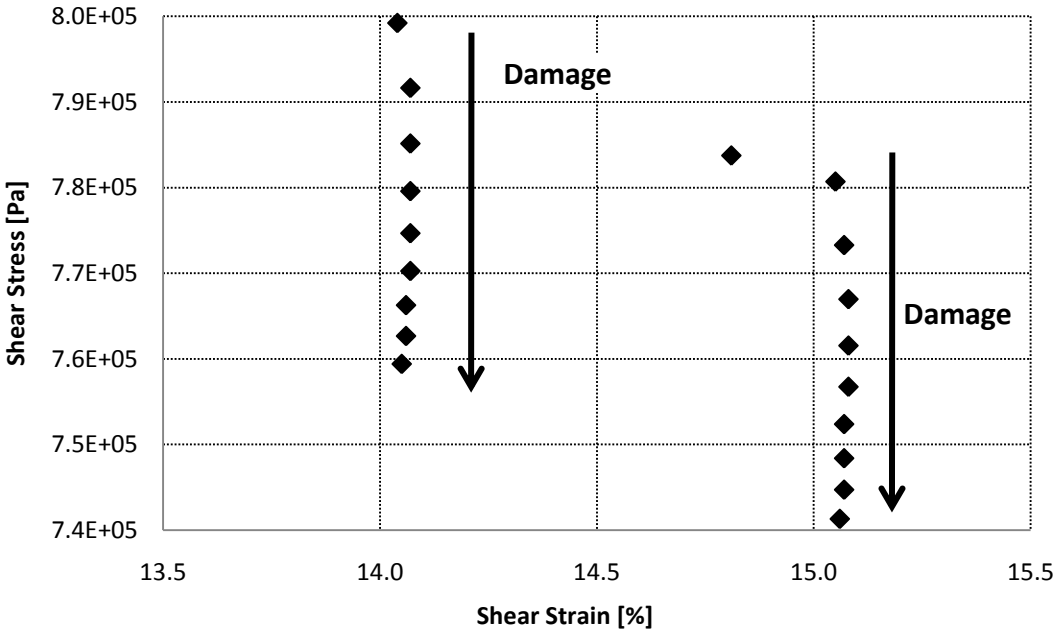

Figure 4.10. Detail of the LAS results for the PG64-28 NEAT binder depicting damage accumulation at 14% and 15% applied strain.

The two PG64-28 binders exhibited much higher stiffness values at 5°C, often resulting in slippage between the interface of the specimen and the plate/spindle in the DSR. Strain levels beyond 5% in the PG64-28 SBS were repeatedly unattainable without slippage, so only data up until 5% applied strain were used for damage analysis. The two Elvaloy®-modified binders had much lower stiffness values at 5°C, and subsequently showed a much more strain-tolerant behavior.

4.4. Stress Relaxation Test Results

It can be seen in Figure 4.11 through Figure 4.14 that the relaxation modulus predictions from frequency sweep data appear to be quite different from the relaxation modulus that was measured directly. One possible source of this is could be that the stress

relaxation test in the DSR is transient in nature, where as the frequency sweep is a cyclic test. It has been shown that differences exist between measured transient response and that which is calculated from cyclic test data (Hertzberg and Manson 1980). It was noted that polymers subjected to repeated cyclic loading (as is done during frequency sweep testing) can experience what is known as “cyclic softening”. An initial reduction in modulus is seen, followed by a steady state condition where modulus is relatively consistent with cyclic load repetition until damage propagates to the point of material failure. Whether this initial softening is damage is subject to debate, but it would explain the trend shown in the figures below where relaxation modulus as calculated from transient testing is generally higher than that which is calculated from frequency sweep test results.

With these differences in mind, the subsequent damage analysis will incorporate the results from both directly measured and predicted relaxation data. Results will be compared in an effort to determine the significance of their differences as well as their ability to accurately indicate fatigue performance.

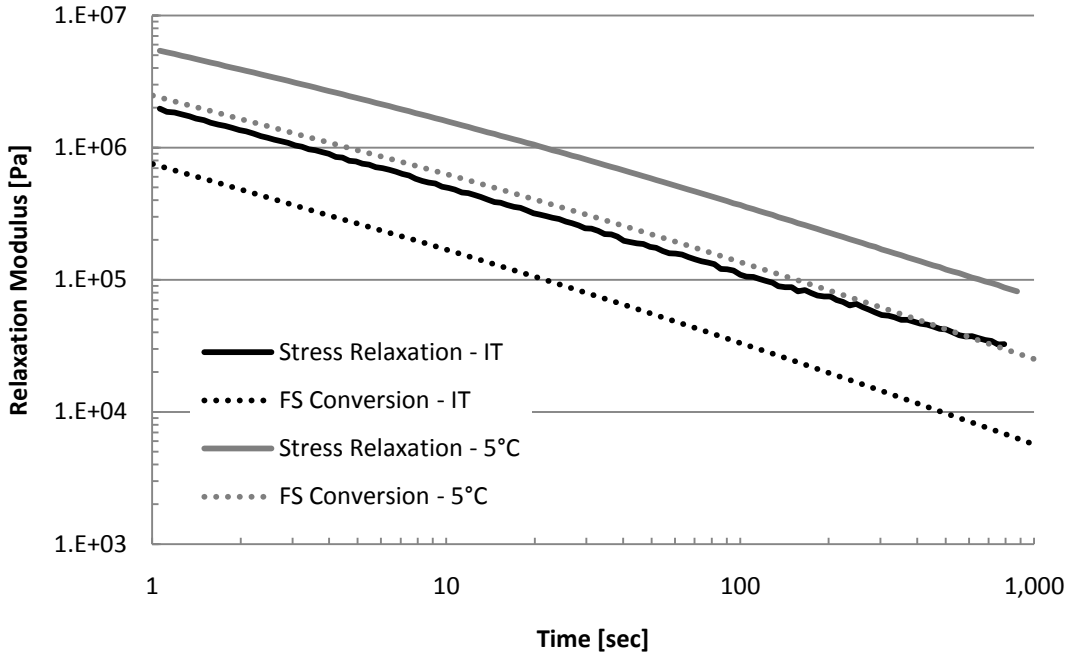

Figure 4.11. Comparison of directly measured and converted relaxation modulus for 64-28 SBS.

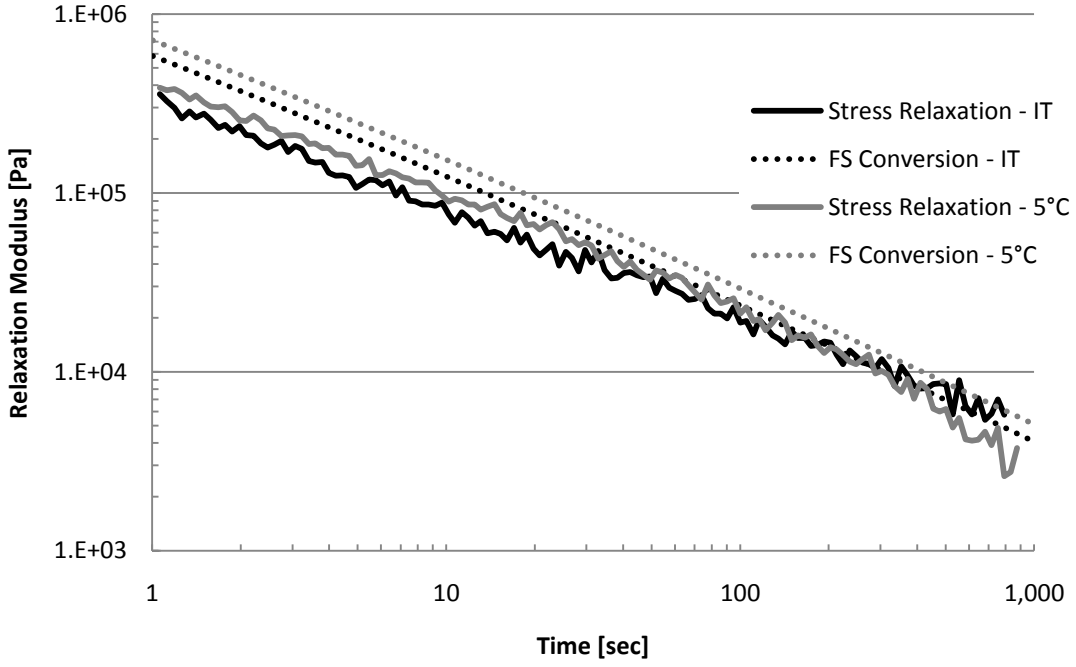

Figure 4.12. Comparison of directly measured and converted relaxation modulus for 64-34 ELV.

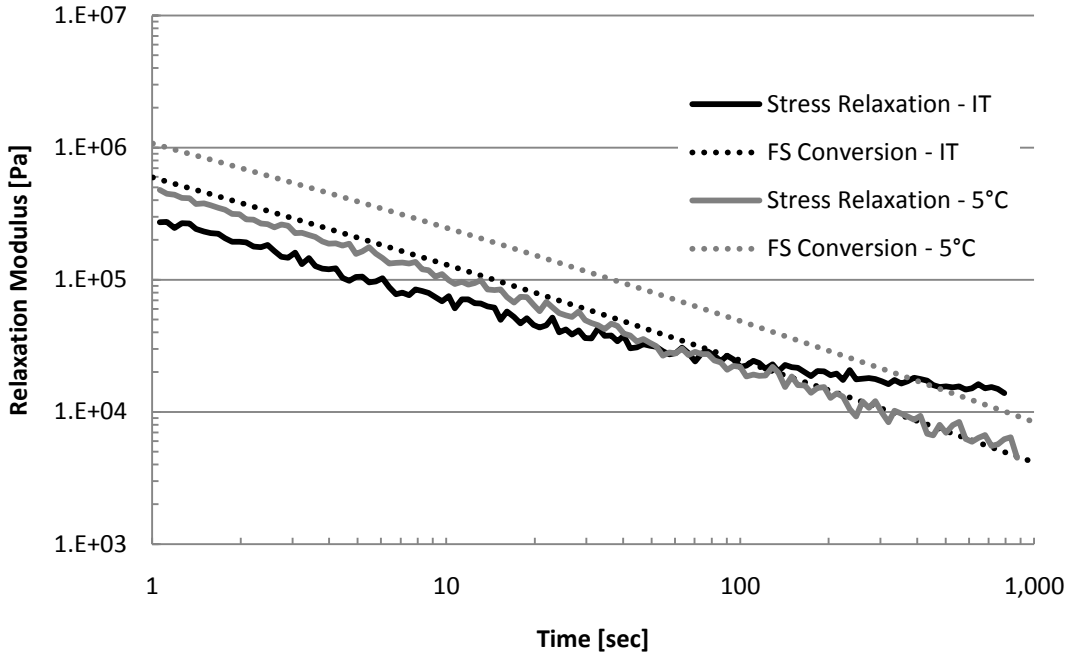

Figure 4.13. Comparison of directly measured and converted relaxation modulus for 58-34 ELV.

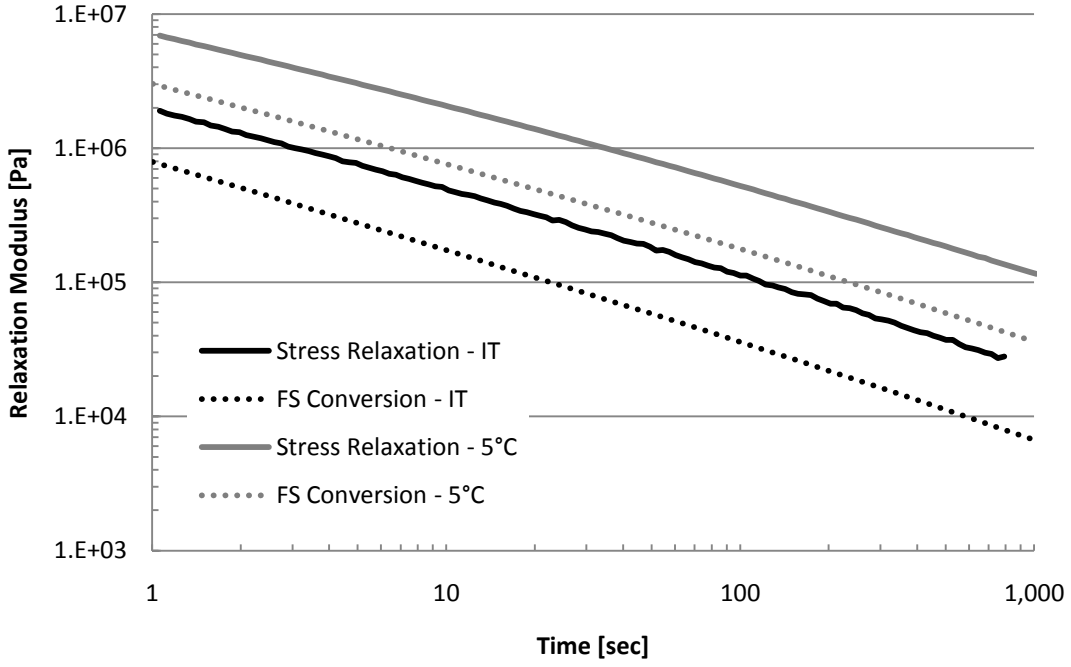

Figure 4.14. Comparison of directly measured and converted relaxation modulus for 64-28 NEAT.

4.5. Damage Analysis and Comparison of Results

One of the main objectives of this research is to develop a test method and subsequent analysis framework that can be used to efficiently evaluate the fatigue performance of asphalt binders. Currently, the time sweep procedure is the most commonly accepted test procedure for comparison to mixture and pavement fatigue performance, as its methodology is the very definition of fatigue evaluation. However, the accelerated method shown here has been compared to the time sweep in an attempt to find a more efficient procedure that can still provide adequate indication of time sweep performance.

Damage accumulation from the LAS data was calculated using Equation (13) in order to determine the VECD model coefficients for the power law given by Equation (14), which were determined using least squares regression and the Solver optimization function in Excel. The coefficients were first determined by using the stress relaxation data to calculate α, and second by using the converted value of α from frequency sweep data. Average coefficients from the two replicates are shown in Table 4.4 and Table 4.5. An example of the output of the damage accumulation calculation is plotted against normalized $|G^*|\sin\delta$ in Figure 4.15. In theory, the relationship shown in Figure 4.15 is characteristic of a material's damage resistance capabilities.

Table 4.4. Values of the LAS VECD coefficients using α from stress relaxation.

Binder	C_0	C_1	C_2	α
64-SBS	12.49	0.191	0.427	2.680
64-ELV	16.65	0.237	0.417	2.783
58-ELV	14.50	0.223	0.413	3.075
64-NEAT	14.62	0.230	0.420	2.552

Table 4.5. Values of the LAS VECD coefficients using α from frequency sweep.

Binder	C_0	C_1	C_2	α
64-SBS	12.49	0.192	0.432	2.42
64-ELV	16.65	0.238	0.425	2.39
58-ELV	14.50	0.225	0.425	2.39
64-NEAT	14.62	0.230	0.422	2.45

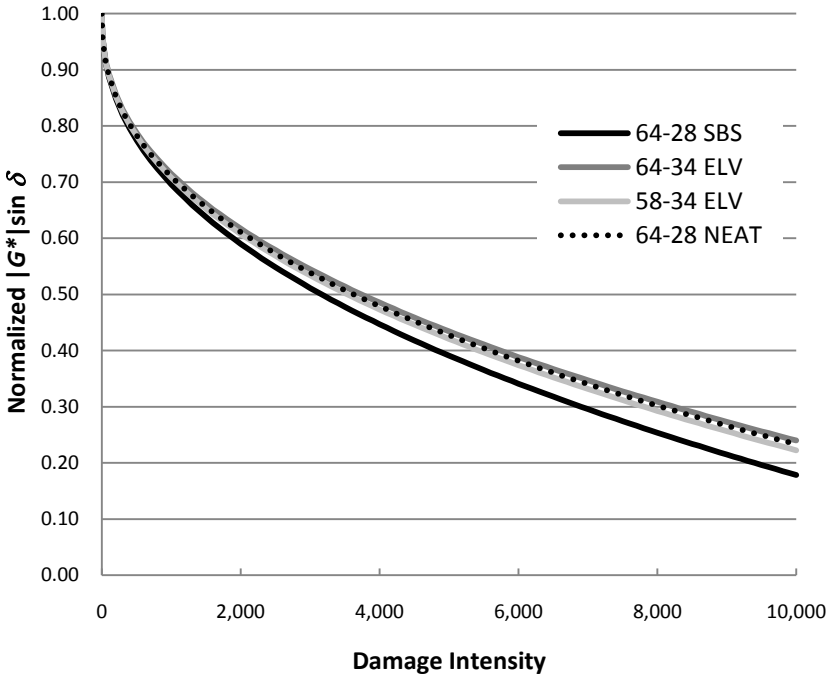

Figure 4.15. Plot of normalized $|G^*| \sin\delta$ versus damage from LAS testing at intermediate temperature (using α from frequency sweep).

For the comparison of the LAS results to those from the time sweep, it should first be noted that applying the same VECD analysis methodology as was used for the LAS to the time sweep data typically does not produce characteristic curves that overlap with their LAS counterparts. The two different test procedures appear to produce damage in differing ways, as shown in Figure 4.16 using the LAS and 5% time sweep test data. Moving forward, making the direct comparison between time sweep and LAS test results using the VECD framework

will most likely require that the effect of the substantially higher strain levels employed by the LAS procedure is accounted for, which may be inducing a non-linear behavior that is not necessarily due to damage.

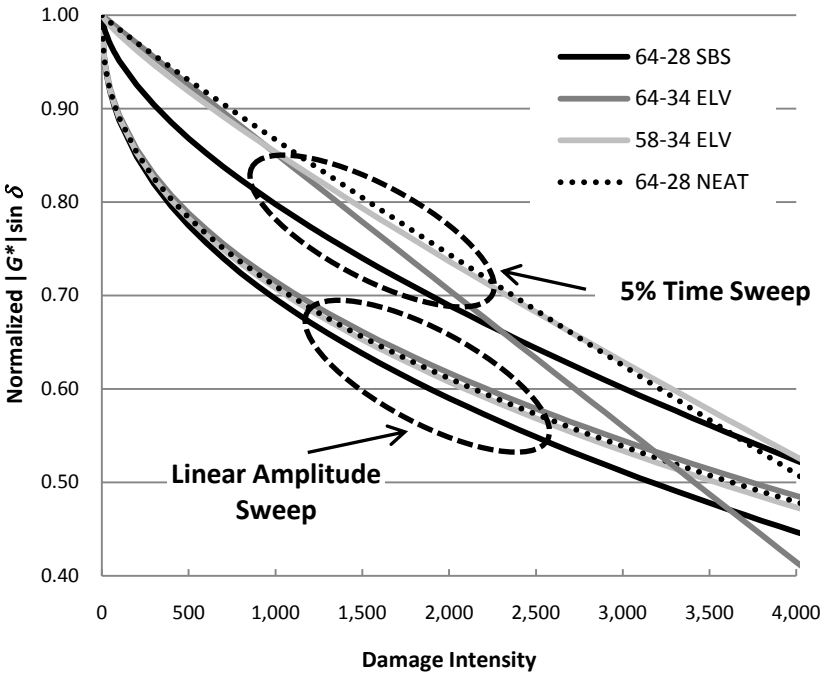

Figure 4.16. Comparison of VECD analysis from LAS & time sweep data.

In an effort to investigate any possible relationship between LAS and time sweep damage accumulation characteristics, damage accumulation from the time sweep data was used to determine the VECD model coefficients, first by using the stress relaxation data to calculate α, and second by using the converted value of α from frequency sweep data. Average coefficients from the two replicates are shown in Table 4.6 through Table 4.9.

Table 4.6. Values of the 5% time sweep VECD coefficients using α from stress relaxation.

Binder	C_0	C_1	C_2	α
64-SBS	9.11	2.23E-02	0.636	2.680
64-ELV	11.83	1.65E-03	0.992	2.783
58-ELV	10.95	3.62E-03	0.870	3.075
64-NEAT	10.99	2.16E-03	0.942	2.552

Table 4.7. Values of the 7% time sweep VECD coefficients using α from stress relaxation.

Binder	C_0	C_1	C_2	α
64-SBS	8.64	1.38E-02	0.678	2.680
64-ELV	11.42	1.29E-03	0.951	2.783
58-ELV	9.62	1.25E-03	0.970	3.075
64-NEAT	9.77	1.02E-03	1.007	2.552

Table 4.8. Values of the 5% time sweep VECD coefficients using α from frequency sweep.

Binder	C_0	C_1	C_2	α
64-SBS	9.11	2.58E-02	0.618	2.42
64-ELV	11.83	1.85E-03	0.992	2.39
58-ELV	10.95	4.72E-03	0.844	2.39
64-NEAT	10.99	2.22E-03	0.940	2.45

Table 4.9. Values of the 7% time sweep VECD coefficients using α from frequency sweep.

Binder	C_0	C_1	C_2	α
64-SBS	8.64	1.31E-02	0.681	2.42
64-ELV	11.42	1.45E-03	0.944	2.39
58-ELV	9.62	1.49E-03	0.962	2.39
64-NEAT	9.77	1.03E-03	1.008	2.45

Then, Equation (18) was used to predict the fatigue life at two applied strain levels, 3% and 5%, based on the VECD coefficients from strain sweep and time sweep analyses in order to compare the fatigue life of these materials as predicted from separate test methods.

The selection of the level of damage accumulation to use in the fatigue life prediction model must be done in a consistent manner for each material. One can select a single value for all materials, but it was found that the level of damage at a consistent level of reduction in $|G^*|\sin\delta$ gave the best relationship. Therefore, the damage intensity corresponding to a 35%

reduction in $|G^*|\sin\delta$ for each characteristic VECD curve was used for input into the fatigue model parameter D_f. The selection of an appropriate fatigue failure criterion for asphaltic materials has been the subject of much debate. The traditional standard to which most subscribe is the 50% reduction in modulus. However, this number is little more than an arbitrary selection that is widely agreed upon for ranking the relative performance of materials. A more objective criterion was developed for the development of the binder time sweep test, which was the N_{P20} parameter employed earlier. Based on the change in dissipated energy, it was decided that deviation of 20% from the initial dissipated energy provided a balance of indicating the accumulation of damage without requiring excessive testing times. The 20% value was determined as the point where deviations in dissipated energy are outside the range of experimental variability. For the LAS analysis, this same value of 20% was initially employed, but it was found that a reasonable correlation between time sweep and LAS could be found at up to a 35% reduction of $|G^*|\sin\delta$. By increasing the level of damage at which failure is established, one can be further reassured that the degradation in material properties is more likely due to damage as opposed to variability. Given this approach, a summary of model inputs and results are given in Table 4.10 through Table 4.15.

Table 4.10. LAS fatigue model parameters and predicted fatigue lives (stress relaxation α).

Binder	*A*	*B*	3% N_f	5% N_f
64-SBS	2.076E+07	5.360	57,525	3,722
64-ELV	2.187E+07	5.566	48,319	2,814
58-ELV	7.190E+07	6.150	83,638	3,614
64-NEAT	8.330E+06	5.104	30,577	2,255

Table 4.11. LAS fatigue model parameters and predicted fatigue lives (frequency sweep α).

Binder	*A*	*B*	3% N_f	5% N_f
64-SBS	6.810E+06	4.832	33,705	2,856
64-ELV	4.317E+06	4.776	22,720	1,981
58-ELV	4.271E+06	4.778	22,428	1,953
64-NEAT	5.491E+06	4.902	25,163	2,057

Table 4.12. 5% time sweep fatigue model parameters and predicted fatigue lives (stress relaxation α).

Binder	*A*	*B*	3% N_f	5% N_f
64-SBS	2.017E+08	5.360	558,902	36,160
64-ELV	1.280E+08	5.566	282,892	16,474
58-ELV	2.596E+08	6.150	302,001	13,051
64-NEAT	6.746E+07	5.104	247,639	18,260

Table 4.13. 5% time sweep fatigue model parameters and predicted fatigue lives (frequency sweep α).

Binder	*A*	*B*	3% N_f	5% N_f
64-SBS	8.624E+07	4.832	426,834	36,165
64-ELV	3.626E+07	4.776	190,826	16,637
58-ELV	2.821E+07	4.778	148,129	12,902
64-NEAT	4.873E+07	4.902	223,330	18,258

Table 4.14. 7% time sweep fatigue model parameters and predicted fatigue lives (stress relaxation α).

Binder	*A*	*B*	3% N_f	5% N_f
64-SBS	3.799E+08	5.360	1,052,687	68,107
64-ELV	4.814E+08	5.566	1,063,663	61,943
58-ELV	1.150E+09	6.150	1,337,834	57,814
64-NEAT	1.356E+08	5.104	497,775	36,704

Table 4.15. 7% time sweep fatigue model parameters and predicted fatigue lives (frequency sweep α).

Binder	*A*	*B*	3% N_f	5% N_f
64-SBS	1.694E+08	4.832	838,424	71,038
64-ELV	1.036E+08	4.776	545,055	47,522
58-ELV	7.918E+07	4.778	415,844	36,219
64-NEAT	9.141E+07	4.902	418,934	34,249

Although the values for estimated fatigue life for each material differ between the test methods used to derive them, one can see a strong correlation between the 5% time sweep and LAS with the values plotted against one another when the frequency sweep data is used to calculate the value of α, as evidenced by Figure 4.17 and Figure 4.18. Additionally, the 7% time sweep test data was used to compare the LAS's ability to indicate fatigue performance at a 7% strain level, and it also showed a favorable correlation (shown in Figure 4.19). However, the correlations are not as strong when using the α calculated from stress relaxation testing, as shown in Figure 4.20. It appears that the use of cyclic testing to determine undamaged material properties for damage analysis of cyclic destructive tests (i.e. LAS and time sweep tests) is beneficial.

While not a 1:1 relationship, the LAS appears to have the ability to indicate fatigue life as measured with the time sweep test. The LAS applies loading at an increasing rate as the amplitude increases, whereas the loading rate is constant in the time sweep test. This increase in loading rate appears to be affecting the damage accumulation rate as calculated by the VECD analysis, which gives a lower fatigue life for the LAS. However, it appears that this effect is consistent between all binders, as the time sweep test and LAS test generally rank the binders in the same fashion.

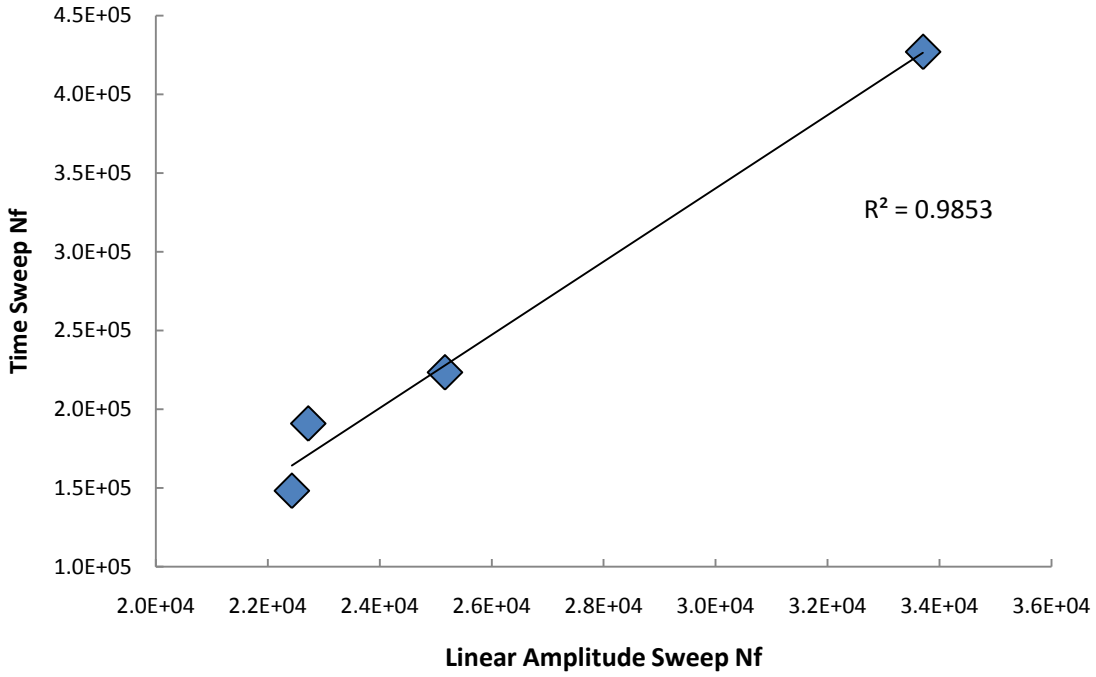

Figure 4.17. Plot of predicted Nf at 3% applied strain from the 5% time sweep and LAS VECD analyses (using frequency sweep α).

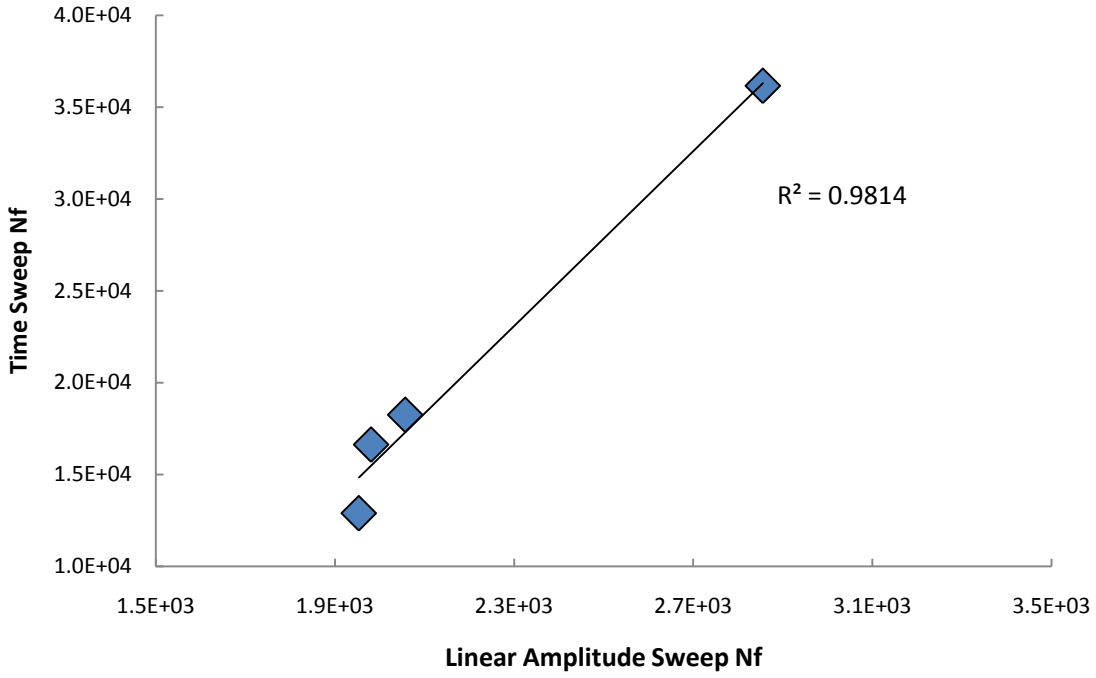

Figure 4.18. Plot of predicted Nf at 5% applied strain from 5% time sweep and LAS VECD analyses (using frequency sweep α).

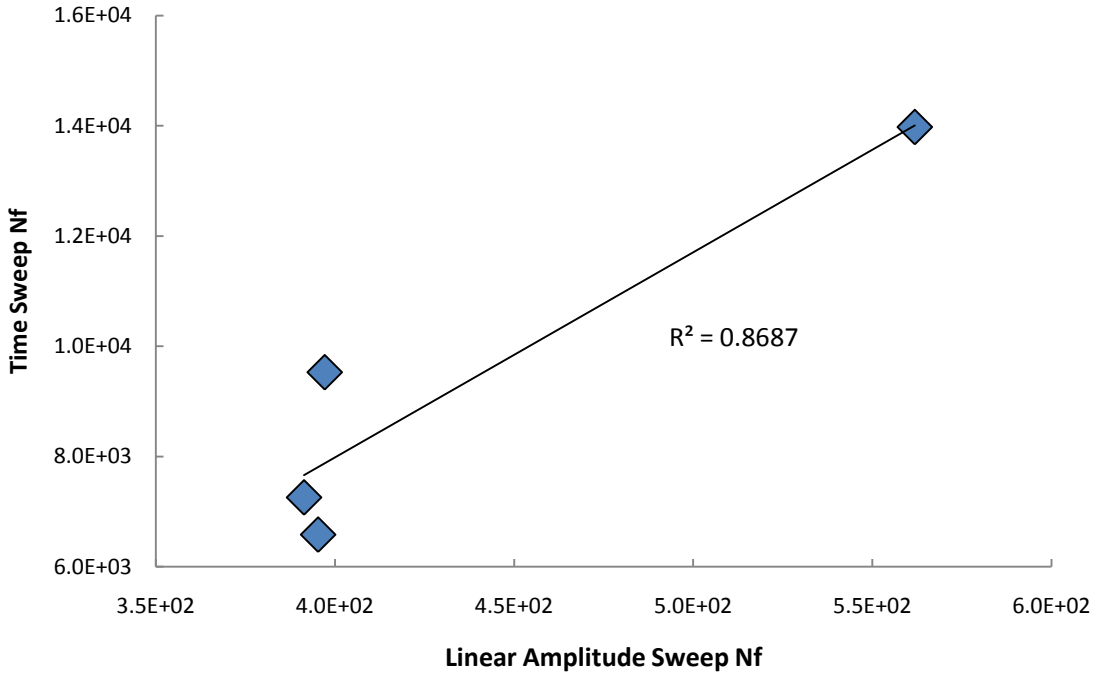

Figure 4.19. Plot of predicted Nf at 7% applied strain from 7% time sweep and LAS VECD analyses (using frequency sweep α).

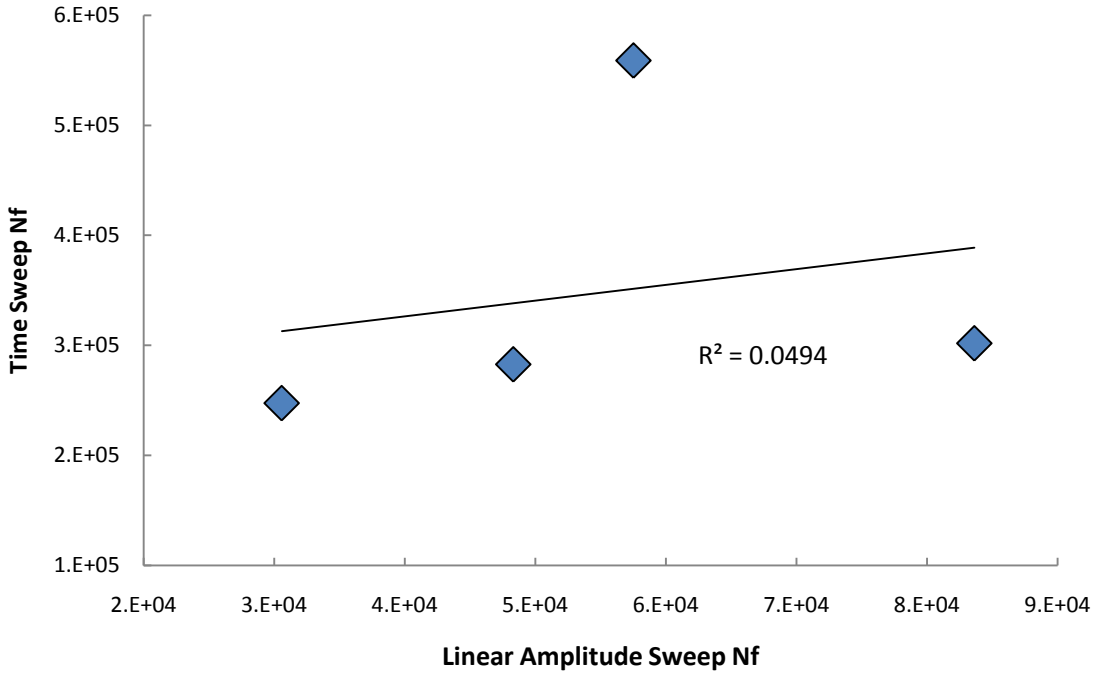

Figure 4.20. Plot of predicted Nf at 3% applied strain from the 5% time sweep and LAS VECD analyses (using stress relaxation α).

The correlation shown in Figure 4.17 is very encouraging, and thus further investigation of the relationships between the accelerated LAS analysis and the time sweep has been pursued. The time sweep binder data measured at 5% strain was characterized by VECD analysis and used to estimate the constant "*A*" in the fatigue law shown in Eq. 18. The LAS data was used to estimate the same constant using VECD analysis. The values of the "*A*" constant from the two tests were compared as shown in Figure 4.21. For notational brevity, this parameter will be referred to as A_{35} from this point forward, as it is calculated based on the failure criterion of 35% reduction in $|G^*|\sin\delta$. It should be noted that the exponent *B* from the fatigue law is based on undamaged rheological properties of the material, and is the same for both time sweep and LAS analysis. However, both A_{35} and *B* are used to calculate the fatigue life of a material, as A_{35} accounts for the damage resistance, and *B* takes the undamaged properties into account. As shown in Figure 4.22, it does not appear one can be indicated from the other, so both need to be measured in order to accurately characterize fatigue performance.

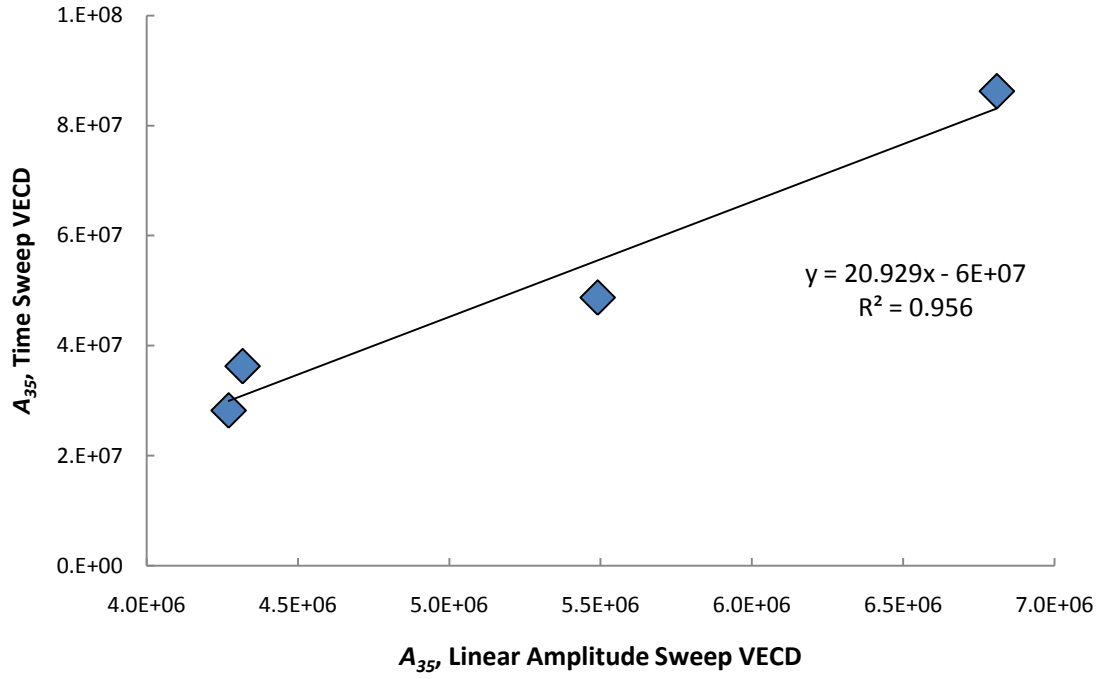

Figure 4.21. Plot of the fatigue law parameter A_{35} derived from VECD analysis of time sweep versus LAS tests.

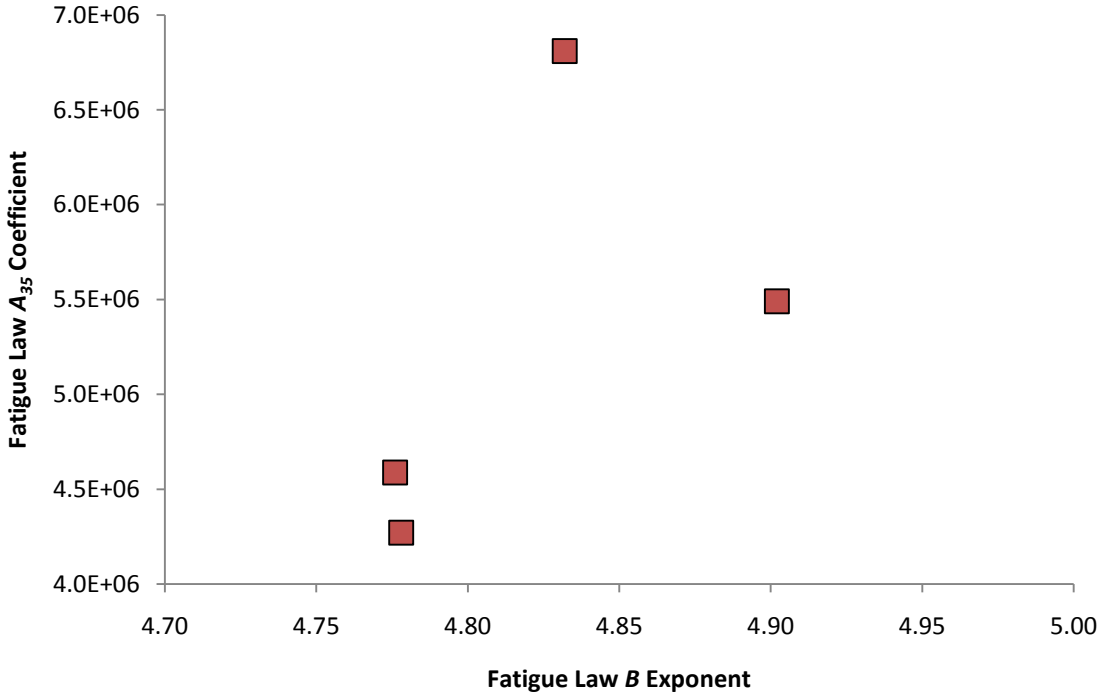

Figure 4.22. Comparison of the fatigue law parameters A_{35} and *B*.

Figure 4.21 shows that there is a good possibility that the parameter A_{35} for the fatigue law given in Equation 18 may be successfully indicated from the LAS test in the place of a time sweep test using a simple linear relationship.

4.6. A Simplified Method for Determining Alpha

With the discovery that the value of α determined from frequency sweep data gives better agreement between linear amplitude and time sweep results, a less rigorous approach for calculating α was investigated for practicality purposes. While the method of converting frequency sweep data to the time domain as described previously will give an estimate of relaxation modulus, the conversion method relies primarily on the relationship between the storage modulus component of complex modulus [denoted as $G'(\omega)$] and the loading frequency. Thus, rather than following the conversion method to completion, the *m*-value from Equation (7) was taken as the absolute value of the slope of the log $G'(\omega)$ vs. log ω curve. The value of α was then determined using the same relationship used previously, where $\alpha = 1 + 1/m$. The VECD analysis was then performed using the revised α value to determine a revised value of A_{35} (shown in Table 4.16), and an analysis of variance (ANOVA) was performed using a 95% confidence level to determine whether the results were statistically different. ANOVA results are given in Table 4.17.

Table 4.16. Results from using the revised method of calculating α.

Binder	Original α	Revised α	Original A_{35}	Revised A_{35}
64-SBS	2.416	2.430	6.810E+06	7.227E+06
64-ELV	2.388	2.401	4.317E+06	4.536E+06
58-ELV	2.389	2.403	4.271E+06	4.529E+06
64-NEAT	2.451	2.460	5.491E+06	5.709E+06

Table 4.17. ANOVA results for comparison of revised and original methods of determining α.

Source of Variation	SS	df	MS	F	P-value	F crit
Binder	1.84E+13	3	6.14E+12	17.23841	**0.000749**	4.066181
Alpha Method	3.1E+11	1	3.1E+11	0.87127	0.377916	5.317655
Interaction	2.68E+10	3	8.93E+09	0.025096	0.994191	4.066181
Within	2.85E+12	8	3.56E+11			
Total	2.16E+13	15				

As is shown in Table 4.17, the method of determining α is not a significant factor. Thus, rather than using the inter-conversion process for estimating relaxation modulus, one can simply calculate the slope of the log $G'(\omega)$ vs. log ω curve and arrive at the same result. This makes practical application of the LAS easier to implement due to a more simplified analysis approach.

4.7. Role of Alpha in Determining Sensitivity of Fatigue Life to Applied Strain Amplitude

The time sweep results at 5% and 7% were also used to determine the effectiveness of using the VECD α parameter to estimate the change in fatigue life due to change in applied strain amplitude. Recall that the exponent of the fatigue law given by Equation (18) ("*B*") is simply two times α. Previously, determining this exponent required experimental fatigue testing at multiple strain amplitudes; the method presented here requires only one test to determine this value. To evaluate whether the *B* exponent derived from the α value could be used effectively in the prediction of fatigue life, it was compared against the value of the exponent derived from numerically fitting the number of cycles to failure from the time sweep

data to the same fatigue law given by Equation (18). The failure criterion for N_f of the time sweep was recalculated from those shown in Table 4.2 and Table 4.3 as the number of cycles corresponding to a 35% reduction in the value of $|G^*|\sin\delta$ (labeled N_{35} in Table 4.18 below), consistent with what was used for the VECD analysis previously shown. As can be seen in Figure 4.23, a moderate linear correlation of 73% exists.

Table 4.18. Analysis of time sweep results for comparison VECD-modeled *B* parameter.

Binder	Avg. N_{35} 5% strain	Avg. N_{35} 7% strain	Fatigue Model *B* Parameter
64 – 28 SBS	49,725	15,300	3.420
64 – 34 ELV	35,700	16,800	2.278
58 – 34 ELV	19,950	12,900	1.271
64 – 28 NEAT	27,750	7,950	3.720

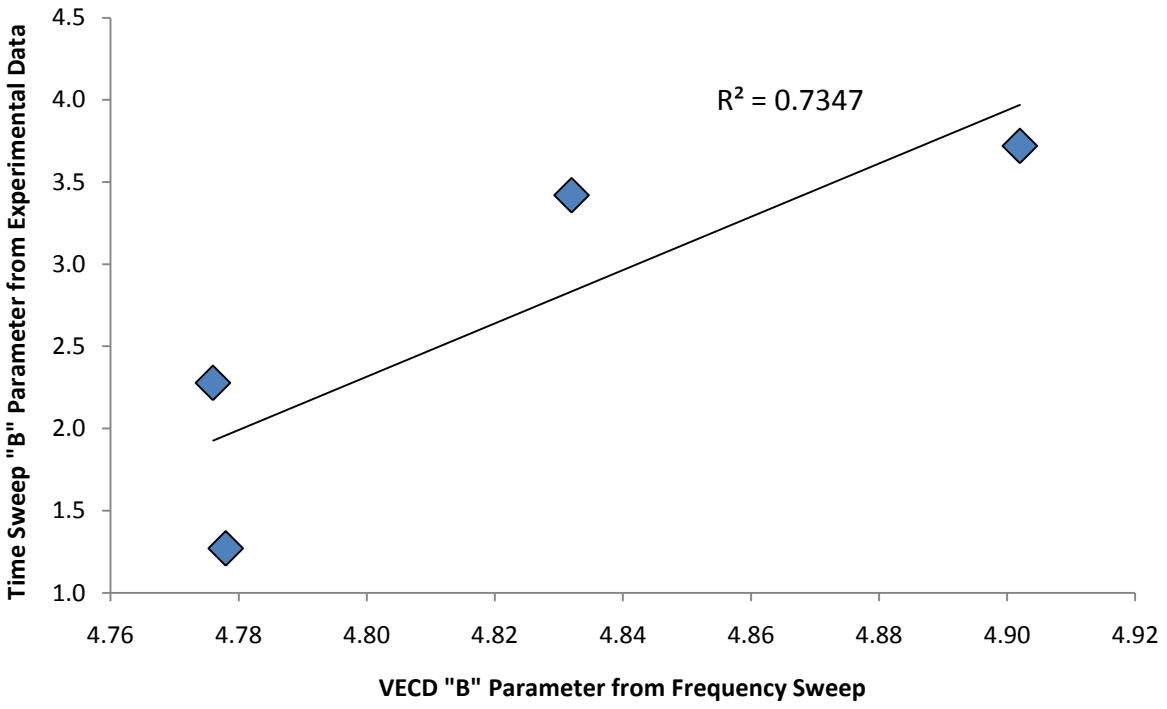

Figure 4.23. Fatigue law exponent "*B*" determined from experimental data versus that which is derived from frequency sweep test results.

The relationship in Figure 4.23 is not 1:1, but suggests that undamaged viscoelastic characteristics may play a role in the effect of load amplitude on fatigue life. Indeed, other research investigating the use of fracture mechanics approaches to predict asphalt cracking resistance has shown that the slope of the creep compliance curve (from which the VECD exponent α can be derived) can be an indicator in the cracking resistance when used in conjunction with model parameters incorporating the level of stress and strain in the pavement (Roque et al. 2004).

4.8. Effect of Testing Temperature on the Predicted Fatigue Life from Linear Amplitude Sweep

LAS testing was also performed at a testing temperature of 5°C for each of the binders. For the PG64 binders, variability was a substantial issue. Operational difficulties were experienced when testing at 5°C, where it was difficult to maintain adhesion between the asphalt specimen and the steel plates of the DSR. The analysis of results of this testing at lower temperatures gave high levels of variability, as evidenced in the coefficients of variation shown in Table 4.19. Due to time constraints, it was not feasible in this study to solve the adhesion problem encountered, or to try a different testing temperature. There is, however, no doubt that fatigue is affected by temperature, but it is unknown if the ranking of binders will change with temperature. A larger effort is required to study variation of fatigue damage of binders with change in temperature. For asphalt mixtures, it is well established in the literature that temperature has a major effect on modulus, and that fatigue resistance is a significant function of modulus.

Table 4.19. LAS fatigue model parameters and coefficients of variation (COV) for A_{35} at 5°C (frequency sweep α).

Binder	A_{35}	B	COV - A_{35}
64-SBS	1.180E+06	5.214	122.12%
64-ELV	5.169E+06	5.606	30.05%
58-ELV	2.408E+06	5.432	4.02%
64-NEAT	2.969E+06	5.350	58.25%

Unlike the testing at 5°C, analyses of results at intermediate temperatures showed no problem of adhesion and thus were much more repeatable. The following section will address the repeatability of the LAS at intermediate temperatures using the larger set of Long Term Pavement Performance (LTPP) binders, as they are representative of a wide range of locations, climates, and performance.

4.9. Repeatability of the Linear Amplitude Sweep

The LTPP binders were used to determine the repeatability of the LAS test, as the data set contains the largest number of binders that are used in a wide range of locations and climates. An analysis of variance was performed on the A_{35} values as shown in Table 4.20, which also include a description of the binders. Table 4.21 includes the results of ANOVA modeling comparing the effect of changing binder type with the effect of replication. As can be seen in Table 4.21, the effect of binder type is strongly significant (very low P-value) , while the effect of replication is insignificant (much higher P-value). This clearly indicates that the LAS test can effectively separate different binders by estimated performance in a repeatable manner.

Table 4.20. Information and results for LTPP binder evaluation using the LAS

Binder	Testing Temp [°C]	Climate Type	Cracked Area [m^2]	A_{35}	B
PG76-10 (04-B901)	37	DN	328	2.078E+06	3.804
PG76-28 (34-0961)	28	WF	178.8	4.050E+06	4.296
PG76-22 (37-0962)	31	WN	0.01*	1.056E+08	4.592
PG58-34 (09-0961)	16	WN	2.1	1.245E+07	4.679
PG64-22 (34-0901)	25	WN	49.5	5.402E+06	4.265
PG52-40 (89-A902)	10	WF	40.1	5.468E+06	4.495
PG64-22 (35-0902)	25	DN	19	7.776E+06	4.338
PG64-28 (09-0902)	22	WN	3.6	4.981E+06	4.388

*Measured distress is zero, but is listed as 0.01 for inclusion on logarithmic plot.

Table 4.21. ANOVA comparison of binder type and replication.

Source of Variation	SS	df	MS	F	P-value	F crit
Binder Type	1.75E+16	7	2.50E+15	71.025	5.72E-06	3.787
Replication	3.76E+13	1	3.76E+13	1.070	0.335	5.591
Error	2.46E+14	7	3.51E+13			
Total	1.78E+16	15				

4.10. Investigation of a Stress-Controlled Linear Amplitude Sweep

In addition to the strain-controlled method described in detail above, a stress-controlled analog to this test was also investigated, as a number of DSR's currently in use in labs today are stress-control machines by design. Testing was performed at the intermediate testing temperatures given in Table 4.1, but rather than increasing the applied strain by 1% at

each loading interval, the applied stress was increased by 50 kPa until an ultimate loading of 1,000 kPa was achieved. As can be seen in Figure 4.24, the material responds quite differently between stress- and strain-controlled modes of loading. For the stress-controlled test, damage is manifested as an increase in the strain response for a constant applied stress level. Under strain-controlled testing, the damage is given by a reduction in stress response for a constant applied strain level.

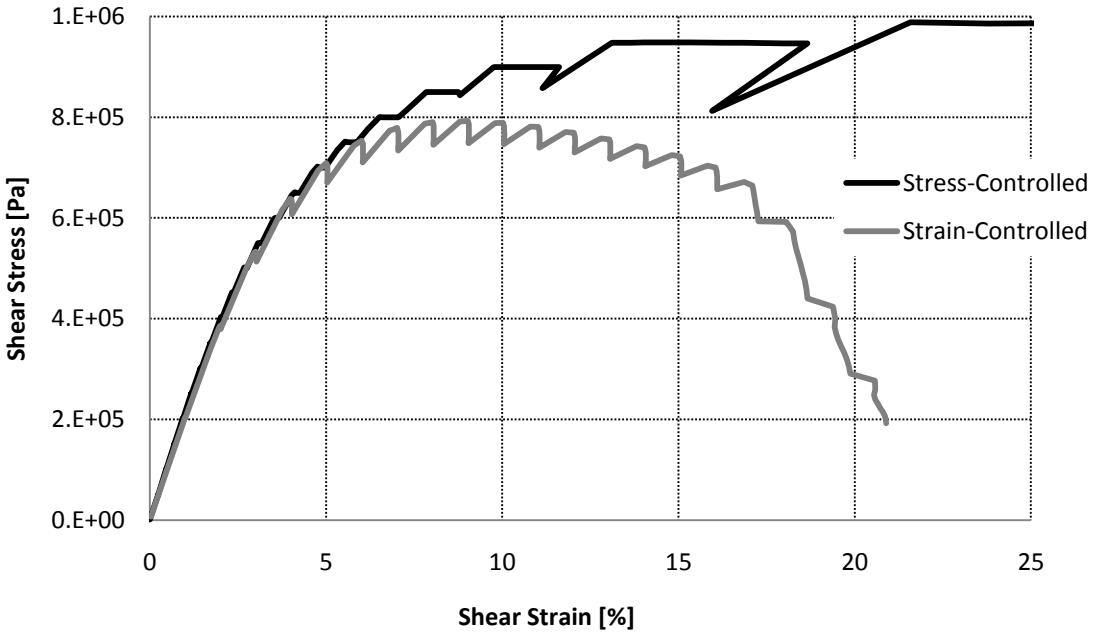

Figure 4.24. Comparison of stress- and strain-controlled LAS output from the 64-28 NEAT binder.

The results from the stress-controlled testing was analyzed in that same fashion as the strain-controlled LAS testing discussed previously. Damage coefficients are shown in Table 4.22, while fatigue law parameters and predicted fatigue lives are shown in Table 4.23. It

should be noted that the α value calculated from frequency sweep data was used for VECD analysis due to the better correlation between strain-controlled LAS and time sweep results.

Table 4.22. Values of the stress-controlled LAS VECD coefficients (frequency sweep α).

Binder	C_0	C_1	C_2	α
64-SBS	12.04	0.113	0.496	2.42
64-ELV	16.97	0.208	0.486	2.39
58-ELV	13.51	0.254	0.416	2.39
64-NEAT	13.89	0.154	0.476	2.45

Table 4.23. Stress LAS fatigue model parameters and predicted fatigue lives at intermediate temperature (frequency sweep α).

Binder	A_{35}	B	3% N_f	5% N_f
64-SBS	9.799E+06	4.832	48,498	4,109
64-ELV	3.512E+06	4.776	18,487	1,612
58-ELV	2.440E+06	4.778	12,813	1,116
64-NEAT	6.331E+06	4.902	29,014	2,372

As shown in Figure 4.25, the stress-controlled test yields the same ranking of material performance as the strain-controlled test. It appears that the differences in which the two types of tests cause damage is resulting in the value of A_{35} being systematically higher for stress-controlled conditions than strain-controlled conditions.

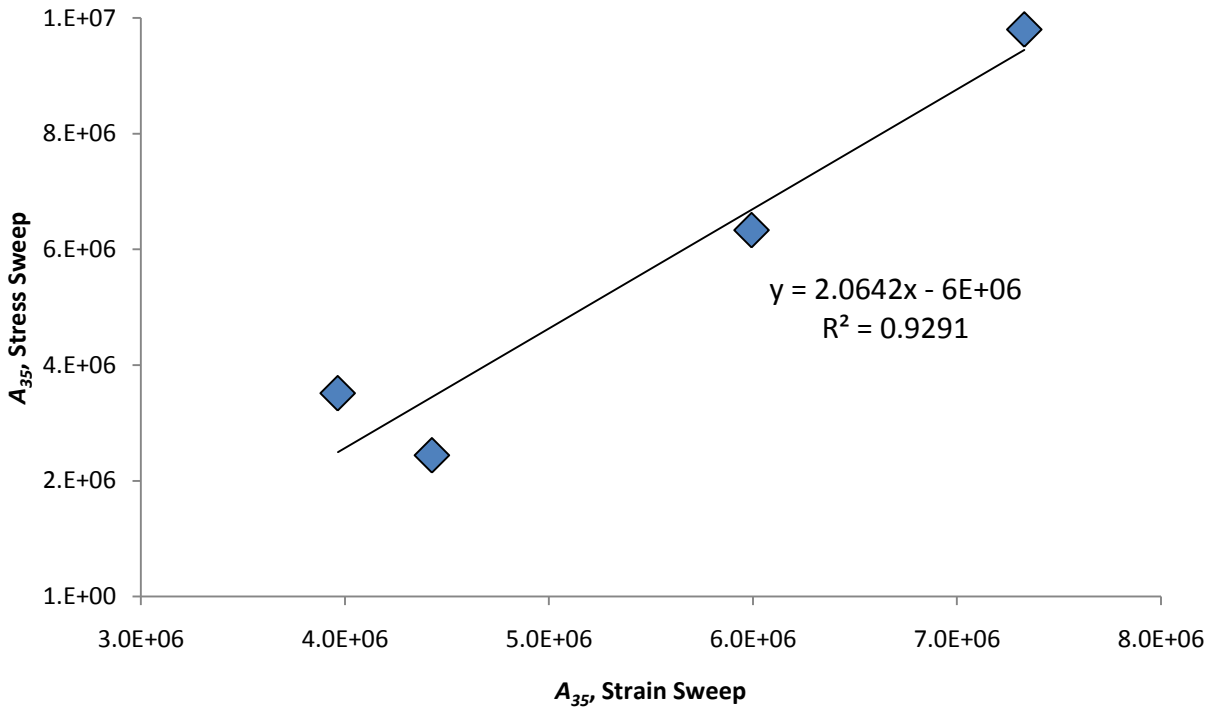

Figure 4.25. Comparison of the A_{35} parameters from stress-controlled and strain-controlled LASs.

Even though the value of predicted fatigue life would differ depending on mode of loading, the strain-controlled test offers a more conservative estimate. Additionally, stress-controlled loading gives abrupt failure, and without a priori knowledge of this failure point, the stress levels that should be targeted for the LAS test are unknown. Strain-controlled testing has been consistently shown to give a peak stress response with a gradual decrease in material integrity over a range of 1 – 20% applied strain. As far as operational issues are concerned, fully-reversed loading in the DSR while running in strain-controlled mode minimizes drift in the mean displacement of the spindle, whereas stress-controlled testing may lead to an increasing mean displacement that could create additional considerations in the mechanical response of the material for damage modeling purposes.

5. VALIDATION EFFORTS

5.1. Comparison of Linear Amplitude Sweep with Laboratory Mixture Fatigue Testing

In order to assess the validity of the LAS's ability to indicate asphalt binder fatigue resistance, a number of binders were collected that were known to have asphalt mixture fatigue data associated with them.

5.1.1. Transportation Pooled Fund Study 5(146) Mixtures

Currently, multiple state highway agencies are participating in a national "transportation pooled fund" (TPF) research project [study number TPF-5(146)] evaluating the use of modified asphalt binders in asphalt mixture overlay layers as a maintenance strategy. The study is being led by the University of Massachusetts – Dartmouth, whose responsibilities include the preparation and testing of asphalt mixture specimens in fatigue. The University of Wisconsin-Madison has assisted in the fatigue characterization of the asphalt binders.

The asphalt concrete specimens consist of a 9.5mm Superpave coarse gradation made with crushed stone from Wrentham, Massachusetts. This gradation was mixed with each of the binders under investigation, listed in Table 5.1 below. Specimens were prepared for mechanical testing in accordance with AASHTO TP 62 (AASHTO 2007) using the Superpave Gyratory Compactor to compact the mixtures, which were then sawn and cored to the final cylindrical testing dimensions of 100 mm in diameter by 150 mm tall.

Table 5.1. Materials used for TPF-5(146) binder fatigue investigation.

Binder	Source	Modification
PG64-28 Control	Aggregate Industries (AI)	None
PG64-28 + PPA	Hudson Asphalt	Poly Phosphoric Acid (PPA)
PG64-34 SBS	SemMaterials	Styrene-Butadiene-Styrene (SBS)
PG76-22 SBS	Citgo Asphalt	Styrene-Butadiene-Styrene (SBS)
PG64-28 + Latex	Base PG64-28 Aggregate Industries (AI)	2.0% Latex (BASF Butanol NX1129)

Specimens were first evaluated using a frequency sweep test procedure in order to determine the time and temperature dependency of the asphalt concrete mechanical properties using the procedure recommended by AASHTO TP 62. Master curves were developed similar to those shown in Figure 4.1 for each mixture in order to determine undamaged characteristics. This was followed by fully-reversed (push-pull) uniaxial fatigue testing on each specimen until failure at 20°C and 10 Hz.

5.1.2. Transportation Pooled Fund Study 5(019) Mixtures

Additional binders (shown in Table 5.2) were used as part of asphalt pavements tested both by using uniaxial push-pull laboratory mixture fatigue tests (as described above), as well as using the FHWA's Accelerated Loading Facility (ALF) under Transportation Pooled Fund Study TPF-5(019) (Kutay et al. 2007). Information regarding the pavement test sections will be discussed in the following section.

Table 5.2. Binder used for the comparison to accelerated pavement testing.

Binder	Description	PG Grade
PG 70-22	Unmodified straight-run (control)	70-22
CR-TB	Terminally blended crumb rubber modified	76-28
SBS LG	Linear-grafted SBS polymer-modified	70-28
Terpolymer	Ethylene terpolymer-modified	70-28

5.1.3. Discussion of Results

The LAS testing on the TPF-5(146) binders was performed at 20°C and 10 Hz, consistent with the mixture testing, and frequency sweep data was used to calculate the damage exponent α due to its ability to better indicate time sweep fatigue performance. The analysis of the TPF-5(146) laboratory mixture fatigue data is presented in an internal project report (Mogawer et al. 2009). VECD concepts were employed to analyze the mixture data as was shown previously by Kutay et. al. (2008). LAS results are given in Table 5.3; fatigue performance ranking of the mixture specimens as provided by Prof. Kutay is provided in Table 5.4, along with the rankings as determined from the LAS analysis.

Table 5.3. Linear amplitude results for laboratory mixture validation binders.

Project	Binder	A_{35}	B	3% N_f	5% N_f
TPF-5(146)	PG64-28 Ctrl	1.083E+07	4.641	135,567	12,660
	PG76-22 SBS	1.214E+07	4.827	140,666	11,951
	PG64-28 Latex	1.993E+07	4.813	280,111	23,965
	PG64-28 PPA	1.792E+07	4.749	153,270	13,552
	PG64-34 SBS	1.011E+08	4.947	22,760,860	1,818,276
TPF-5(019)	PG 70-22	8.043E+06	4.788	41,800	3,623
	CR-TB	1.071E+08	5.162	369,195	26,433
	Terpolymer	4.278E+08	5.363	1,181,039	76,276
	SBS LG	8.139E+07	4.732	449,645	40,095

Table 5.4. Comparison of fatigue performance ranking between mixture and binder testing.

Project	Binder	Mixture Ranking	A_{35} Ranking
TPF-5(146)	PG64-28 Ctrl	E	E
	PG76-22 SBS	C	D
	PG64-28 Latex	B	B
	PG64-28 PPA	D	C
	PG64-34 SBS	A	A
TPF-5(019)	PG 70-22	D	D
	CR-TB	C	B
	Terpolymer	A	A
	SBS LG	B	C

Note: "A" indicates best performance.

As can be seen in Table 5.4, the LAS can correctly identify the best and worst performing mixtures for fatigue resistance. While discrepancies do exist in between the extremes, the general trend is consistent. Considerations such as strain distribution in the binder phase of the mixture (as was discussed previously in Section 2.3.2) are difficult to account for. However, the comparison to mixture data is promising, and the most pressing issue is how the LAS results can be translated to actual pavement performance under both simulated and actual in-service traffic loading, which are presented in the following sections.

5.2. Comparison of Linear Amplitude Sweep with Accelerated Pavement Testing

5.2.1. Description of TPF-5(019) Experiment

The test sections, represented in Figure 5.1, were subjected to repeated wheel loading, with their fatigue performance being recorded as cumulative crack length (m) due to fatigue failure after 100,000 passes, and number of passes to 50-m in cumulative crack length. The test sections were produced using a single dense gradation of 12.5-mm Superpave mix design,

and were constructed in two lifts of 50-mm over a crushed aggregate base. The accelerated wheel testing was performed at a controlled temperature of 19°C with a simulated wheel load of 74 kN.

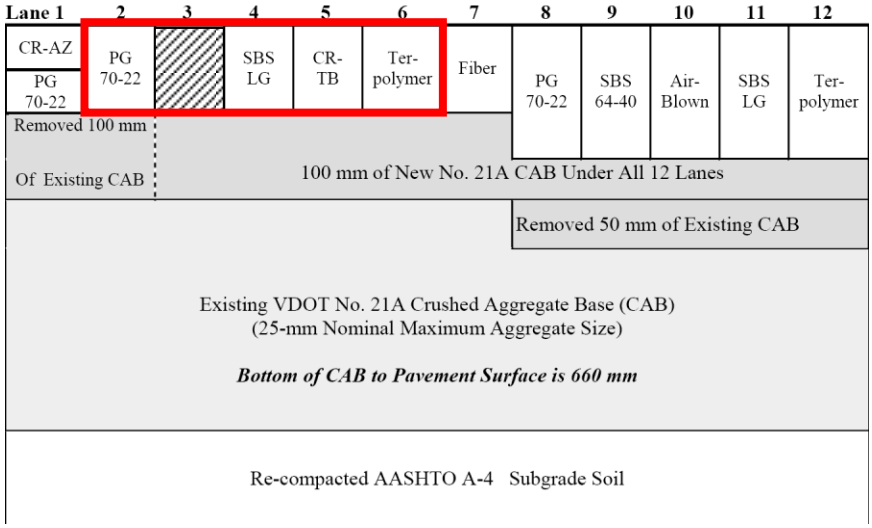

Figure 5.1. Layout of ALF pavement test sections, with Lanes 2 through 6 highlighted as those investigated for this study (Kutay et al. 2007).

For LAS binder testing, RTFO-aged material was used in order to simulate the short-term age (oxidative state) of the binders in the test sections. All tests were performed at 19°C.

5.2.2. Discussion of Results

Results of the LAS testing are given in Table 5.5, with the ethylene terpolymer showing the best performance and the unmodified control binder showing the poorest performance. In addition to the binder test results, the measured fatigue cracking after 100,000 passes for the accelerated pavement testing lanes is also listed in Table 5.5. The best performing pavement is the SBS-LG, but is ranked second-to-last based on the LAS ranking. However, when compared against each other, the remaining three binders rank consistently

between LAS and accelerated pavement results. This comparison is plotted in Figure 5.2, with the SBS-LG shown as an outlier.

Table 5.5. LAS fatigue model parameters and predicted fatigue lives.

Binder	*A*	*B*	3% N_f	5% N_f	ALF Cracking [m]
Terpolymer	3.831E+07	5.363	105,750	6,830	9
CR-TB	7.731E+06	5.162	26,639	1,907	24.9
PG 70-22	1.559E+06	4.788	8,103	702	90.6
SBS LG	3.618E+06	4.732	19,986	1,782	0

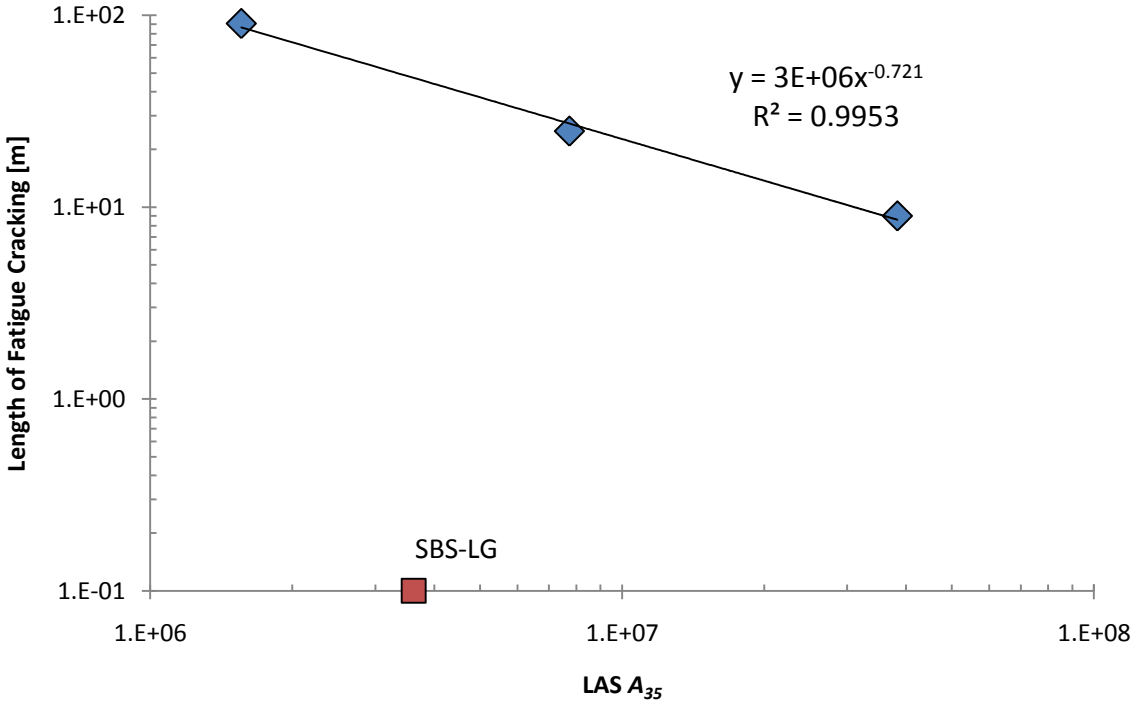

Figure 5.2. ALF pavement cracking plotted against LAS results (SBS-LG plotted as outlier).

With only three data points, it is difficult to attribute the correlation to the fatigue performance of the binders. However, the removal of the outlier gives a near-perfect correlation that would indicate that higher values of A_{35} lead to reduced cracking under

simulated traffic loading. It should be noted that the FHWA accelerated pavement tester cannot apply wheel loads at traditional highway traffic speeds of 60+ miles per hour; it employs wheel speeds of 2.5 to 11 miles per hour, and thus cannot be directly related to actual in-service traffic-related fatigue distress. It does provide a convenient method of simulation, but actual field performance data will be required to confirm these results.

5.3. Comparison of Linear Amplitude Sweep with Long-Term Pavement Performance Data

5.3.1. Description of LTPP Program

Upon the discovery of the afore mentioned relationship between LAS and time sweep test results, further steps are now being taken to validate these findings with historical pavement performance data. The United States Long Term Pavement Performance (LTPP) program monitors a select number of highways, recording the extent of the pavement distresses among many other factors. Raw materials for each of these pavements were sampled and stored during their construction, and a limited amount of asphalt binder has been made available to test new evaluation methods, such as the LAS, against measured field performance data.

5.3.2. Description of Pavement Sections

Eight binders have initially been tested, but future work will expand this number to approximately 30 binders to refine testing limits. Information regarding the seven binders, along with the measured VECD fatigue model parameters, was previously shown in Table

4.20. Testing was performed at the SuperPave intermediate temperature for each binder in an attempt to account for the local climate conditions for each highway section. Various climate types were also included, listed as Dry-No Freeze (DN), Wet-No Freeze (WN), and Wet-Freeze (WF). The measure fatigue distress is listed as the total cracked area of the pavement in square meters.

5.3.3. Discussion of Results

Preliminary investigation of the results of LTPP binders showed that the value of A_{35} as measured from the LAS correlates well with the measured fatigue cracking in the pavement sections, as shown in Figure 5.3. Binder (37-0962) was not included in fitting of the displayed trend line and calculation of the R^2 value, as the pavement section this outlier binder was used in showed no measureable fatigue distress, but it is included on the plot in order to show the general trend that the in-service fatigue distress was reduced as the binder A_{35} value increased.

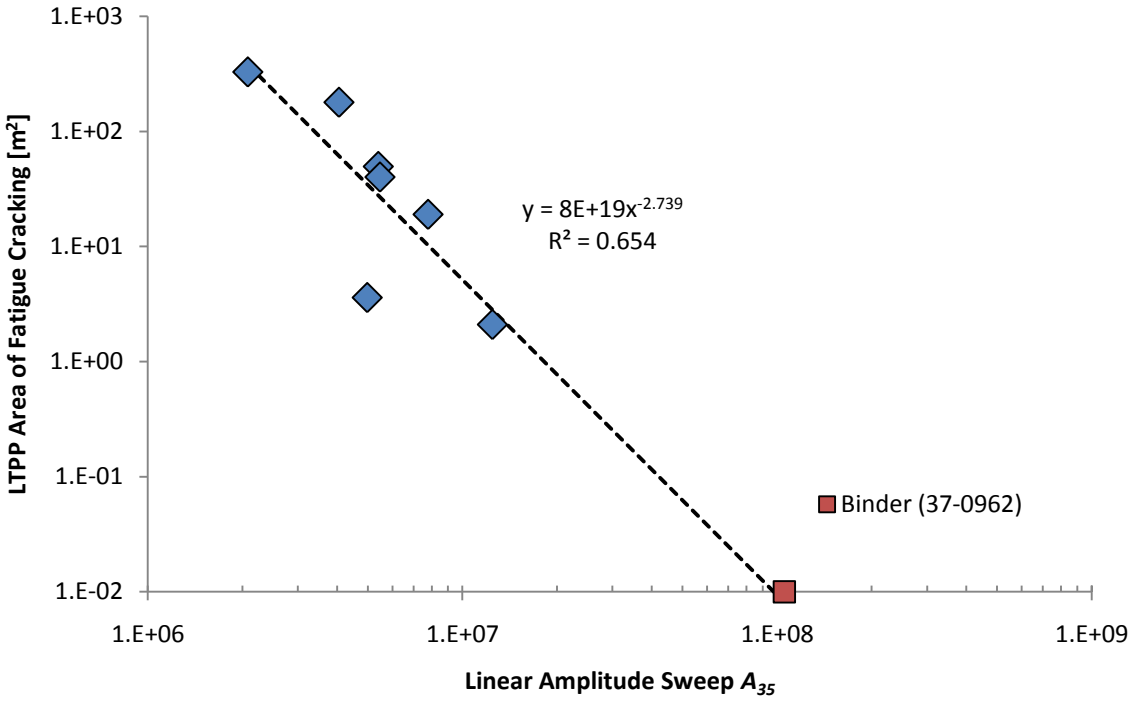

Figure 5.3. Plot of LAS results versus measured fatigue cracking of in-service asphalt pavements.

While the correlation in Figure 5.3 is promising, the LTPP field data was investigated further in order to gain information regarding the amount of traffic for each section. Table 5.6 below gives the yearly traffic in thousands of Equivalent 18-kip Single Axle Loads, or ESAL's. Data is not available for some years, so the latest recorded data point will be used to capture the traffic levels for those years.

Table 5.6. Traffic information for LTPP pavement sections.

	Thousands of ESAL's [kESAL's]							
Year	PG76-10 (04-B901)	PG76-28 (34-0961)	PG76-22 (37-0962)	PG58-34 (09-0961)	PG64-22 (34-0901)	PG52-40 (89-A902)	PG64-22 (35-0902)	PG64-28 (09-0902)
1995	1053	406*	473	530	414*	77*	125	531
1996	1277	406*	542	538	414*	77*	172	538
1997	1094	406*	503	473	414*	77*	172*	474
1998	988	406	20	91	414	77*	1132	91
1999	716	527	175	117	526	77*	1132*	116
2000	2934	427	222	117*	428	77	1132*	116*
2001	1459	496	257	117*	495	77*	1132*	116*
2002	2406	507	371	117*	507	77*	1132*	116*
2003	2642	743	276	33	739	77*	1132*	34
2004	1190	407	276*	3	409	77*	1096	3
2005	1121	467	276*	3*	469	77*	952	3*
2006	1121*	467*	276*	3*	469*	77*	801	3*

Note: (*) indicates data not available for that year, so latest available traffic data is used.

The fatigue cracking data for each section was then normalized to the amount of estimated traffic volume up until the year the fatigue data was measured, given in Table 5.7. The data for Figure 5.3 was then re-plotted using the normalized fatigue cracking instead, now shown in Figure 5.4. With the measured pavement fatigue distress now in units of cracked area per thousand ESAL's, a more valid comparison between binder estimated fatigue parameter (A_{35}) and field performance can be made.

Table 5.7. Traffic data and normalized fatigue cracking results.

Binder	Cracked Area [m^2]	Year of Fatigue Measurement	Total Estimated kESAL's	Normalized Fatigue Cracking [m^2/kESAL]
PG76-10 (04-B901)	328	2005	16,880	1.94E-02
PG76-28 (34-0961)	178.8	2005	5,198	3.44E-02
PG76-22 (37-0962)	0.01*	2005	3,391	2.95E-06
PG58-34 (09-0961)	2.1	2005	2,139	9.82E-04
PG64-22 (34-0901)	49.5	2004	4,760	1.04E-02
PG52-40 (89-A902)	40.1	2003	693	5.79E-02
PG64-22 (35-0902)	19	2003	7,261	2.62E-03
PG64-28 (09-0902)	3.6	2007	2,144	1.68E-03

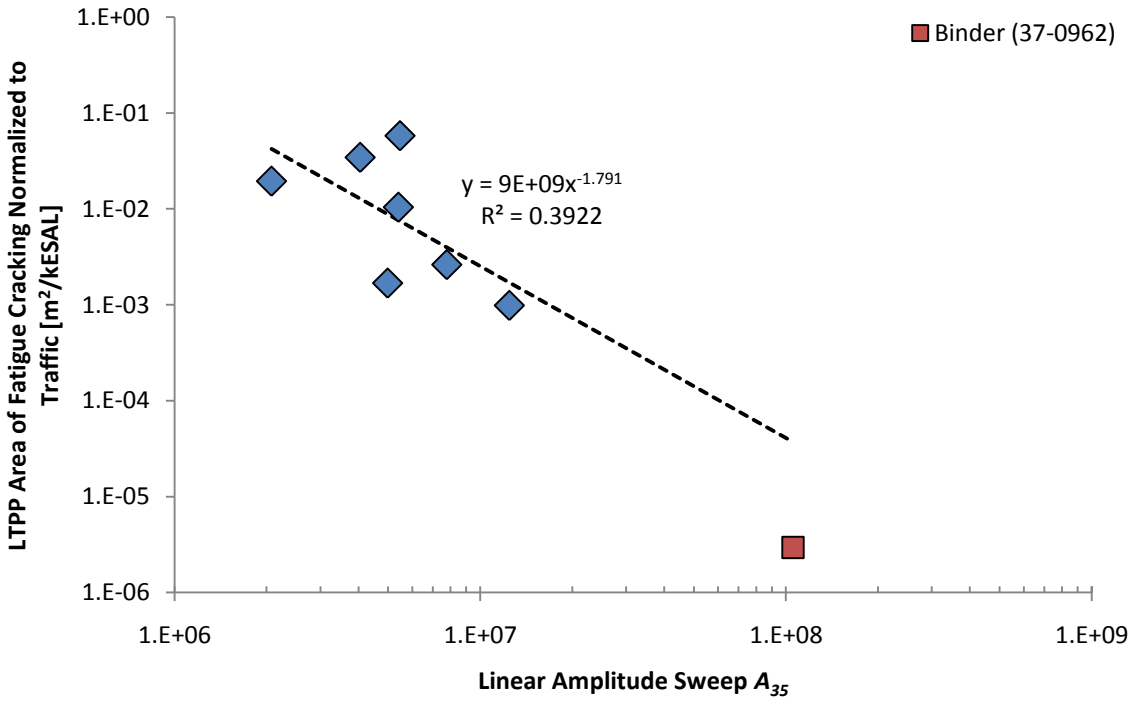

Figure 5.4. Plot of LAS results versus measured fatigue cracking normalized to estimated traffic volume.

When the measured distress is normalized to traffic, the relationship maintains the trend that the higher the value of A_{35}, the less cracking is witnessed for in-service pavements. It should be noted that relating these two parameters as shown above requires the assumption that the applied strain level in each of the pavement sections is the same; if pavement sections are appropriately instrumented to measure actual deflections under traffic loading, the fatigue law as determined by the LAS can be used to match the actual pavement strain more accurately.

6. CONCLUSIONS & RECOMMENDATIONS

The main contribution of this study is the introduction of a method to quantify fatigue damage accumulation of asphalt binders using a short-duration test procedure that can be easily implemented into current practice. This was made possible by integrating results from the testing into an analysis procedure based on Viscoelastic Continuum Damage (VECD) concepts. The use of VECD analysis to characterize asphalt mixtures has been in use by researchers for a number of years, and it has been successfully applied in the field of asphalt mixtures to both monotonic and constant applied load amplitude cyclic (time sweep) tests. However, the application of these methods to asphalt binders has encountered a number of challenges. Monotonic testing of binders showed that, in some cases, the undamaged material response to loading is difficult to predict when some types of binder modification are used (e.g. polymers). The duration of time sweep tests is undefined, since it monitors the change in material properties with respect to number of loading cycles, and some high-performing binders can take many hours to show enough degradation to accurately assess their fatigue properties.

These challenges in applying VECD concepts to binders have been resolved by using the Linear Amplitude Sweep (LAS) test. By selecting a specific ramping sequence of strains, and by combining the results with the results of a frequency sweep, it has been shown that estimation of the fatigue performance of asphalt binders can be correlated to mixture performance in the laboratory and to field fatigue performance.

The accelerated loading scheme is found to give highly repeatable results and it takes less than 10 minutes to perform. The estimation of binder fatigue behavior was first validated against binder time sweep testing, followed by comparisons with asphalt mixture fatigue

results, and finally with in-service (field) pavement fatigue performance. The following points summarize the main findings.

6.1. Findings from Test Method Development

- ANALYSIS OF LAS RESULTS: By incorporating analysis methods based on Viscoelastic Continuum Damage (VECD) mechanics, the damage accumulation rate from the LAS test is used to determine the coefficients for the fatigue law relating number of cycles to failure and applied strain level. The coefficients were found to correlate favorably with the same coefficients as derived from time sweep testing.

  The fatigue law parameter governing the sensitivity of fatigue life to applied strain level has been shown to be related to relaxation properties of the binder. Although measuring the relaxation properties of asphalt binder is possible, it was found that that converting cyclic testing data from the frequency domain to the time domain gave stronger correlations for fatigue performance. One explanation could be due to the differences in mechanical behavior of viscoelastic materials when tested in oscillatory cyclic loading as opposed to transient loading.

- LAS TESTING TEMPERATURE: The intermediate testing temperature for the fatigue parameter $|G^*|\sin\delta$ used in the current specification limit appears to be suitable for the LAS testing. This temperature is related to the average pavement temperature for the specific climate conditions under investigation, which provides insight to material behavior at a critical point in the operating temperature range for an asphalt binder. At high temperatures, the material is primarily viscous and not prone to cracking, whereas at

low temperatures the material is so stiff that traffic loading is unlikely to cause the flexural deflections required to induce fatigue damage.

- MODE OF LOADING IN THE LAS: Changing the mode of applied load gave differing estimates for predicted fatigue life between stress- and strain-controlled LAS tests. However, the ranking of fatigue performance was consistent for both modes. Strain-controlled loading is recommended for a number of reasons:
  - Under fully-reversed loading in the DSR, running in strain-controlled mode minimizes drift in the mean displacement of the spindle (permanent deformation).
  - Stress-controlled loading gives abrupt failure, and without a priori knowledge of this failure point, the stress levels that should be targeted for the LAS test are unknown. Strain-controlled testing was consistently shown to give a peak stress response with a gradual decrease in material integrity over a range of 1 – 20% applied strain.
  - Pavement fatigue is typically modeled as a strain-controlled behavior, where flexural deformations are limited only by the available room for deflection in the pavement base layers.
- REPEATABILITY AND SIGNIFICANCE OF THE LAS TEST RESULTS: Analysis of variance for the results of binders used in the Long Term Pavement Performance (LTPP) confirmed that the performance of the binders as measured using the LAS procedure is significantly dependent upon the binder type, while also showing that the effect of variability (as measured by replicate testing) was insignificant.

6.2. Findings from Validation Efforts

- BINDER-TO-LABORATORY MIXTURE VALIDATION: While the first portion of this study focused on the validation of the LAS against another binder fatigue test method, the second portion incorporated laboratory-prepared asphalt mixture fatigue results. The ranking of fatigue resistance of the binders as measured using the LAS procedure was largely confirmed by constant strain amplitude cyclic fatigue testing of asphalt mixtures, as the LAS was able to differentiate the mixtures with the best performance from poor-performing mixtures .

- BINDER-TO-PAVEMENT VALIDATION: The primary finding from the validation efforts was a promising correlation between the fatigue coefficient at 35% damage (A_{35}) and fatigue cracking of monitored LTPP pavement sections. In-service pavement information is the best application of binder-to-pavement performance relationships. The fatigue distress measured for these sections was normalized to the amount of traffic estimated on these sections. The corresponding A_{35} value from LAS testing was able to provide a good indication of the normalized fatigue performance. This strategy will be valuable in future work to evaluate more binders with available in-service fatigue distress data in order to provide rational specification limits, which will be discussed in the following section.

6.3. Development of Specification Limits

The primary source of information regarding rational specification limits should be actual in-service pavement performance data. The LAS test results estimated from damage in binders were shown to compare favorably with the amount of fatigue distress measure for a selected number of LTPP data sets used in this study. As shown in Figure 6.1 and Figure 6.2, the results of the binder testing are plotted alongside the inverse of the amount fatigue cracking per thousand ESAL's of traffic loading in order to achieve a direct trend of increasing values indicating better performance. It can be seen that, in general, a higher value of A_{35} corresponds to a lower level of fatigue cracking. Thus, a minimum value of A_{35} would be a reasonable place to start for a revised fatigue-related specification.

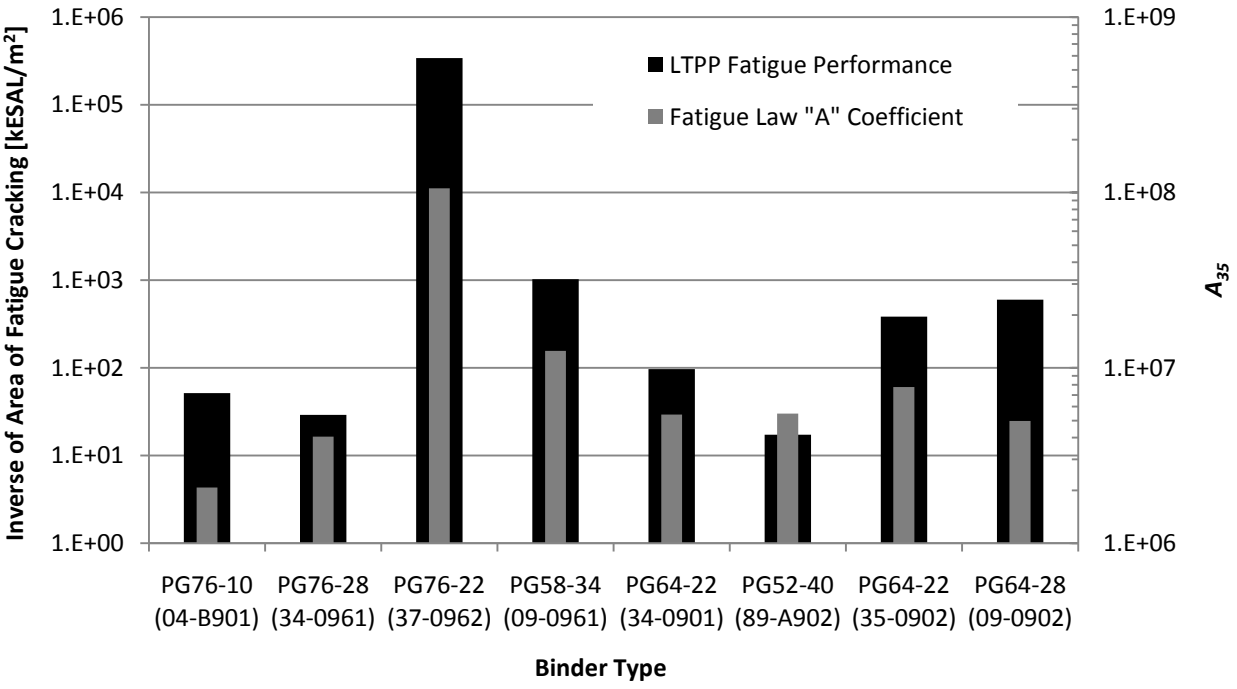

Figure 6.1. Performance of LTPP sections with corresponding A_{35} values.

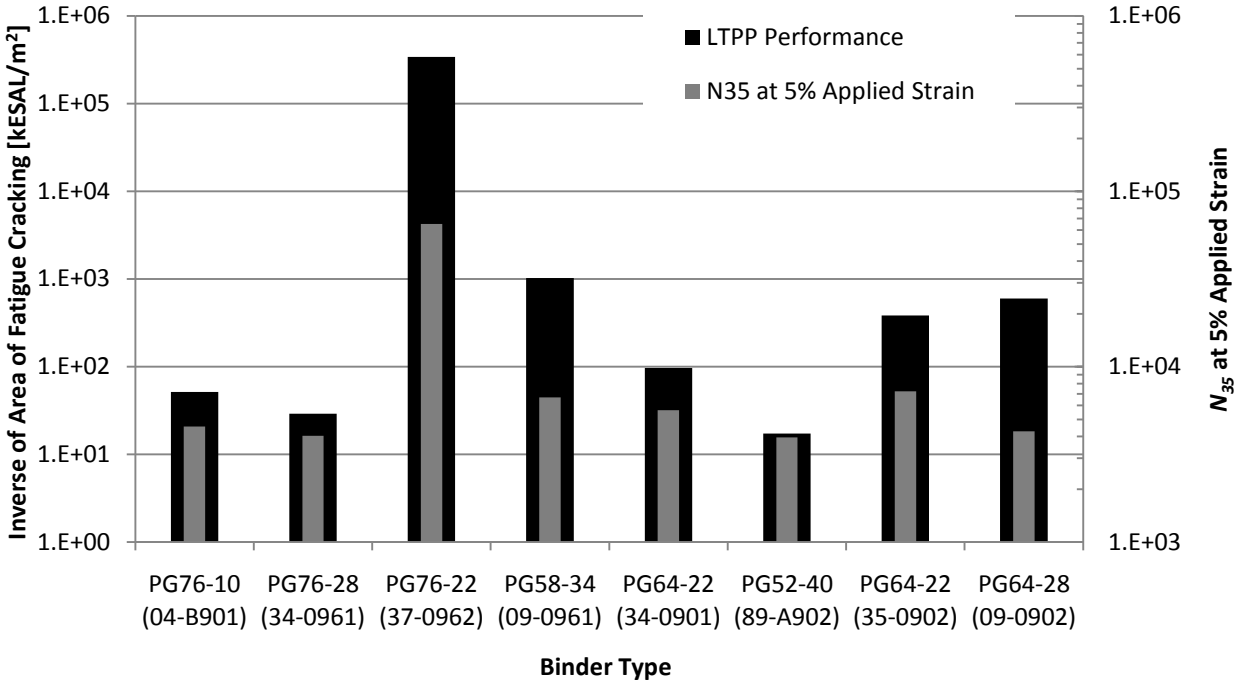

Figure 6.2. Performance of LTPP sections with corresponding N_{35} values at 5% applied strain.

However, A_{35} only provides the number of cycles to failure for a single load amplitude. Therefore, the fatigue law exponent *B* must also be considered. This value determines the sensitivity of fatigue life to applied strain, therefore it would be ideal to have this value as close to zero as possible, indicating that the material does not change its fatigue susceptibility with increasing amplitudes of applied load. As such, an appropriate specification limit would set the value of the exponent *B* to a maximum value. However, a high value of *B* could be offset given a high enough value for A_{35}. With this consideration, it is recommended that a fatigue law benchmark be established, where the derived fatigue law coefficients from LAS testing yield a relationship that results in a fatigue life at or above the benchmark relationship over a specified range of applied strain amplitudes. An example of this concept is shown in Figure 6.3, where two different materials meet the specification requirements in different ways.

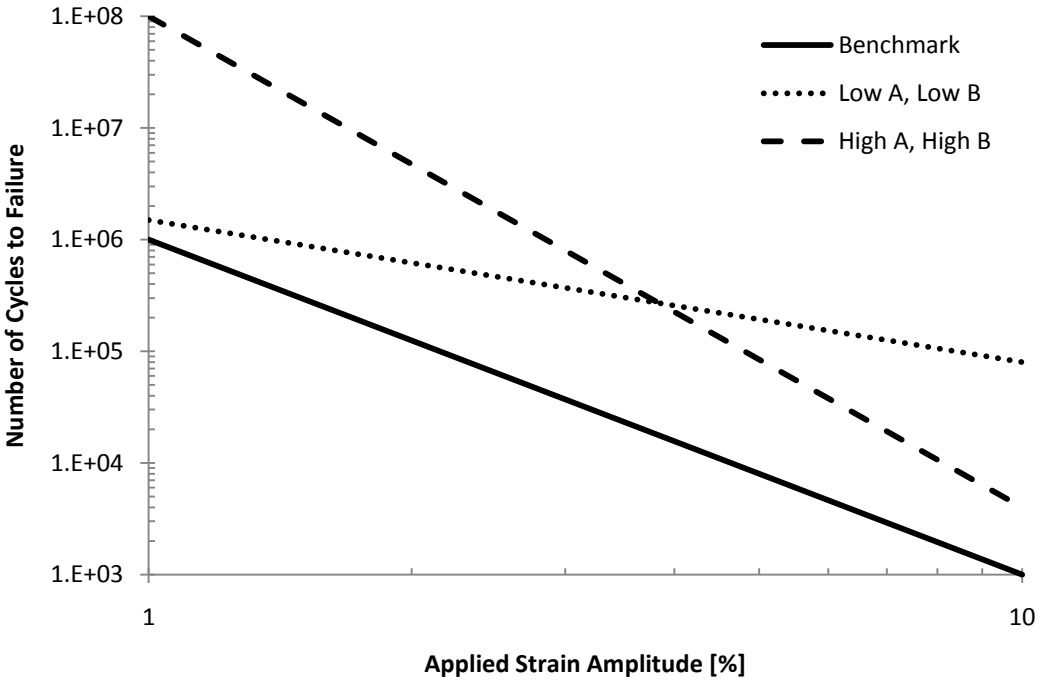

Figure 6.3. Concept for specification limit using fatigue law benchmark.

Using the above concept, a minimum limit would still be in place for A_{35}. The second condition would then set a minimum value of N_{35} at 5% applied strain amplitude (which corresponds to a mixture strain of approximate 1,000με, typically considered a significantly high strain in pavements). Based on the preliminary data in this study, if one selects the in-service pavement distress limit as 100 kESAL's per square meter of fatigue cracking (where half of the pavements studied failed this criterion, as shown in Figure 6.1 and Figure 6.2), that would correspond to limits for A_{35} and N_{35} of 1 x 10^7 and 1 x 10^4, respectively. However, there are currently 22 additional LTPP binders available for testing at UW-Madison, and future work will examine each of these binders in order to refine the exact specification limits. In

order to facilitate inter-laboratory use of the LAS procedure, a draft standard procedure in AASHTO format is presented in Appendix 1.

6.4. Recommendations for Future Work

While the results from this study provide a significant contribution to the existing state of practice for measuring asphalt binder fatigue, there are some issues that should be further investigated. Among them is the subject of healing. As described in the literature review, the presence of secondary bonds in the asphalt binder allow for ease in both breaking bonds in the material as well as reforming them. The characteristics of this self-healing behavior is the subject of much current research, and is certainly relevant to fatigue if the healing can recover the damage accumulation under repeated cyclic loading. It has been said that the true fatigue behavior of an asphalt paving mixture is the ratio of damage accumulation rate to healing rate (Roque et al. 2004). The LAS procedure cannot account for healing rate using the methodology presented here, but future efforts to create a "unified fatigue damage model" will require the healing characteristics of the asphalt be accounted for.

The separation of non-linearity from damage accumulation is another research path that could yield more accurate estimates of fatigue life. While non-linearity is typically not a desirable material behavior, it is theoretically not damage, so the model parameters accounting for predicted undamaged material response could possibly incorporate additional terms to account for non-linearity.

Another recommendation for future work will be to investigate the applicability of the methods used in the VECD analysis to account for temperature sensitivity of the mechanical

properties. This is primarily achieved by employing a normalized modulus in the calculation of damage, such that this normalized value can be converted to the specific modulus by multiplying by the undamaged modulus of the material at the desired temperature. This methodology was applied to uniaxial mixture testing using monotonic strain energy density to characterize damage, but it is currently unknown whether this can be extended to cyclic shear testing that employs dissipated energy to characterize damage.

7. REFERENCES

W. R. Institute. (2007). "Asphalt Research Consortium Year 1 Work Plan." Federal Highway Administration, Washington, D.C.

AASHTO TP 62. "Determining Dynamic Modulus of Hot-Mix Asphalt Concrete Mixtures", *American Association of State & Highway Transportation Officials.*

Anderson, D. A., Le Hir, Y. M., Marasteanu, M. O., Planche, J.-P., Martin, D., and Gauthier, G. (2001). "Evaluation of fatigue criteria for asphalt binders." *Transportation Research Record*, No.1766, 48-55.

Andriescu, A., Hesp, S. A. M., and Youtcheff, J. S. (2004). "Essential and plastic works of ductile fracture in asphalt binders." *Transportation Research Record*, No.1875, 1-8.

Bahia, H. U., Hanson, D. I., Zeng, M., Zhai, H., Khatri, M. A., and Anderson, R. M. (2001). *Characterization of Modified Asphalt Binders in Superpave Mix Design*, NCHRP Report 459, National Academy Press.

Bahia, H. U., Zhai, H., Zeng, M., Hu, Y., and Turner, P. (2002). "Development of binder specification parameters based on characterization of damage behavior." *J. Assn. Asphalt Paving Technologists,* Vol. 70, 442-470.

Bonnetti, K. S., Nam, K., and Bahia, H. U. (2002). "Measuring and defining fatigue behavior of asphalt binders." *Transportation Research Record*, No.1810, 33-43.

Chailleux, E., Bodin, D., Roche, C. d. L., Leguern, M., and Vignard, N. (2009). "Fatigue behaviour of bitumen in tension-compression loading mode: Rheological analysis and comparison with mix fatigue." *Advanced Testing and Characterization of Bituminous Materials, RILEM TC 206*.

Chomton, G., and Valayer, P. J. (1972). "Applied rheology of asphalt mixes, practical application." *Proceedings, Third International Conference on the Structural Design of Asphalt Pavements,* Vol. 1,

Christensen Jr, D. W., and Bonaquist, R. (2005). "Practical application of continuum damage theory to fatigue phenomena in asphalt concrete mixtures." *J. Assn. Asphalt Paving Technologists,* Vol. 74, 963-1001.

Daniel, J. S., Bisirri, W., and Kim, Y. R. (2004). "Fatigue evaluation of asphalt mixtures using dissipated energy and viscoelastic continuum damage approaches." *J. Assn. Asphalt Paving Technologists,* Vol. 73, 557-583.

Daniel, J. S., and Kim, Y. R. (2001). "Laboratory evaluation of fatigue damage and healing of asphalt mixtures." *Journal of Materials in Civil Engineering*,Vol.13, No.6, 434-440.

Daniel, J. S., and Kim, Y. R. (2002). "Development of a simplified fatigue test and analysis procedure using a viscoelastic, continuum damage model." *J. Assn. Asphalt Paving Technologists,* Vol. 71, 619-650.

Deacon, J. A. (1965). "Fatigue of asphalt concrete," Dissertation, University of California, Berkeley.

Delgadillo, R., and Bahia, H. (2005). "Rational fatigue limits for asphalt binders derived from pavement analysis." *J. Assn. Asphalt Paving Technologists,* Vol. 74, 97-137.

Ferry, J. D. (1980). *Viscoelastic properties of polymers*, John Wiley & Sons Inc.

Hertzberg, R. W., and Manson, J. A. (1980). *Fatigue of engineering plastics*, Academic Press.

Johnson, C. M., Bahia, H. U., and Coenen, A. (2009a). "Comparison of Bitumen Fatigue Testing Procedures Measured in Shear and Correlations with Four-Point Bending Mixture Fatigue." 2nd Workshop on Four Point Bending, Guimaraes, Portugal.

Johnson, C. M., Bahia, H. U., and Wen, H. (2009b). "Practical Application of Viscoelastic Continuum Damage Theory to Asphalt Binder Fatigue Characterization." *J. Assn. Asphalt Paving Technologists,* Vol. 78,

Kachanov, L. M. (1986). *Introduction to Continuum Damage Mechanics*, Martinus Nijhoff.

Kim, S., Loh, S. W., Zhai, H., and Bahia, H. U. (2001). "Advanced characterization of crumb rubber-modified asphalts, using protocols developed for complex binders." *Transportation Research Record: Journal of the Transportation Research Board*,Vol.1767, 15-24.

Kim, Y., Lee, H. J., Little, D. N., and Kim, Y. R. (2006). "A simple testing method to evaluate fatigue fracture and damage performance of asphalt mixtures." *J. Assn. Asphalt Paving Technologists,* Vol. 75, 755-788.

Kim, Y. R., and Little, D. N. (1990). "One-dimensional constitutive modeling of asphalt concrete." *Journal of Engineering Mechanics*,Vol.116, No.4, 751-772.

Kim, Y. R., Little, D. N., D'Angelo, J., Davis, R., Rowe, G., Reinke, G., Marasteanu, M., Masad, E., Roque, R., Tashman, L., and Lytton, R. L. (2002a). "Use of dynamic mechanical analysis (DMA) to evaluate the fatigue and healing potential of asphalt binders in sand asphalt mixtures." *J. Assn. Asphalt Paving Technologists,* Vol. 71, 176-206.

Kim, Y. R., Little, D. N., and Lytton, R. L. (2002b). "Use of dynamic mechanical analysis (DMA) to evaluate the fatigue and healing potential of asphalt binders in sand asphalt mixtures." *J. Assn. Asphalt Paving Technologists,* Vol. 71, 176-206.

Kose, S. (2002). "Development of a Virtual Test Procedure for Asphalt Concrete," Ph.D. Dissertation, University of Wisconsin, Madison.

Krajcinovic, D. (1996). *Damage Mechanics*, Elsevier Science.

Kutay, M. E., Gibson, N., and Youtcheff, J. (2008). "Conventional and viscoelastic continuum damage (VECD) based fatigue analysis of polymer modified asphalt pavements." *J. Assn. Asphalt Paving Technologists,* Vol. 77,

Kutay, M. E., Shenoy, A., and Qi, X., (2007). "Full-Scale Accelerated Performance Testing for Superpave and Structural Validation." Federal Highway Administration Turner-Fairbank Highway Research Center.

Lee, H. J., Daniel, J. S., and Kim, Y. R. (2000). "Continuum damage mechanics-based fatigue model of asphalt concrete." *Journal of Materials in Civil Engineering*,Vol.12, No.2, 105-112.

Lee, H. J., and Kim, Y. R. (1998a). "Viscoelastic constitutive model for asphalt concrete under cyclic loading." *Journal of Engineering Mechanics*,Vol.124, No.1, 32-40.

Lee, H. J., and Kim, Y. R. (1998b). "Viscoelastic continuum damage model of asphalt concrete with healing." *Journal of Engineering Mechanics*,Vol.124, No.11, 1224-1232.

Lee, H. J., Kim, Y. R., and Lee, S. W. (2003). "Prediction of asphalt mix fatigue life with viscoelastic material properties." *Transportation Research Record*, No.1832, 139-147.

Lemaitre, J. (1992). *A Course on Damage Mechanics*, Springer-Verlag.

Martono, W., and Bahia, H. U. (2008). "Developing a surrogate test for fatigue of asphalt binders." *Proceedings from the 87th Annual Meeting of the Transportation Research Board,* Vol.

Martono, W., Bahia, H. U., and D'Angelo, J. (2007). "Effect of testing geometry on measuring fatigue of asphalt binders and mastics." *Journal of Materials in Civil Engineering*,Vol.19, No.9, 746-752.

Masad, E., Somadevan, N., Bahia, H. U., and Kose, S. (2001). "Modeling and experimental measurements of strain distribution in asphalt mixes." *Journal of Transportation Engineering*,Vol.127, No.6, 477-485.

Miner, M. A. (1945). "Cumulative damage in fatigue." *Journal of applied mechanics*,Vol.12, No.3, 159-164.

Mogawer, W. S., Austerman, A. J., Kutay, M. E., and Zhou, F., (2009). "TPF-5(146) Internal Project Report."

Monismith, C. L. (1958). "Flexibility Characteristics of Asphaltic Paving Mixtures." *J. Assn. Asphalt Paving Technologists,* Vol. 27, 74-106.

Monismith, C. L., Epps, J. A., Kasianchuk, D. A., and McLean, D. B., (1970). "Asphalt Mixture Behavior in Repeated Flexure." *TE 70-5*, Institute of Transportation and Traffic Engineering, University of California, Berkeley.

Park, S. W., Kim, Y. R., and Schapery, R. A. (1996). "Viscoelastic continuum damage model and its application to uniaxial behavior of asphalt concrete." *Mechanics of Materials*,Vol.24, No.4, 241-255.

Pell, P. S. (1962). "Fatigue Characteristics of Bitumen and Bituminous Mixes." *Proceedings, International Conference on the Structural Design of Asphalt Pavements,* Vol. 1, 310.

Read, J., and Whiteoak, D. (2003). *The Shell Bitumen Handbook, Fifth edition*, Thomas Telford.

Roque, R., Birgisson, B., Drakos, C., and Dietrich, B. (2004). "Development and field evaluation of energy-based criteria for top-down cracking performance of hot mix asphalt." *J. Assn. Asphalt Paving Technologists,* Vol. 73, 229-260.

Santagata, E., Baglieri, O., Dalmazzo, D., and Tsantilis, L. (2009). "Rheological and Chemical Investigation on the Damage and Healing Properties of Bituminous Binders." *J. Assn. Asphalt Paving Technologists,* Vol. 78,

Schapery, R. A. (1975). "A theory of crack initiation and growth in viscoelastic media. III-Analysis of continuous growth." *International Journal of Fracture*,Vol.11, 549-562.

Schapery, R. A. (1984). "Corresponsdence principles and a generalized J integral for large deformation and fracture analysis of viscoelasic media." *International Journal of Fracture*,Vol.25, No.3, 195-223.

Schapery, R. A., and Park, S. W. (1999). "Methods of Interconversion Between Linear Viscoelastic Material Functions - Part II: An Approximate Analytical Method." *International Journal of Solids & Structures*,Vol.36, 1677-1699.

Schütz, W. (1996). "A history of fatigue." *Engineering Fracture Mechanics*,Vol.54, No.2, 263-300.

Shenoy, A. (2002). "Fatigue testing and evaluation of asphalt binders using the dynamic shear rheometer." *Journal of Testing and Evaluation*,Vol.30, No.4, 303-312.

Tsai, B.-W., Monismith, C. L., Dunning, M., Gibson, N., D'Angelo, J., Leahy, R., King, G., Christensen, D., Anderson, D., Davis, R., and Jones, D. (2005). "Influence of asphalt binder properties on the fatigue performance of asphalt concrete pavements." *J. Assn. Asphalt Paving Technologists,* Vol. 74, 733-789.

Wang, L. B., Frost, J. D., and Lai, J. S. (1999). "Noninvasive Measurement of Permanent Strain Field Resulting from Rutting in Asphalt Concrete." *Transportation Research Record*,Vol.1687, 85-94.

Williams, M. L., Landel, R. F., and Ferry, J. D. (1955). "The temperature dependence of relaxation mechanisms in amorphous polymers and other glass-forming liquids." *Journal of the American Chemical Society*,Vol.77, No.14, 3701-3707.

Witczak, M. W., and El-Basyouny, M. M. (2004). *Appendix II-1: Calibration of Fatigue Cracking Models for Flexible Pavements*, Guide for Mechanistic-Empirical Design of New and Rehabilitated Pavement Structures: Final Report, National Cooperative Highway Research Program.

Witczak, M. W., and Fonseca, O. A. (1996). "Revised predictive model for dynamic (complex) modulus of asphalt mixtures." *Transportation Research Record*,Vol.1540, 15-23.

Witczak, M. W., Kaloush, K., Pellinen, T., El-Basyouny, M., and Quintus, H. (2002). *Simple Performance Test For Superpave Mix Design*, NCHRP Report 465, National Academy Press.

Yoder, E. J., and Witczak, M. W. (1975). *Principles of pavement design*, John Wiley & Sons Inc.

8. Appendix 1: Draft Standard Procedure for the Linear Amplitude Sweep

Standard Method of Test for

Estimating Fatigue Resistance of Asphalt Binders Using the Linear Amplitude Sweep

AASHTO Designation: T XXX-10

1. SCOPE

1.1. This test method covers the indication of asphalt binders' resistance to fatigue damage by means of cyclic loading employing a linearly ramping amplitude sweep test. The amplitude sweep is conducted using the Dynamic Shear Rheometer at the continuous intermediate temperature performance grade (PG Grade) of the asphalt binder. The test method can be used with material aged using AASHTO T 240 (RTFOT) and/or AASHTO R 28 (PAV) to simulate the estimated aging for in-service asphalt pavements.

1.2. The values stated in SI units are to be regarded as the standard.

1.3. *This standard does not purport to address all of the safety problems, if any, associated with its use. It is the responsibility of the user of this standard to establish appropriate safety and health practices and determine the applicability of regulatory limitations prior to use.*

2. REFERENCED DOCUMENTS

2.1. *AASHTO Standards*:
M 320, Standard Specification for Performance Graded Asphalt Binder
T 240, Effect of Heat and Air on Rolling Film of Asphalt (Rolling Thin-Film Oven Test)
R 28, Accelerated Aging of Asphalt Binder Using a Pressurized Aging Vessel (PAV)
T 315, Determining the Rheological Properties of Asphalt Binder Using a Dynamic Shear Rheometer (DSR)

2.2. *ASTM Standards*:
D 8, Standard Terminology Relating to Materials for Roads and Pavements
D 2872, Standard Test Method for Effect of Heat and Air on a Moving Film of Asphalt (Rolling Thin-Film Oven Test)
D 6521, Standard Practice for Accelerated Aging of Asphalt Binder Using a Pressurized Aging Vessel (PAV)
D 7175, Standard Test Method for Determining the Rheological Properties of Asphalt Binder Using a Dynamic Shear Rheometer

3. TERMINOLOGY

3.1 Definitions

3.1.1 Definitions of terms used in this practice may be found in Terminology D 8 determined from common English usage, or combinations of both.

4. SUMMARY OF TEST METHOD

4.1 Asphalt binder is first aged using Test Method AASHTO T 240 (ASTM D 2872) (RTFOT) to represent short-term aging of asphalt pavements, or the material may be further aged using AASHTO R 28 (ASTM D 6521-08) prior to testing in order to simulate long-term aging of asphalt pavements. A sample is prepared consistent with Test Method AASHTO T 315 (ASTM D 7175-05) (DSR) using the 8-mm parallel plate geometry with a 2-mm gap setting. The sample is tested in shear using a frequency sweep to determine rheological properties, and is then followed by a series of oscillatory load cycles at systematically increasing amplitudes at a constant frequency to cause accelerated fatigue damage. The continuum damage approach is used to calculate the fatigue resistance from rheological properties and amplitude sweep results.

5. SIGNIFICANCE AND USE

5.1. This method is intended to evaluate the ability of an asphalt binder to resist fatigue damage by employing cyclic loading at increasing amplitudes in order to accelerate damage. The characteristics of the rate of damage accumulation in the material can be used to indicate the fatigue performance of the asphalt binder given pavement structural conditions and/or expected amount of traffic loading using predictive modeling techniques.

6. PROCEDURE

6.1. *Condition the asphalt binder in accordance with T 240 (RTFOT) for short-term performance, or follow with R 28 (PAV) for long-term performance.*

6.2. *Sample preparation* – The sample for the Amplitude Sweep is prepared following T 315 for 8-mm plates. The temperature control also follows the T 315 requirements.

6.2.1. This test may be performed on the same sample that was previously used to determine the rheological properties in the DSR on PAV residue as specified in M 320.

6.3. *Test protocol* – Two types of testing are performed in succession. The first is designed to obtain information on the rheological properties, and the second is intended to measure the damage characteristics of the material.

6.3.1 *Determination of "alpha" parameter* – In order to perform the damage analysis, information regarding the undamaged material properties (represented by the parameter α) must be determined. The frequency sweep procedure outlined in Section 6.3.1.1 is used.

6.3.1.1 *Frequency sweep* –Frequency sweep test data is used to determine the damage analysis "alpha" parameter. The frequency sweep test is performed at the selected temperature, and applies oscillatory shear load of constant amplitude over a range of loading frequencies. For this test method, the frequency sweep test is selected from the DSR manufacturer's controller software, employing an applied load of 0.1% strain over a range of frequencies from 0.1 – 30 Hz. Data is sampled at a rate of ten unique frequencies per decade, or the following specific frequencies can be used (all in Hz):

0.1	0.4	0.7	1.0	4.0	7.0	10	16	22	28
0.2	0.5	0.8	2.0	5.0	8.0	12	18	24	30
0.3	0.6	0.9	3.0	6.0	9.0	14	20	26	

Dynamic shear modulus [|*G**|, Pa] and phase angle [δ, degrees] is recorded at each frequency.

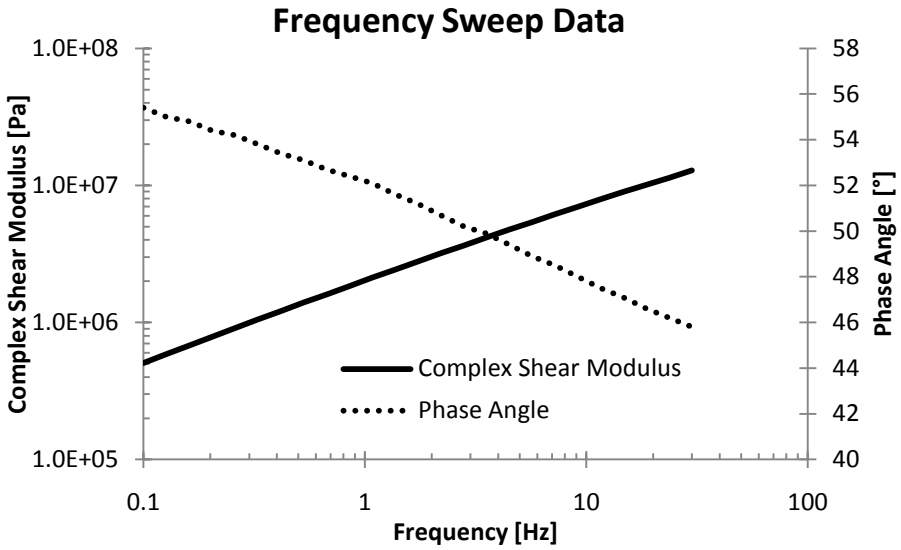

FIGURE 6.1 – Example output from frequency sweep test.

6.3.2. *Amplitude sweep* – The second test is run at the selected temperature using oscillatory shear in strain-control mode at a frequency of 10 Hz. The loading scheme consists of 10 second intervals of constant strain amplitude, where each interval is followed by another interval of increased strain amplitude as follows: 0.1%, 1.0%, 2.0%, 3.0%, 4.0%, 5.0%, 6.0%, 7.0%, 8.0%, 9.0%, 10%, 11%, 12%, 13%, 14%, 15%, 16%, 17%, 18%, 19%, 20%. Peak shear strain and peak shear stress is recorded every 10 load cycles (1 sec), along with phase angle [δ, degrees] and dynamic shear modulus [|*G**|, Pa].

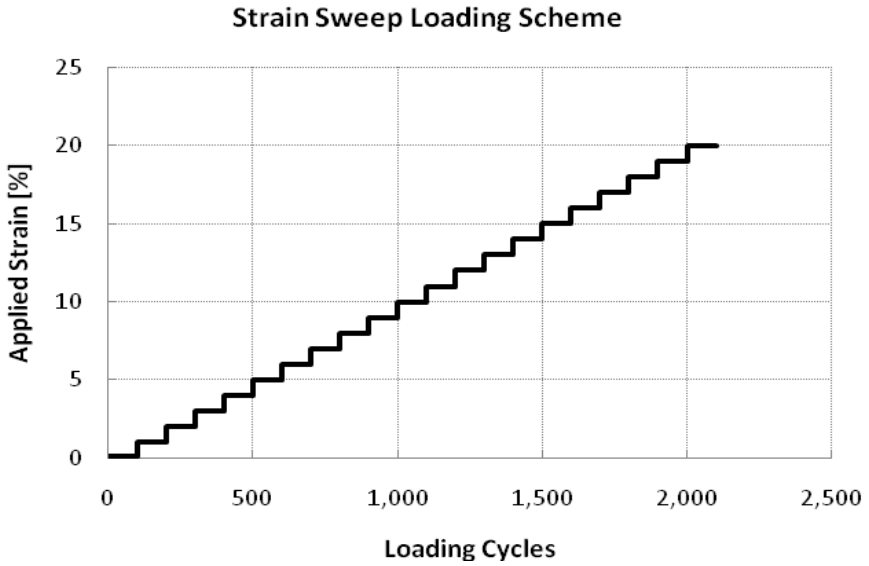

FIGURE 6.2 – Loading scheme for amplitude sweep test

7. CALCULATION AND INTERPRETATION OF RESULTS

7.1 In order to determine the parameter α from frequency sweep test data, the following calculations are performed.

7.1.1. First, data for the dynamic modulus [$|G^*|(\omega)$] and phase angle [$\delta(\omega)$] for each frequency is converted to storage modulus, $G'(\omega)$:

$$G'(\omega) = |G^*|(\omega) \times \cos \delta(\omega)$$

7.1.2. A best-fit straight line is applied to the plot of log ω as the abscissa and log $G'(\omega)$ as the ordinate to the form of

$$\log G'(\omega) = m \, (\log \omega) + b$$

7.1.3. The value obtained for m is recorded as the value α by performing the following transformation:

$$\alpha = 1 + 1 / (m)$$

7.2. For the results of the amplitude sweep test, the data is analyzed as follows:

- NOTE: The following damage calculation method is adapted from Y.R. Kim et al. (11.1).

7.2.1. The damage accumulation in the specimen is calculated using the following summation:

$$D(t) \cong \sum_{i=1}^{N} [\pi I_D \gamma_0^2 (|G^*| \sin \delta_{i-1} - |G^*| \sin \delta_i)]^{\frac{\alpha}{1+\alpha}} (t_i - t_{i-1})^{\frac{1}{1+\alpha}}$$

Where I_D = initial damaged value of $|G^*|$ from the 1.0% applied strain interval, MPa.
γ_0 = Applied strain for a given data point, dimensionless.
$|G^*|$ = dynamic shear modulus, MPa.
α = Value reported in Section 7.1.3.
t = Testing time, sec.

7.2.2. Summation of damage accumulation begins with the first data point for the 1.0% applied strain interval. The incremental value of $D(t)$ at each subsequent point is added to the value of $D(t)$ from the previous point. This is performed up until the final data point from the entire test at 20% applied strain.

7.2.3. For each data point at a given time t, values of $|G^*| \cdot \sin \delta$ and $D(t)$ is recorded (it is assumed that $|G^*| \cdot \sin \delta$ at $D(0)$ is equal to the average undamaged value of $|G^*| \cdot \sin \delta$ from the 0.1% strain interval, and $D(0) = 0$). The relationship between $|G^*| \cdot \sin \delta$ and $D(t)$ can then be fit to the following relationship using least squares regression (or other suitable curve-fitting method):

$$|G^*| \cdot \sin \delta = C_0 - C_1 (D)^{C2}$$

Where C_0 is the average value of $|G^*| \cdot \sin \delta$ from the 0.1% strain interval, and C_1 and C_2 are curve-fit coefficients.

7.3. The value of $D(t)$ at failure, D_f, is defined as that which corresponds to a 35% reduction in undamaged $|G^*| \cdot \sin \delta$ (C_0). The calculation is as follows:

$$D_f = (0.35)(C_0 / C_1)\text{^}(1 / C_2)$$

7.4. The following parameters (A and B) for the binder fatigue performance model can now be calculated and recorded as follows:

$$A = \frac{f(D_f)^k}{k(\pi I_D C_1 C_2)^{\alpha}}$$

Where f = Loading frequency (10 Hz).
$k = 1 + (1 - C_2)\alpha$

and

$B = 2\alpha$.

7.5. The binder fatigue performance parameter N_f can now be calculated as follows:

$$N_f = A(\gamma_{max})^{-B}$$

Where γ_{max} = the maximum expected binder strain for a given pavement structure, dimensionless.

8. REPORT

8.1. *Report the following, if known*:

8.1.1. Sample identification,

8.1.2. PG Grade and Test Temperature, nearest 0.1°C

8.1.3. Fatigue model parameters A and B, 4 significant figures.

8.1.4. Binder fatigue performance parameter N_f, nearest whole number.

9. PRECISION AND BIAS

9.1. To be determined upon results of inter-laboratory testing.

10. KEYWORDS

10.1. Asphalt binder, fatigue, DSR.

11. REFERENCES

11.1. Kim, Y., Lee, H. J., Little, D. N., and Kim, Y. R. (2006). "A simple testing method to evaluate fatigue fracture and damage performance of asphalt mixtures." *J. Assn. Asphalt Paving Technologists*, Vol. 75, pp. 755-788.

[1] The numbers in parentheses refer to the list of references at the end of this standard.

APPENDIX

X1. SAMPLE CALCULATIONS

X1.1. Example data from the amplitude sweep test is given in Table X1.1.

Table X1.1 – Example data output from amplitude sweep test

Testing Time	Shear Stress	Shear Strain	Dynamic Modulus	Phase Angle	$\lvert G^*\rvert \cdot \sin \delta$
[sec]	[MPa]	[%]	[MPa]	[°]	[MPa]
34	0.212	1.996	10.646	49.18	8.057
35	0.212	2.001	10.619	49.22	8.041
36	0.212	2.003	10.595	49.26	8.028
37	0.211	2.003	10.574	49.29	8.016
38	0.211	2.004	10.555	49.32	8.005
39	0.211	2.003	10.539	49.34	7.995
40	0.210	2.003	10.524	49.37	7.987

X1.2. The following values have already been assumed:

$D(33) = 10.77$
$\alpha = 2.58$
$I_D = 8.345$ MPa
$|G^*| \cdot \sin \delta_{t=33} = 8.075$ MPa

X1.3. *Sample calculations:*

X1.3.1. To calculate the accumulation of damage from $t = 33$ sec to $t = 34$ sec,

$$D(34) = D(33) + [\pi I_D \gamma_0^2 (|G^*| \sin \delta_{i-1} - |G^*| \sin \delta_i)]^{\frac{\alpha}{1+\alpha}} (t_i - t_{i-1})^{\frac{1}{1+\alpha}}$$

$$D(34) = D(33) + [\pi (8.345)(1.996)^2 (8.075 - 8.057)]^{\frac{2.58}{1+2.58}} (34 - 33)^{\frac{1}{1+2.58}}$$

$$D(34) = 12.36$$

X1.3.2. This procedure is repeated, giving the following results shown in Table X1.2.

Table X1.2 – Example data output and damage calculation from amplitude sweep test

Testing Time	Shear Stress	Shear Strain	Dynamic Modulus	Phase Angle	$\|G^*\|\cdot\sin\delta$	$D(t)$
[sec]	[MPa]	[%]	[MPa]	[°]	[MPa]	
34	0.212	1.996	10.646	49.18	8.057	12.36
35	0.212	2.001	10.619	49.22	8.041	13.79
36	0.212	2.003	10.595	49.26	8.028	15.06
37	0.211	2.003	10.574	49.29	8.016	16.26
38	0.211	2.004	10.555	49.32	8.005	17.35
39	0.211	2.003	10.539	49.34	7.995	18.40
40	0.210	2.003	10.524	49.37	7.987	19.26

X2.1 The following example plots may be useful in visualizing the results:

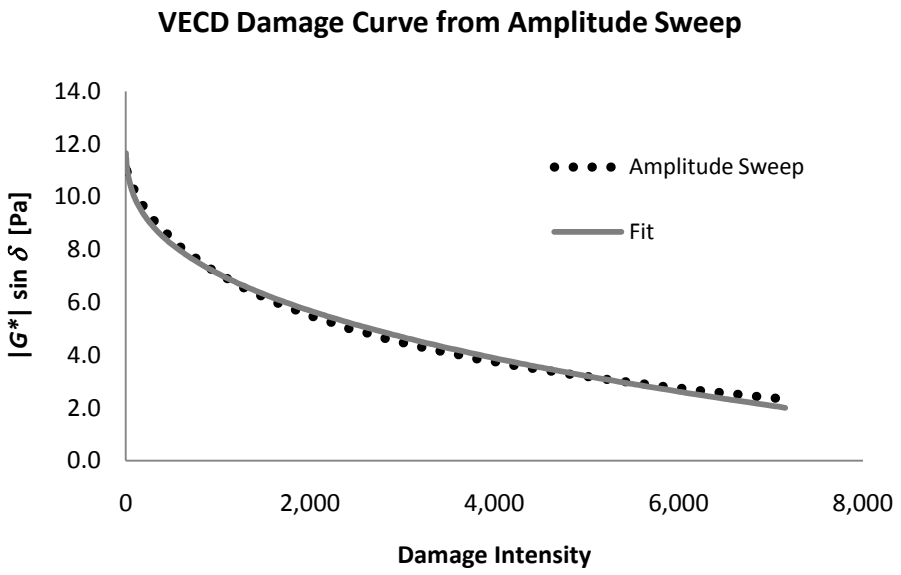

FIGURE X2.1 – Example $|G^*|\cdot\sin\delta$ versus damage plot with curve-fit from Section 7.2.

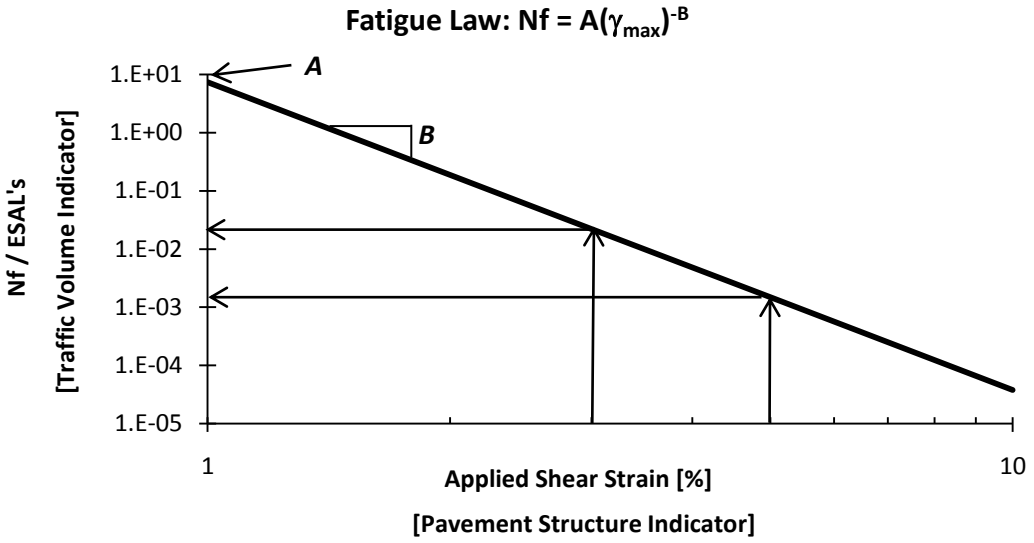

FIGURE X2.2 – Plot of fatigue parameter N_f (normalized to 1 million ESAL's) versus applied binder shear strain on a log-log scale. Allowable fatigue life can be determined for given strain amplitudes, as shown by the arrows.

9. APPENDIX 2: TEST DATA

Test Development Results

Time Sweep – 5% Applied Strain (Intermediate Temperature)

	Alpha		Time Sweep 5% A_{35}							
Binder	SR	FS	SR1	SR2	SR AVG	SR COV	FS1	FS2	FS AVG	FS COV
64-28 SBS Polymer	2.680	2.416	1.902E+08	2.132E+08	**2.017E+08**	**8.06%**	8.148E+07	9.100E+07	**8.624E+07**	**7.81%**
64-34 Terpolymer	2.783	2.388	1.607E+08	9.534E+07	**1.280E+08**	**36.10%**	4.597E+07	2.654E+07	**3.626E+07**	**37.90%**
58-34 Terpolymer	3.075	2.389	2.606E+08	2.586E+08	**2.596E+08**	**0.54%**	2.848E+07	2.793E+07	**2.821E+07**	**1.38%**
64-28 Unmodified	2.552	2.451	6.154E+07	7.338E+07	**6.746E+07**	**12.41%**	4.439E+07	5.307E+07	**4.873E+07**	**12.60%**

Time Sweep – 7% Applied Strain (Intermediate Temperature)

	Alpha		Time Sweep 7% A_{35}							
Binder	SR	FS	SR1	SR2	SR AVG	SR COV	FS1	FS2	FS AVG	FS COV
64-28 SBS Polymer	2.680	2.416	4.959E+08	2.639E+08	**3.799E+08**	**43.18%**	1.781E+08	1.607E+08	**1.694E+08**	**7.26%**
64-34 Terpolymer	2.783	2.388	5.006E+08	4.621E+08	**4.814E+08**	**5.66%**	1.076E+08	9.951E+07	**1.036E+08**	**5.52%**
58-34 Terpolymer	3.075	2.389	1.184E+09	1.116E+09	**1.150E+09**	**4.18%**	8.139E+07	7.697E+07	**7.918E+07**	**3.95%**
64-28 Unmodified	2.552	2.451	1.274E+08	1.438E+08	**1.356E+08**	**8.55%**	8.586E+07	9.696E+07	**9.141E+07**	**8.59%**

KEY: SR – *Values determined from direct stress relaxation testing to estimate* α
FS – *Values determined from using inter-converted stress relaxation from frequency sweep testing to estimate* α
COV – *Coefficient of variation*

Strain-Controlled Linear Amplitude Sweep (Intermediate Temperature)

	Alpha		Strain-Controlled Linear Amplitude Sweep A_{35}							
Binder	SR	FS	SR1	SR2	SR AVG	SR COV	FS1	FS2	FS AVG	FS COV
64-28 SBS Polymer	2.680	2.416	1.900E+07	2.252E+07	**2.076E+07**	**11.99%**	6.289E+06	7.331E+06	**6.810E+06**	**10.82%**
64-34 Terpolymer	2.783	2.388	2.387E+07	1.986E+07	**2.187E+07**	**12.98%**	4.668E+06	3.965E+06	**4.317E+06**	**11.51%**
58-34 Terpolymer	3.075	2.389	6.843E+07	7.536E+07	**7.190E+07**	**6.82%**	4.114E+06	4.427E+06	**4.271E+06**	**5.18%**
64-28 Unmodified	2.552	2.451	7.533E+06	9.126E+06	**8.330E+06**	**13.52%**	4.987E+06	5.994E+06	**5.491E+06**	**12.97%**

Strain-Controlled Linear Amplitude Sweep (5°C)

	Alpha		Strain-Controlled Linear Amplitude Sweep A_{35} – 5°C							
Binder	SR	FS	SR1	SR2	SR AVG	SR COV	FS1	FS2	FS AVG	FS COV
64-28 SBS Polymer	2.607	2.508	3.164E+06	2.255E+05	**1.695E+06**	**122.60%**	2.198E+06	1.610E+05	**1.180E+06**	**122.12%**
64-34 Terpolymer	2.803	2.394	3.556E+07	2.169E+07	**2.863E+07**	**34.25%**	6.268E+06	4.071E+06	**5.169E+06**	**30.05%**
58-34 Terpolymer	2.716	2.422	7.691E+06	7.225E+06	**7.458E+06**	**4.42%**	2.476E+06	2.339E+06	**2.408E+06**	**4.02%**
64-28 Unmodified	2.675	2.566	6.393E+06	2.555E+06	**4.474E+06**	**60.66%**	4.192E+06	1.746E+06	**2.969E+06**	**58.25%**

KEY: SR – *Values determined from direct stress relaxation testing to estimate* α
FS – *Values determined from using inter-converted stress relaxation from frequency sweep testing to estimate* α
COV – *Coefficient of variation*

Mixture/Pavement Validation LAS Testing Results

		Alpha	Strain-Controlled Linear Amplitude Sweep A_{35}			
Binder	**Temperature [°C]**	FS	FS1	FS2	FS AVG	FS COV
70-22 Unmodified	19	2.394	1.568E+06	1.550E+06	**1.559E+06**	**0.85%**
Crumb Rubber – Terminal Blend	19	2.581	8.224E+06	7.239E+06	**7.731E+06**	**9.01%**
Ethylene Terpolymer	19	2.682	4.113E+07	3.549E+07	**3.831E+07**	**10.40%**
SBS - Linearly Grafted	19	2.366	3.470E+06	3.766E+06	**3.618E+06**	**5.80%**
64-28 Unmodified	20	2.321	1.107E+07	1.059E+07	**1.083E+07**	**3.09%**
76-22 Citgo	20	2.413	1.211E+07	1.217E+07	**1.214E+07**	**0.36%**
64-28 2% Latex Rubber	20	2.406	1.844E+07	2.142E+07	**1.993E+07**	**10.57%**
64-28 Polyphosphoric Acid	20	2.374	1.396E+07	2.188E+07	**1.792E+07**	**31.23%**
64-34 SEM Matls.	20	2.474	1.128E+08	8.934E+07	**1.011E+08**	**16.40%**
PG76-10 (04-B901)	37	1.902	2.261E+06	1.896E+06	**2.078E+06**	**12.42%**
PG76-28 (34-0961)	28	2.148	4.318E+06	3.782E+06	**4.050E+06**	**9.36%**
PG76-22 (37-0962)	31	2.296	1.175E+08	9.369E+07	**1.056E+08**	**15.93%**
PG58-34 (09-0961)	16	2.340	1.271E+07	1.219E+07	**1.245E+07**	**2.95%**
PG64-22 (34-0901)	25	2.132	5.127E+06	5.677E+06	**5.402E+06**	**7.20%**
PG52-40 (89-A902)	10	2.248	5.222E+06	5.714E+06	**5.468E+06**	**6.36%**
PG64-22 (35-0902)	25	2.169	7.811E+06	7.742E+06	**7.776E+06**	**0.63%**
PG64-28 (09-0902)	22	2.194	5.130E+06	4.832E+06	**4.981E+06**	**4.22%**

KEY: SR – *Values determined from direct stress relaxation testing to estimate* α
FS – *Values determined from using inter-converted stress relaxation from frequency sweep testing to estimate* α
COV – *Coefficient of variation*